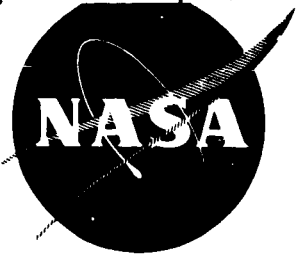


FF No. 602(B)

**N68-10050**  
(ACCESSION NUMBER)  
**98**  
(PAGES)  
**CR-72307**  
(NASA CR OR TMX OR AD NUMBER)

(THRU)  
**1**  
(CODE)  
**22**  
(CATEGORY)

**NASA CR-72307**  
**MAY 6, 1967**



**TOPICAL REPORT**

**COMPARISON OF LOAD BEARING AND  
NON-LOAD BEARING RADIATORS  
FOR  
NUCLEAR RANKINE SYSTEMS**

by

**R. D. Cockfield**

prepared for

**NATIONAL AERONAUTICS AND SPACE ADMINISTRATION**

**CONTRACT NASw-1449**

**ADVANCED NUCLEAR SYSTEMS OPERATION**

**GENERAL  ELECTRIC**

**MISSILE AND SPACE DIVISION  
Valley Forge Space Technology Center  
P.O. Box 8661 • Philadelphia 1, Penna.**

## NOTICE

This report was prepared as an account of Government sponsored work. Neither the United States, nor the National Aeronautics and Space Administration (NASA), nor any person acting on behalf of NASA:

- A.) Makes any warranty or representation, expressed or implied, with respect to the accuracy, completeness, or usefulness of the information contained in this report, or that the use of any information, apparatus, method, or process disclosed in this report may not infringe privately owned rights; or
- B.) Assumes any liabilities with respect to the use of, or for damages resulting from the use of any information, apparatus, method or process disclosed in this report.

As used above, "person acting on behalf of NASA" includes any employee or contractor of NASA, or employee of such contractor, to the extent that such employee or contractor of NASA, or employee of such contractor prepares, disseminates, or provides access to, any information pursuant to his employment or contract with NASA, or his employment with such contractor.

Requests for copies of this report should be referred to

National Aeronautics and Space Administration  
Office of Scientific and Technical Information  
Box 33  
College Park, Md. 20740

NASA CR-72307  
GE ANSO 6300-203  
May 6, 1967

TOPICAL REPORT

COMPARISON OF LOAD BEARING AND NON-LOAD BEARING  
RADIATORS FOR NUCLEAR RANKINE SYSTEMS

by

R. D. Cockfield

prepared for

NATIONAL AERONAUTICS AND SPACE ADMINISTRATION

CONTRACT NASw-1449

Technical Management  
NASA Lewis Research Center  
Cleveland, Ohio  
James P. Couch

**ADVANCED NUCLEAR SYSTEMS OPERATION**

**GENERAL  ELECTRIC**

**MISSILE AND SPACE DIVISION**  
Valley Forge Space Technology Center  
P.O. Box 8661 • Philadelphia 1, Penna.

## ABSTRACT

A comparison is made between load bearing radiators in a conical configuration, and non-load bearing radiators in a flat panel configuration, for a nuclear Potassium - Rankine powerplant. For a typical unmanned interplanetary probe mission the load bearing radiator showed a payload advantage of four percent at a power level of 300 kWe, and an advantage of thirty percent at 1200 kWe. The comparison shows that the non-load bearing radiator does not achieve the payload advantage for interplanetary missions that might be anticipated by virtue of its ability to dispose of launch structure.

~~PRECEDING PAGE BLANK NOT FILMED.~~

## TABLE OF CONTENTS

Section		Page
ABSTRACT	.....	iii
1	SUMMARY .....	1- 1
2	ASSUMPTIONS FOR RADIATOR COMPARISON .....	2- 1
	2.1 Powerplant Specifications .....	2- 1
	2.2 Radiator Configuration .....	2- 2
	2.3 Meteoroid Criteria .....	2-10
	2.4 Structural Criteria .....	2-12
	2.5 References .....	2-17
3	NON-LOAD BEARING RADIATOR .....	3- 1
	3.1 Spacecraft Description .....	3- 1
	3.2 Structural Analysis .....	3-17
	3.3 Thermal Stresses .....	3-18
	3.4 Fabrication and Assembly of Non-Load Bearing Radiator .....	3-20
	3.5 References .....	3-26
4	LOAD BEARING RADIATORS .....	4- 1
	4.1 Spacecraft Description .....	4- 1
	4.2 Structural Analysis of the Conical Radiator .....	4- 8
	4.3 Thermal Stresses .....	4-13
	4.4 Fabrication and Assembly-Load Bearing Radiator .....	4-14
	4.5 References .....	4-17
5	CONCLUDING REMARKS .....	5- 1
APPENDICES		
A	SAMPLE CALCULATION FOR STRUCTURAL ANALYSIS OF LAUNCH STRUCTURE .....	A-1
B	STRESSES DUE TO TUBE TO FIN THERMAL GRADIENTS .....	B-1
C	MISSION PERFORMANCE ANALYSIS .....	C-1

## LIST OF ILLUSTRATIONS

Figure	Title	Page
2-1	Feed Line Schematic for Flat Panel 300 kWe Powerplant .....	2- 4
2-2	Feed Line Schematic for Flat Panel 1200 kWe Powerplant .....	2- 5
2-3	Feed Line Schematic for Conical 300 kWe Powerplant .....	2- 6
2-4	Feed Line Schematic for Conical 1200 kWe Powerplant .....	2- 7
2-5	Unmanned Shield Weights for 300 kWe Powerplant .....	2- 9
2-6	Unmanned Shield Weights for 1200 kWe Powerplant .....	2- 9
2-7	Launch Loads on Radiator for Three-Stage Saturn V .....	2-13
2-8	Launch Loads on Radiator for two-Stage Saturn V .....	2-14
2-9	Trend in Launch Vehicle Dynamic Loads .....	2-14
2-10	Effect of Payload Stiffness on the Natural Frequency of the Combined Launch Vehicle. ....	2-16
3-1	Spacecraft Concept for 300 kWe Powerplant with Flat Panel Radiator ....	3- 3
3-2	Spacecraft Concept for 1200 kWe Powerplant with Flat Panel Radiator ...	3- 5
3-3	Tube Cross-Sections for Primary Radiator on 1200 kWe Spacecraft .....	3- 8
3-4	Weight Comparison for Flat Panel and Conical Radiator Configuration ...	3-10
3-5	Separation Sequence for 1200 kWe Spacecraft .....	3-11
3-6	Support Structure for Power Conversion Equipment .....	3-13
3-7	Detail of Launch Structure Separation Device .....	3-14
3-8	Detail of Launch Structure to Payload Structure Joint .....	3-15
3-9	Detail of Tubular Cluster Joint in Truss Frame .....	3-16
3-10	Comparison of Launch Structure Weight Distribution, Actual with Ideal ...	3-18
3-11	Assembly Sequence for Flat Panel Radiator .....	3-21
3-12	Portable Welding Tool, 2-inch Diameter Tube .....	3-24
3-13	Detail of Feed Line to Header Joints .....	3-25

## LIST OF ILLUSTRATIONS (Cont)

Figure	Title	Page
4-1	Spacecraft Concept - 300kWe Powerplant with Conical Radiator .....	4- 3
4-2	Spacecraft Concept - 1200kWe Powerplant with Conical Radiator .....	4- 5
4-3	Assembly Sequence for Conical Radiator .....	4-15
5-1	Weight Comparison for Jupiter Fly-by Mission .....	5- 3
5-2	Payload Comparison for Jupiter Fly-by Mission .....	5- 4

## LIST OF TABLES

Number	Title	Page
2-1	Powerplant Specifications .....	2- 2
3-1	Flat Panel Radiator Parameters for 300 kWe Powerplant .....	3- 2
3-2	Flat Panel Radiator Parameters for 1200 kWe Powerplant .....	3- 7
3-3	Comparison of Candidate Materials for Launch Structure at 300°F .....	3-17
3-4	Summary of Thermal Stress Analyses .....	3-19
3-5	Space Requirements for Welding Equipment .....	3-26
4-1	Conical Radiator Parameters for 300 kWe Powerplant .....	4- 2
4-2	Conical Radiator Parameters for 1200 kWe Powerplant .....	4- 7
4-3	Definitions of Structural Failure Modes .....	4-10
4-4	Summary of Stress Analysis for the 300 kWe Conical Radiator .....	4-11
4-5	Summary of Stress Analysis for the 1200 kWe Conical Radiator .....	4-12
5-1	Weight Comparison for Jupiter Fly-by Mission .....	5- 2

# 1. SUMMARY

This report is the second topical report under contract NASW-1449, "A Study of Radiator Structural and Mechanical Requirements." The study deals with the problems of large space radiators for nuclear Rankine power systems. The first topical report discussed the interrelations between the radiator and unmanned spacecraft, and presented parametrically the data describing these interrelations. This second report presents a comparison between load bearing and non-load bearing radiator concepts.

The comparison is made to determine if the non-load bearing has an advantage for an interplanetary probe mission. The load bearing radiator has several advantages resulting from its simplicity and ability to provide a less restricted payload volume. If the non-load bearing radiator concept is to show any advantage over the load bearing radiator, it would be for an interplanetary probe mission where it can take advantage of disposing of its launch structure. If such an advantage does not exist, then other considerations would favor the selection of a load bearing radiator.

The non-load bearing radiator requires an aerodynamic shroud and additional support structure during launch. However, since the shroud can be ejected shortly after launch and the structure ejected prior to initiating low thrust electric propulsion, the weight penalty imposed can only be evaluated by comparing the delivered payloads associated with the two concepts.

Analysis of an unmanned Jupiter fly-by mission shows that the load bearing radiator concept results in a four percent payload advantage at a power level of 300 kWe and a 30 percent payload advantage at a power level of 1200 kWe. These two cases correspond to spacecraft launched on a three-stage Saturn V with a 500 day trip time, and a spacecraft launched on a two-stage Saturn V with an 800 day trip time.

Although the exact payload differences are dependent to some extent on the assumptions made in this study, the comparison suffices to show that the non-load bearing radiator does not offer the advantage that may have been anticipated for an interplanetary mission.

## 2. ASSUMPTIONS FOR RADIATOR COMPARISON

### 2.1 POWERPLANT SPECIFICATIONS

The radiator concepts compared in this study are associated with nuclear powerplants having the characteristics listed in Table 2-1. These characteristics were specified by NASA-Lewis and are representative of current Potassium - Rankine powerplant concepts. The comparison is made for two power levels, corresponding to the radiator area limitations of the three-stage and two-stage Saturn V launch vehicles. In each case, the power level is limited by the area requirements of the flat panel radiator configuration. A conical radiator with the same heat rejection capability fits within a smaller envelope. The launch capabilities of the Saturn vehicles in terms of maximum radiator area and mass distribution were determined in Task "A" of this study, and are reported in Reference 2-1.

The distribution of the heat rejected is indicated in Table 2-1. Two percent of the total thermal power is rejected by low temperature radiators. The comparison made in this study, however, is concerned only with the higher temperature primary and secondary radiators associated with the powerplant. The low temperature radiators associated with the payload could be of aluminum construction and deployed from the payload section, which in turn may deploy away from the powerplant. The fins and armor of these low temperature radiators would be relatively thin and not suited to a load bearing function. The use of an organic coolant in these radiators would make deployment relatively easy, and, in fact the large area requirements may make deployment essential.

For simplicity, the powerplant conversion efficiencies were assumed to be such that the net electrical power of the two powerplant sizes would be 300 kWe and 1200 kWe, respectively. This makes possible comparison with previous studies conducted at these power levels and simplifies the task of estimating component weights. For convenience, in the remainder of this report the power levels will be referred to by the net electrical power, rather than the total thermal power.

TABLE 2-1. POWERPLANT SPECIFICATIONS

Launch Vehicle	THREE-STAGE SATURN V	TWO-STAGE SATURN V
Total power	3 MWt	12 MWt
Heat rejected by primary radiator	2.46 MWt	9.84 MWt
Heat rejected by secondary radiator	0.48 MWt	1.92 MWt
Heat rejected by low temperature radiator	0.06 MWt	0.24 MWt
Primary radiator coolant	NaK	NaK
Secondary radiator coolant	K	K
Primary radiator inlet	1300°F	1300°F
Secondary radiator inlet/outlet	850/750°F	850/750°F
Pump efficiency	20%	20%
Radiator material	Beryllium with stainless steel liners and plumbing	
Life	5 Years	
Meteoroid Nonpenetration probability	0.999	

Pump efficiency is specified so that proper account may be taken of the pumping work in determining the optimum radiator design. This penalty is a second order effect and is not sensitive to the actual value of pump efficiency chosen.

## 2.2 RADIATOR CONFIGURATION

The two extremes in radiator configuration are the cone-cylinder shape which rejects heat from one fin surface only and the flat panel configuration which rejects heat from both fin surfaces with a maximum view factor. The conical configuration is ideally suited to the role of a load bearing radiator, while the flat panel radiator, being the ideal for thermal performance, is the logical choice for a non-load bearing radiator. In this study then, the comparison will be made between conical and flat panel configurations, and the terms "conical" and "flat panel" will be used interchangeably with "load bearing" and "non-load bearing", respectively.

One advantage of the flat panel configuration is that it can be preferentially oriented in the plane of the solar ecliptic during flight to reduce the effect of the incident solar flux. However, at the radiator temperatures specified for this study, the effective sink temperature has little effect on thermal performance. The conservative assumption is made that the powerplant will be operated initially at full power in Earth orbit so that near Earth incident fluxes are used in the thermal analysis. The conical radiator will see a solar flux of approximately  $440 \text{ Btu/hr-ft}^2$  combined with Earth emission and albedo of approximately  $220 \text{ Btu/hr-ft}^2$ . The flat panel radiator, in a plane parallel to the solar flux, will see only a fraction of the Earth emission and albedo. The corresponding effective sink temperatures, assuming an emittance of 0.90 and an absorptance of 0.75, are  $120^\circ\text{F}$  for the conical radiator and  $-51^\circ\text{F}$  for the flat panel radiator.

The specified pump efficiency of 20 percent affects the radiator weight through the use of a pump penalty. The pump penalty factor is defined as the specific powerplant weight, divided by pump efficiency. In this study, the pumping power for each radiator is multiplied by a pump penalty factor of 200 lb/kWe. The resulting pump penalty is then added to the radiator weight to give a "system weight." Optimization is performed by minimizing the "system weight" rather than radiator weight. The pump work is affected by the feed line lengths, which are included in the pressure drop analysis of the radiator. Because of fundamental differences in the two configurations, it is not possible to use the same feed line network for both the flat panel and conical radiators. A schematic of the feed lines assumed for each of the radiators is shown in Figures 2-1 through 2-4. For the 300 kWe powerplants, it was assumed that two independent loops would be used, although only one set of turbomachinery may be required. For the 1200 kWe powerplant, four independent loops are shown, allowing the power conversion components to be chosen in multiples of 300 kWe. Because the flat panel configuration fits within a larger launch vehicle envelope, the feed line lengths are greater than those of an equivalent conical radiator. Also the feed lines for the flat panel radiators must be routed to take advantage of the meteoroid protection provided by the launch structure. In the conical radiator, the feed lines are protected by the radiator.

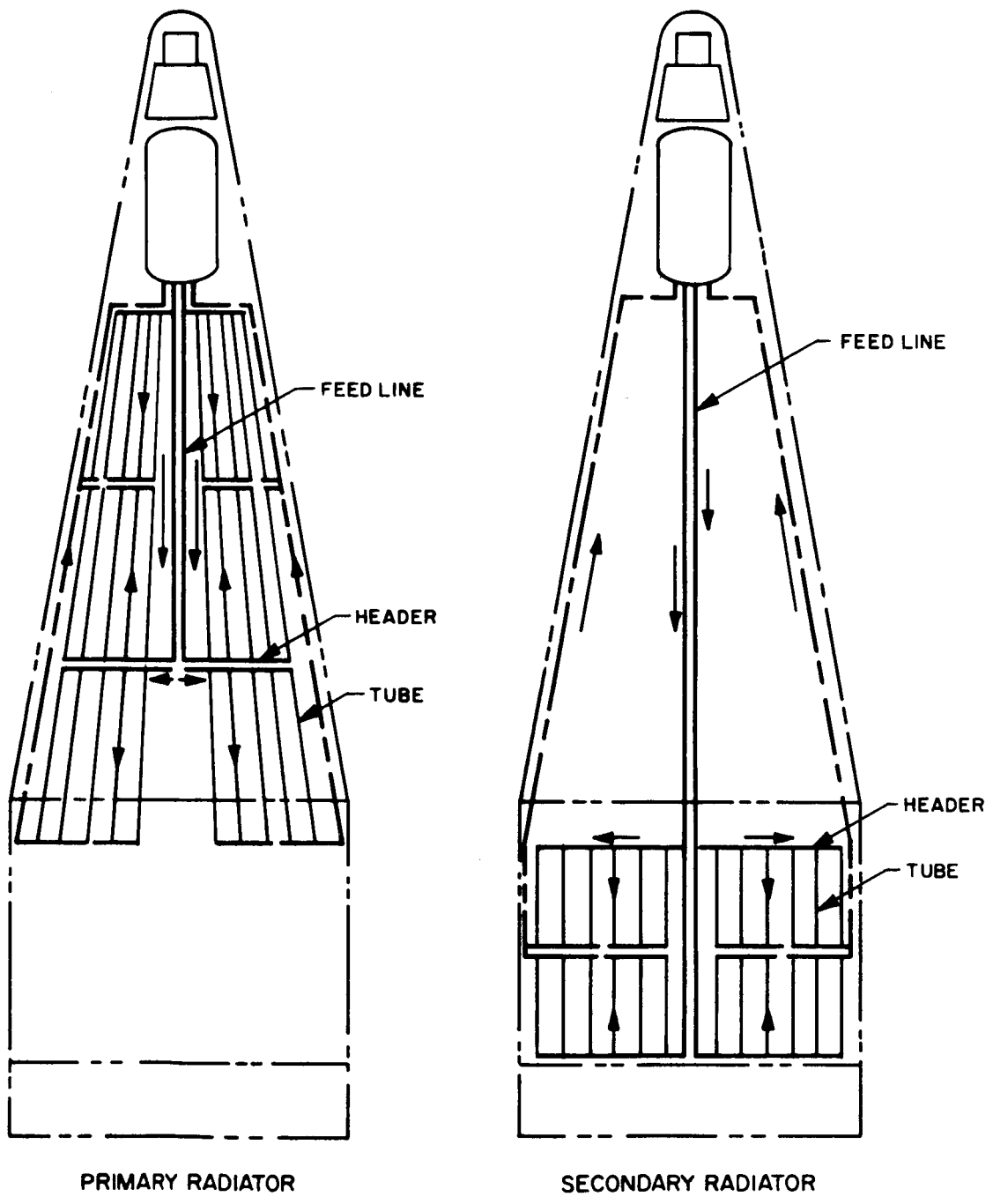


Figure 2-1. Feed Line Schematic for Flat Panel 300 kWe Powerplant

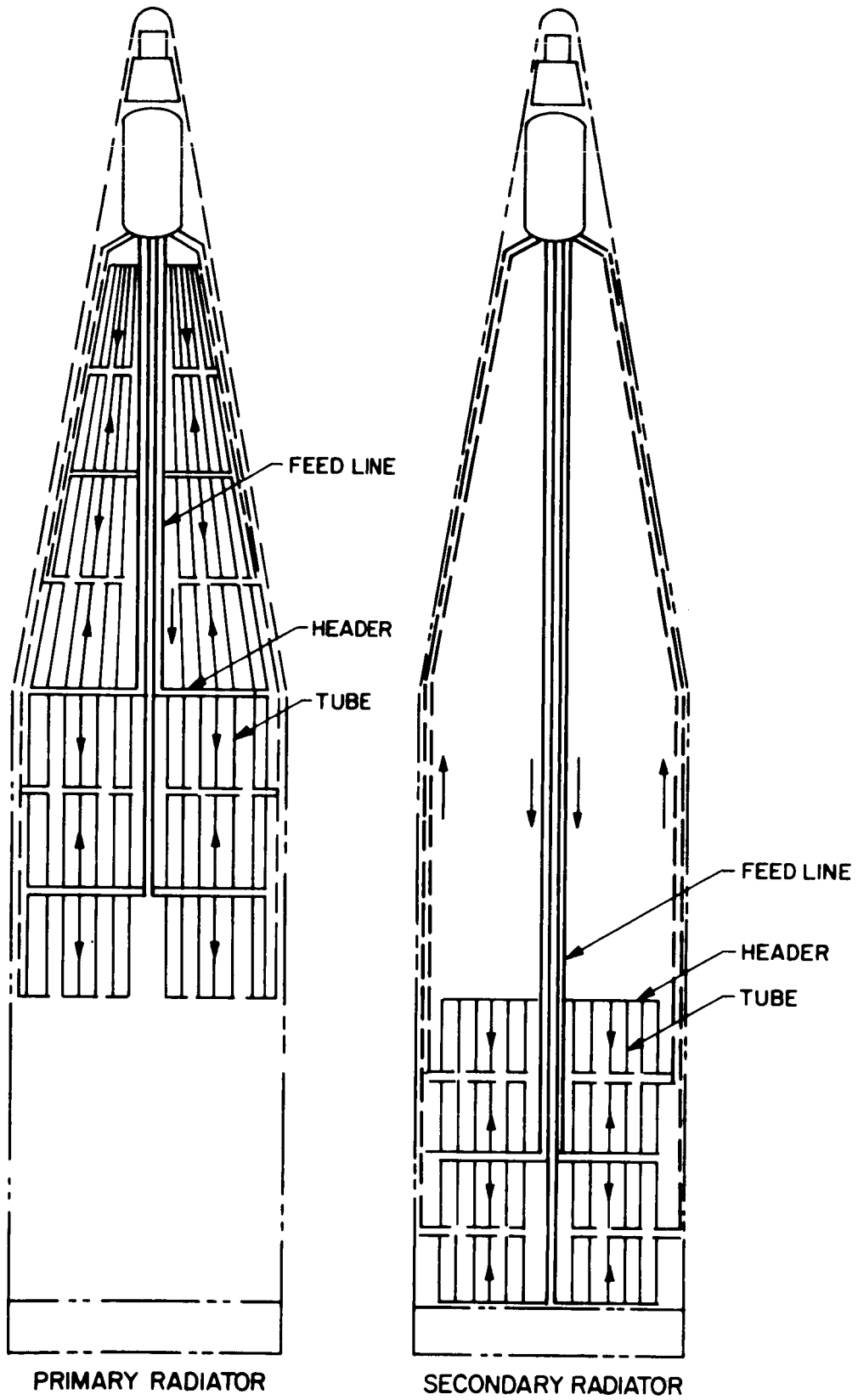
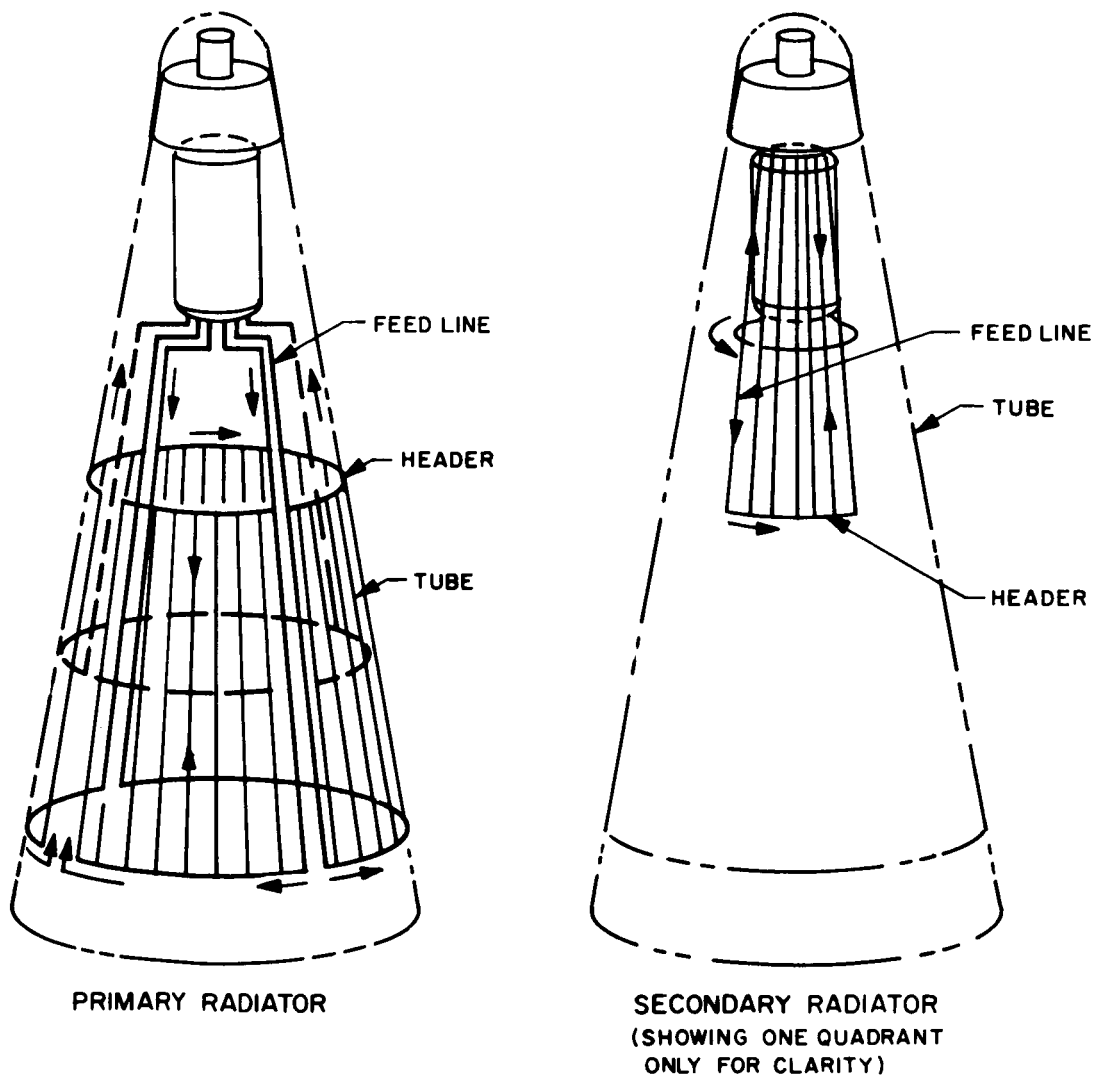


Figure 2-2. Feed Line Schematic for Flat Panel 1200 kWe Powerplant



PRIMARY RADIATOR

SECONDARY RADIATOR  
(SHOWING ONE QUADRANT  
ONLY FOR CLARITY)

Figure 2-3. Feed Line Schematic for Conical 300 kWe Powerplant

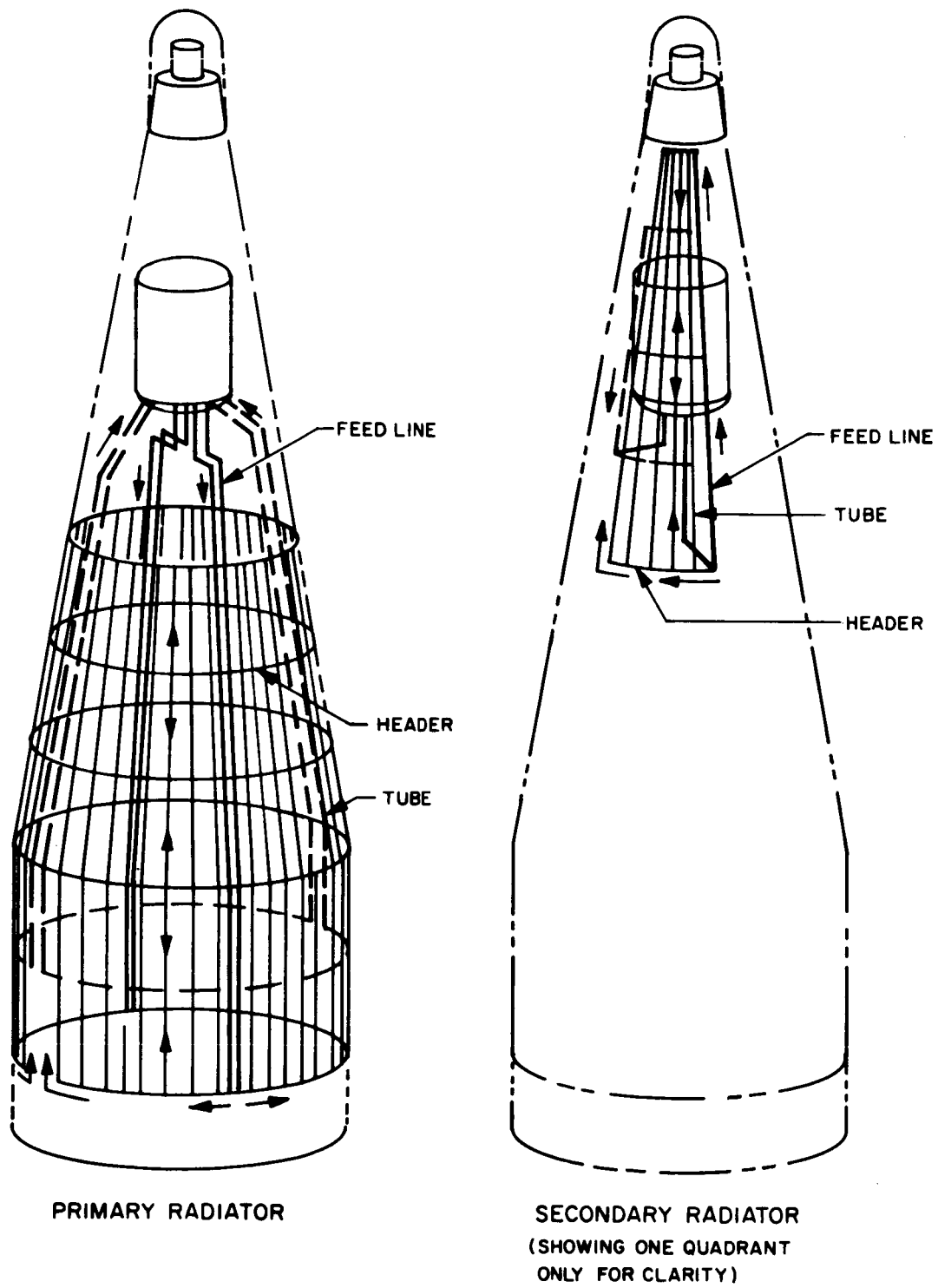


Figure 2-4. Feed Line Schematic for Conical 1200 kWe Powerplant

Thermal, meteoroid, and hydraulic analysis of the radiators was performed using the SPARTAN III computer code. This code has the capability of performing weight optimization while varying up to twenty independent variables simultaneously. Performance calculations from the code have shown excellent agreement with a liquid metal test radiator. Included in the radiator weight calculated by the computer code are the weights of liners, armor, fins, headers, feed lines, and coolant inventory.

An advantage of the flat panel radiator configuration is that it requires less nuclear radiation shielding. In Task "A" of this study (Reference 2-1), it was shown that the advantage in reduced scatter shielding weight is negligible or vanishes when the radiator half-cone angle is ten degrees. However, the flat panel radiator retains a shielding weight advantage by virtue of a greater separation distance, resulting from the fact that its envelope dimensions are greater for the same heat rejection capability. Because some of the powerplant specifications were different than those assumed in the prior task, revised shield weights were determined. Except as noted, the assumptions and method of analysis are the same as those discussed in the previous topical report. The results are shown in Figures 2-5 and 2-6, for a radiator half-cone angle of ten degrees. It should be noted that these shield weights are appropriate to an unmanned mission only.

A consequence of the choice of a non-load bearing radiator in a flat panel configuration is that a rigid frame is required surrounding each panel. Since the radiator is the heaviest component of the powerplant, most of the launch loads are carried by this frame in the plane of the radiator. Load paths to the launch vehicle interface are therefore directed principally through two axial members. These members are of necessity a significant part of the launch structure and must remain with the radiator after launch. The remainder of the launch structure can be ejected prior to initiating electric propulsion. Because of the strongly directed load paths in the non-disposable structure, the launch structure is best designed as a space frame. A space frame also lends itself to simple separation schemes since it attaches at specific hard points where pyrotechnic release devices can be located. A shell structure in this application would be loaded adversely along two axial elements and would be less efficient than a frame; in addition, separation would require a more elaborate pyrotechnic system. In this study, therefore, the concept shown for the

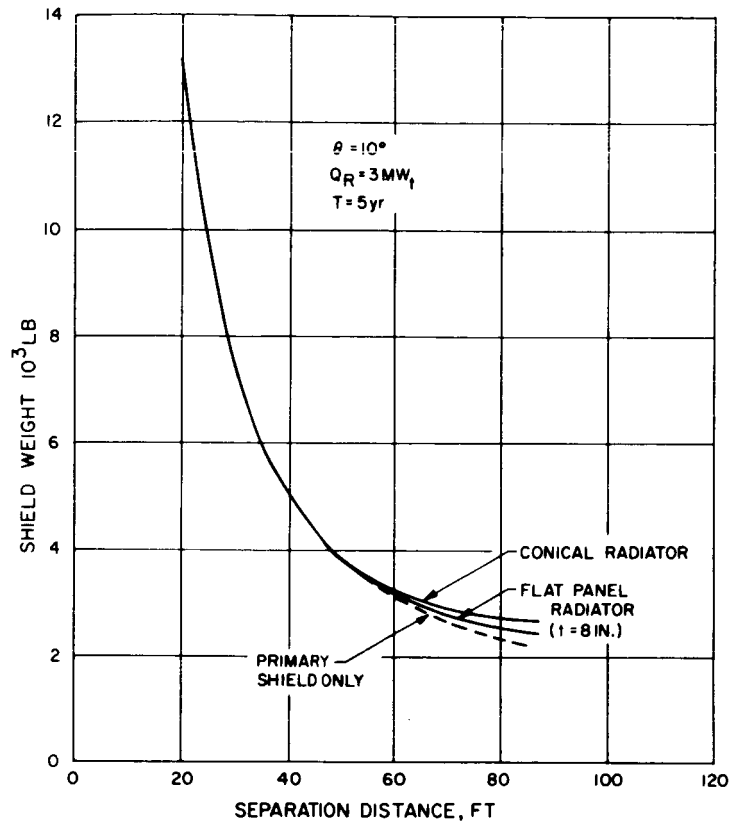


Figure 2-5. Unmanned Shield Weights for 300 kW Powerplant

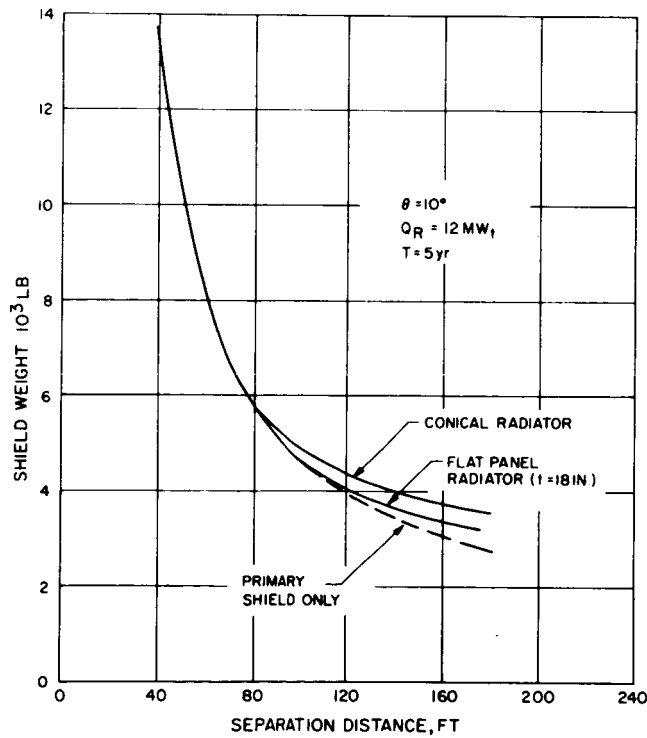


Figure 2-6. Unmanned Shield Weights for 1200 kW Powerplant

launch structure with the non-load bearing radiator is a tubular space frame that utilizes the two axial members of the non-disposable structure. Frame bays are sized to match the radiator panel sizes so that attachments occur at rigid intersections with the lateral members of the non-disposable structure. A further consequence is that an aerodynamic shroud over the entire payload is required. If a concept were used in which the shroud also performed the function of primary launch structure, the entire structure would have to be carried into orbit or beyond escape. The advantage of being able to dispose of the aerodynamic shroud at low altitude would be lost. As will be shown later, the penalty imposed by the aerodynamic shroud has a significant effect on the comparison of payload capabilities.

### 2.3 METEOROID CRITERIA

The meteoroid protection criteria used in this study reflect current recommendations of NASA-Lewis. The meteoroid environment assumed is the Whipple 1963A flux density model with an average meteoroid velocity of 20 km/sec and a meteoroid density of 0.5 g/cc. Many of the previous radiator studies at GE-MSD assumed an average velocity of 30 km/sec and a meteoroid density of 0.44 g/cc. The more recent estimates result in a 22 percent reduction in armor thickness compared with previous estimates. The use of estimates of near Earth environment may be conservative for an outward interplanetary probe mission, since the flux is generally considered to decrease with heliocentric distance. Loeffler, (Reference 2-2), suggests a flux density decreasing at the rate  $(R)^{-1.5}$ , where R is the heliocentric distance. If the flux is integrated between Earth and Jupiter, assuming a constant velocity and an  $(R)^{-1.5}$  relation, the average flux is only 29 percent of the near Earth flux. However, the flux intensities in the asteroid belt and near Jupiter are anomalous, possibly comparable in intensity to the near Earth environment. Estimates of the flux in traversing the asteroid belt vary by an order of magnitude on either side of the near Earth environment, and the near Jupiter environment is as yet unexplored. A study of Jupiter fly-by missions, reported in Reference 2-3, assumes a Jupiter environment three times more severe than Earth's. Volkoff, (Reference 2-4), estimates a protection requirement ratio relative to near Earth of 0.432 for a Jupiter orbit mission based on a time integrated environment. In the absence of reliable experimental data, the more conservative estimates of near Earth environment are used in this study.

A possible advantage of the flat panel radiator that has been suggested is that it can be oriented to take advantage of the directional distribution of the meteoroid flux. In the near Earth environment, the flux is observed to be concentrated in the ecliptic plane. Reference 2-5 has shown that a reduction in armor thickness of up to 45 percent may be possible. However, the assumed anisotropy of the meteoroid flux distribution is based on near Earth observation only. It is not known how the distribution may vary beyond the Earth environment. In this study, no attempt will be made to account for anisotropy of the meteoroid flux.

The conservative assumptions of meteoroid environment, along with the relatively severe nonpenetration probability, have the effect of penalizing the flat panel radiator since it is unable to take advantage of a meteoroid bumper effect.

The damage criteria used in determining meteoroid protection requirements is that proposed by Loeffler, et al (Reference 2-5).

$$t_a = Kay \rho_p^{1/6} \rho_t^{-1/6} V^{2/3} E_t^{-1/3} \left( \frac{\alpha A_v \tau}{-\log_e P(o)} \right)^{1/3\beta} \left( \frac{1}{\beta + 1} \right)^{1/3\beta}$$

where

- $t_a$  = required armor thickness in inches
- $K$  =  $0.231 \text{ in.}^{1/3} \text{ cm}^{1/2} \text{ ft}^{-7/6} \text{ lb}^{1/2} \text{ gm}^{-1/2} \text{ sec}^{2/3}$
- $a$  = damage thickness factor
- $\gamma$  = materials cratering coefficient
- $\rho_p$  = meteoroid density in  $\text{gm/cm}^3$  (0.5)
- $\rho_t$  = armor material density in  $\text{lb/ft}^3$
- $V$  = meteoroid velocity in feet per second (65,500)
- $E_t$  = Young's Modulus of Elasticity at operating temperature in  $\text{lb/in.}^2$
- $\alpha$  =  $5.3 \times 10^{-11}$
- $\beta$  = 1.34

$A_v$  = vulnerable (external surface) area of armor in ft<sup>2</sup>

$\tau$  = mission time in days

$P(o)$  = design probability of no critical damage

The constants  $a$  and  $\gamma$  vary from material to material and with damage mode. The cratering coefficient  $\gamma$  for a wide range of materials has been determined experimentally.

The cratering coefficient for beryllium at 1300°F is taken as 2.28, based on the test data reported in Reference 2-6. The incipient damage factor for beryllium armor with a stainless steel liner as a function of dimple height has not been determined experimentally. However, tests with aluminum armor have shown that with an 0.028 inch thick stainless steel liner, an armor thickness based on a damage factor of 1.75 will limit damage to a dimple in the liner no greater than 20 percent of the liner diameter (Reference 2-7). It is assumed that a similar damage factor can be applied to beryllium armor, since the cratering coefficient should account for any differences in material behavior. In all calculations, the vulnerable area is based on the outside dimensions of the armor, in accordance with the procedure recommended by NASA-Lewis.

The conical radiator gains an advantage over the flat panel radiator in meteoroid protection because of its self shielding effect. Armor thickness on the back side of the tubes can be substantially reduced because of the bumper protection provided by the fins. A bumper factor of 0.25 has been suggested by Lieblein as being appropriate to the offset tube configuration conceived for SNAP-8 radiators. This value may be conservative for other configurations, since test data has shown bumper factors as low as 0.20 may be possible. Reference 2-8 presents typical test data substantiating this factor. The bumper relation used at GE-MSD for radiator analysis is a function of the ratio of bumper thickness to armor thickness. For the offset tube fin configurations analyzed in this study, the bumper factor was found to be in the range 0.214 to 0.243.

## 2.4 STRUCTURAL CRITERIA

In Task A of this study it was shown that the launch conditions which result in critical loads on the payload are the maximum " $q \alpha$ " condition and the maximum axial acceleration condition. Maximum bending loads occur when the product of dynamic pressure

and angle of attack reach a maximum, and the maximum axial loads occur at the instant of first stage engine cut off. For a load bearing radiator, the maximum " $q \alpha$ " condition loads as shown in Figures 2-7 and 2-8 are used for design. The launch structure which supports the non-load bearing radiator, however, is covered by an aerodynamic shroud so that it is subjected to inertia loads only. The condition used to design this structure is an axial acceleration of 4.7g limit.

If the launch structure were designed to an axial load condition only, an unrealistic result would be obtained, since it is obvious that the structure must also have some lateral stiffness. A difficulty arises in attempting to specify a realistic load condition for lateral stiffness since it is known that static lateral accelerations during launch are generally low. One approach is to design to an artificial but conservative condition such as 12g axial combined with 5g lateral, which will certainly envelope all possible load conditions including response to dynamic excitation. This approach is reasonable for small payloads, but excessively conservative for a payload whose size and mass are no longer insignificant compared with the launch vehicle. The load factors must decrease as the payload size increases, as evidenced by the trend shown in Figure 2-9. The proper approach, which is

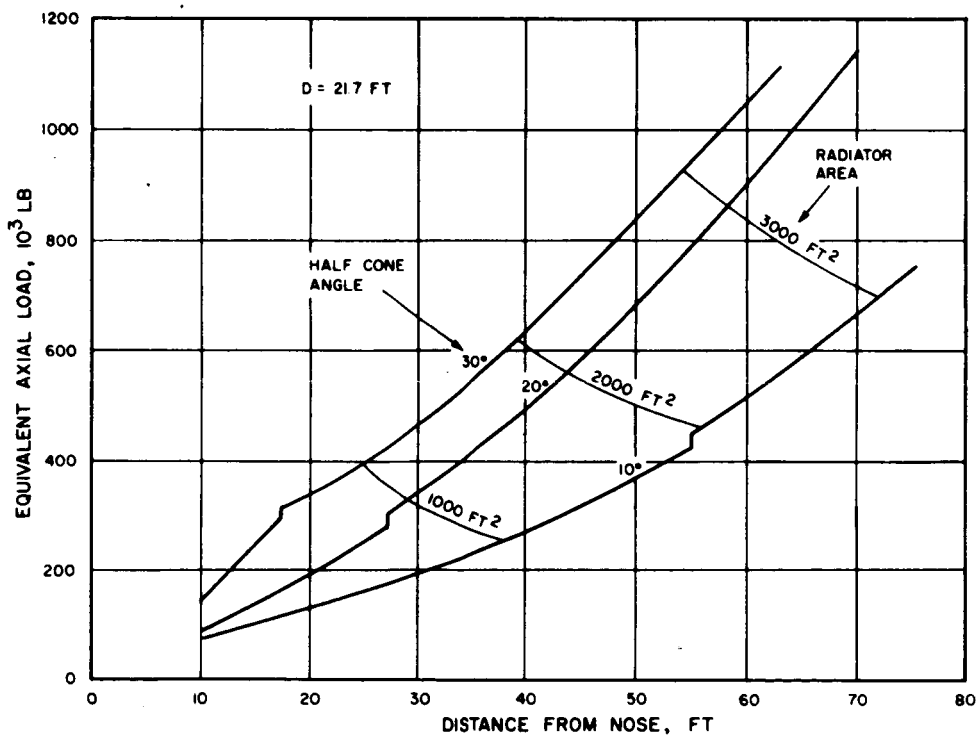


Figure 2-7. Launch Loads on Radiator for Three-Stage Saturn V

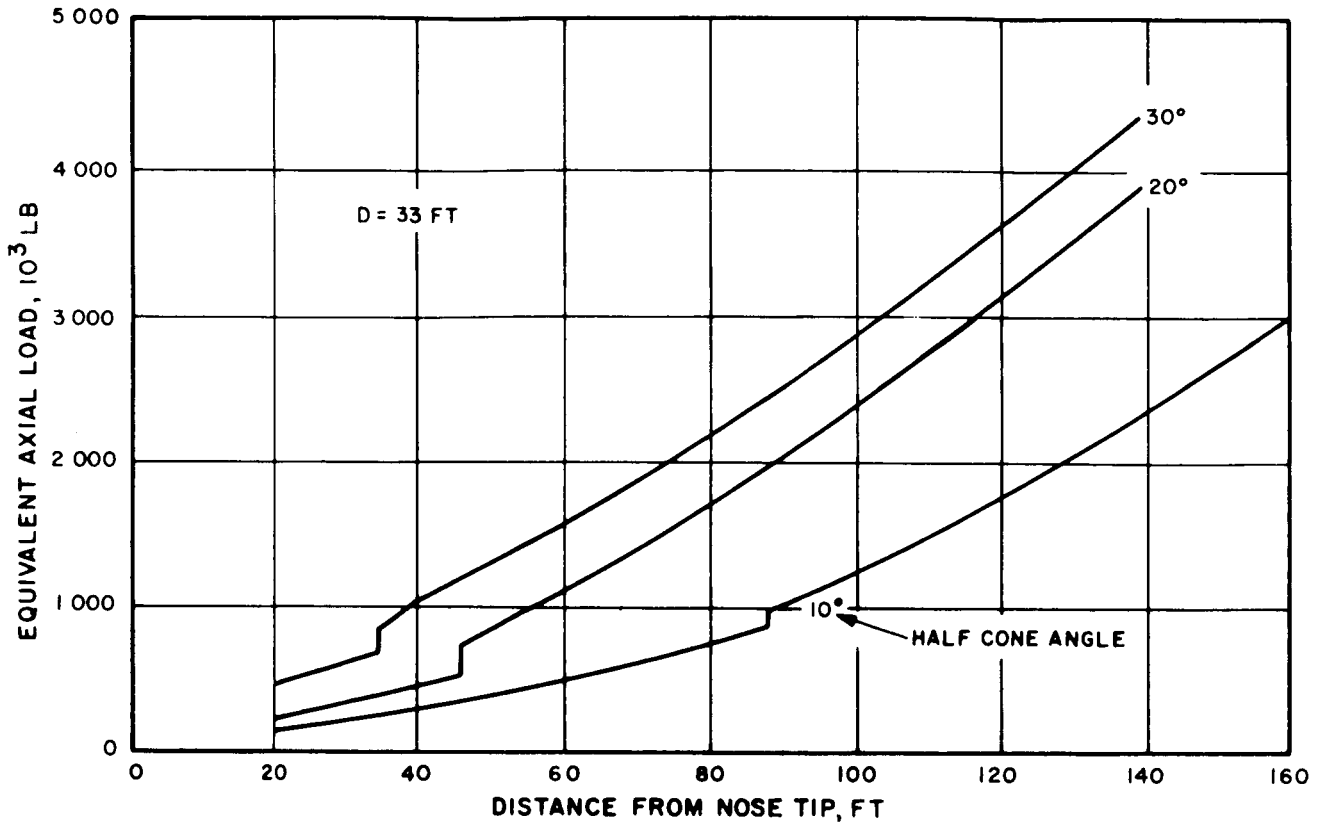


Figure 2-8. Launch Loads on Radiator for Two-Stage Saturn V

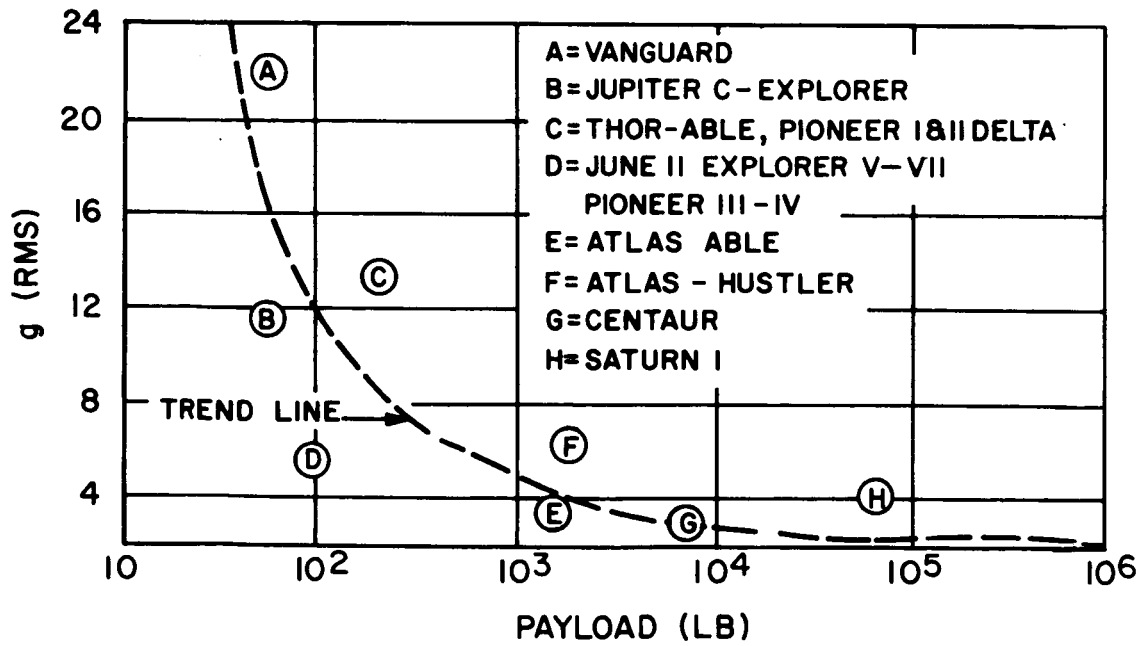


Figure 2-9. Trend in Launch Vehicle Dynamic Loads

beyond the scope of this study, is to analyze the combined dynamics of the payload and launch vehicle during launch. A simple approach to the problem can be made, however, by comparison with the dynamics of the Apollo spacecraft payload on the Saturn V launch vehicle, a combination which has been analyzed in detail. The Apollo payload and S-IVB stage together have a natural frequency in the free-free bending mode of 4.04 cps, while the entire launch vehicle has a natural frequency of 1.0 cps. If a payload launched by the two-stage Saturn V has a natural frequency less than 4.04 cps, the natural frequency of the entire launch vehicle will be reduced. The natural frequencies can be related by Dunkerley's equation (Reference 2-9).

$$\left(\frac{1}{f_{SV}}\right)^2 = \left(\frac{1}{f_{SI}}\right)^2 + \left(\frac{1}{f_{SII}}\right)^2 + \left(\frac{1}{f_P}\right)^2$$

where

$f_{SV}$  = natural frequency of the Saturn V launch vehicle

$f_{SI}$  = natural frequency of the S-IC stage

$f_{SII}$  = natural frequency of the S-II stage

$f_P$  = natural frequency of the payload

Figure 2-10 shows the effect of the payload stiffness on the overall vehicle stiffness, based on this approximation. The consequences of a reduced overall stiffness on the launch vehicle attitude control system are not easily assessed without a detailed dynamic analysis. To maintain the same trajectory accuracy with a more flexible vehicle, increased gimbal angles and rates may be required, which could cause excessive bending loads on the lower stages of the launch vehicle. When the payload is enclosed by an aerodynamic shroud, lack of stiffness in the payload structure will mean a requirement for additional clearance between the payload and shroud to accommodate larger deflections. It is apparent that a desirable criteria for lateral stiffness of the payload structure on the two-stage Saturn V is that the natural frequency be no less than 4.04 cps, so that the entire launch vehicle stiffness is no worse than that for which the Saturn V is presently designed; 1 cps in the first bending mode. The same criteria applied to the three-stage Saturn V would require that the natural frequency of the payload structure, together with the S-IVB stage, be no

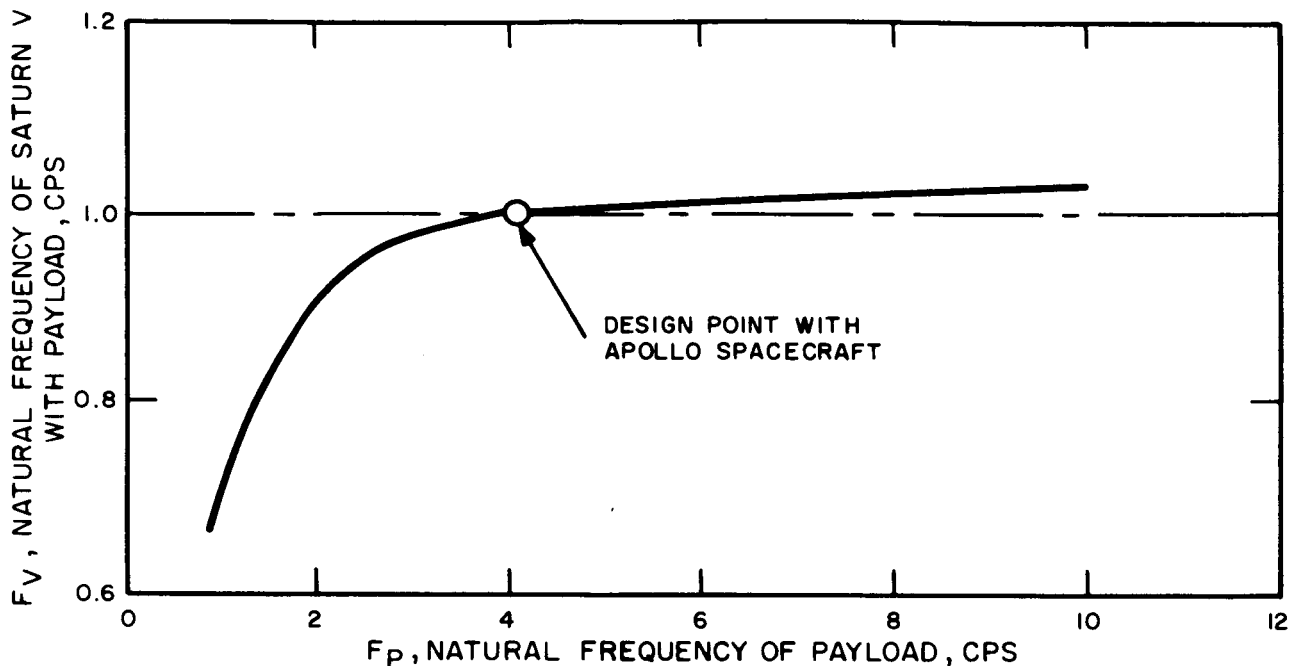


Figure 2-10. Effect of Payload Stiffness on the Natural Frequency of the Combined Launch Vehicle

less than 4.04 cps, in the first bending mode, or 4.13 cps for the payload alone. As will be shown later, this criteria is more critical for design of the structure used with the non-load bearing radiator than the axial load condition.

An additional stiffness criteria for the structure used with the non-load bearing radiator must be met during electric propulsion thrusting, after the launch structure has been ejected. In this configuration, the spacecraft has a greatly reduced bending stiffness in the plane of the flat panel radiator. If the stiffness is too low, large deflections during attitude control maneuvers may prevent achieving the pointing accuracy required for communications and scientific measurements. A low natural frequency in this bending mode may also restrict the choice of attitude control limit cycle in order to prevent resonance. Without defining the attitude control system, it is not possible to establish this stiffness criteria quantitatively. However, the need for stiffness in this part of the structure (the flight structure) is recognized in the structural design.

## 2.5 REFERENCES

- 2-1. Cockfield, R. D. , "Definition of Spacecraft and Radiator Interrelations for Nuclear Rankine Systems," NASA CR-72245, January 26, 1967.
- 2-2. Loeffler, I. J. , N. Clough, and S. Lieblein, "Recent Developments in Space Power System Meteoroid Protection," AIAA Paper No. 64-759, September, 1964.
- 2-3. - - - - - , "A Study of Jupiter Flyby Missions," General Dynamics Report FZM-4625, May 17, 1966.
- 2-4. Volkoff, J. J. , "Protection Requirements for the Resistance of Meteoroid Penetration Damage of Interplanetary Spacecraft Systems," JPL Technical Report No. 32-410, July 1, 1964.
- 2-5. Loeffler, I. J. , S. Lieblein, and N. Clough, "Meteoroid Protection for Space Radiators," In "Progress in Astronautics and Aeronautics, Vol II, Power Systems for Space Flight," Academic Press, New York, 1963.
- 2-6. Diedrich, J. H. , I. J. Loeffler, and A. R. McMillan, "Hypervelocity Impact Damage Characteristics in Beryllium and Graphite Plates and Tubes," NASA TN D-3018, September, 1965.
- 2-7. Clough, N. and J. H. Diedrich, "Results of Hypervelocity Impacts into Space Radiator Materials," In CONF - 651026, "AIAA Specialists Conference on Rankine Space Power Systems, Volume 1," October, 1965.
- 2-8. Posever, F. C. , F. L. Fish, and C. N. Scully, "An Evaluation of Impact on Meteoroid Shielding Configurations for Velocities up to 60,000 Feet Per Second" AIAA Fifth Annual Structures and Materials Conference, April 1964.
- 2-9. Den Hartog, J. P. , "Mechanical Vibrations" McGraw-Hill Book Company, New York, 1940.

## 3. NON-LOAD BEARING RADIATOR

### 3.1 SPACECRAFT DESCRIPTION

The non-load bearing radiators defined for the comparison made in this study are flat panel configurations. The spacecraft concept employing a non-load bearing radiator for a 300 kWe powerplant, launched on a three-stage Saturn V, is shown in Figure 3-1. Figure 3-2 shows a similar concept with a 1200 kWe powerplant, launched on a two-stage Saturn V. In each case, the radiator fits within a fairing envelope defined by a 10-degree half-cone angle and an overall length that is limited by the structural capability of the launch vehicle. Clearances between the inside of the aerodynamic fairing and the powerplant are shown, based on an estimate of the relative deflections that will occur during launch.

The powerplant is mounted above a section which houses all other spacecraft systems: electric propulsion, communications, guidance and control, and scientific instrumentation. For the purposes of the comparison made in this study, this payload section is largely undefined. It is apparent, however, that payload volume will be limited because of the flat panel radiator configuration. For this reason, an envelope is shown extending below the launch vehicle interface, into the unoccupied volume of the Instrument Unit.

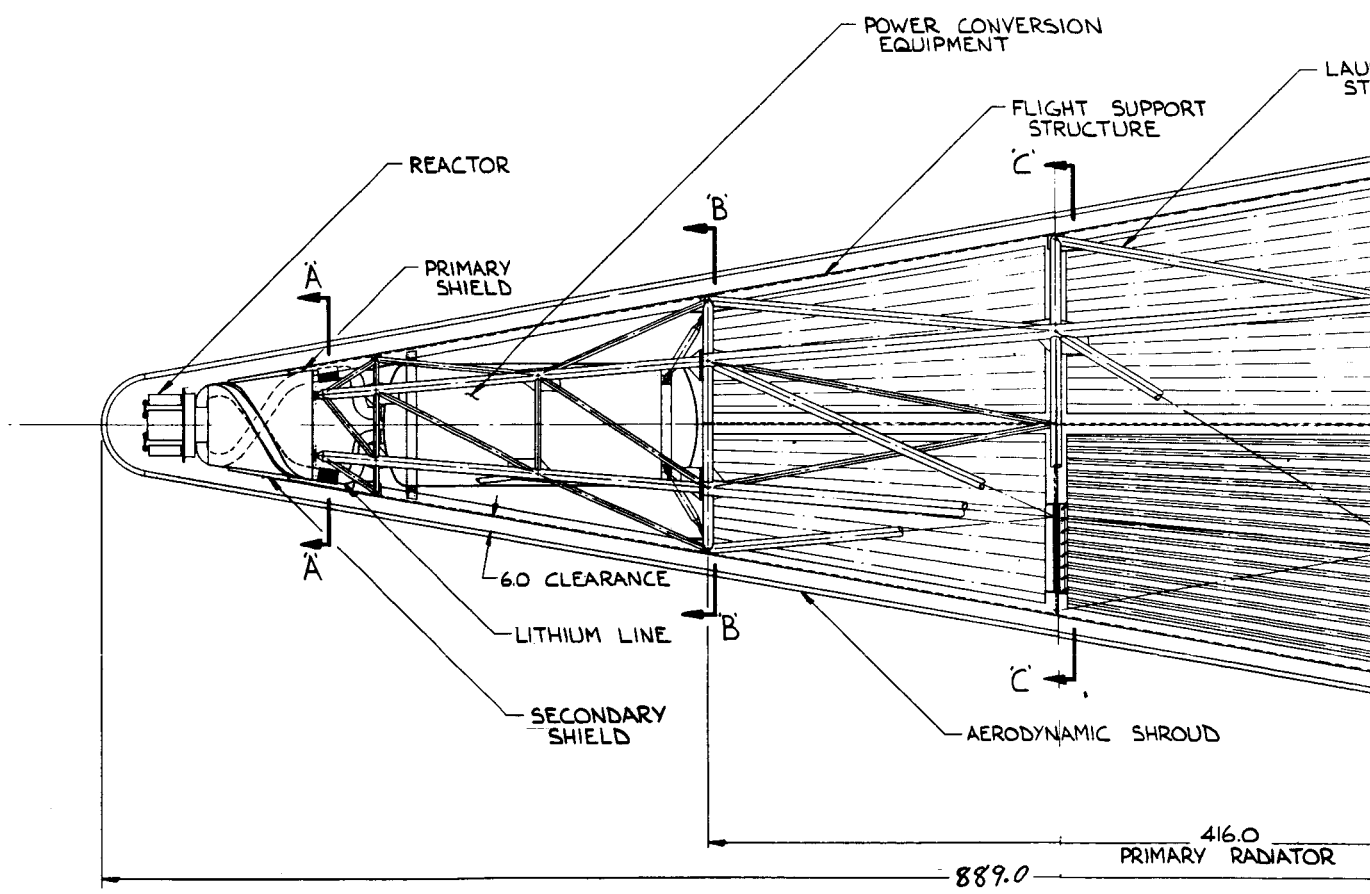
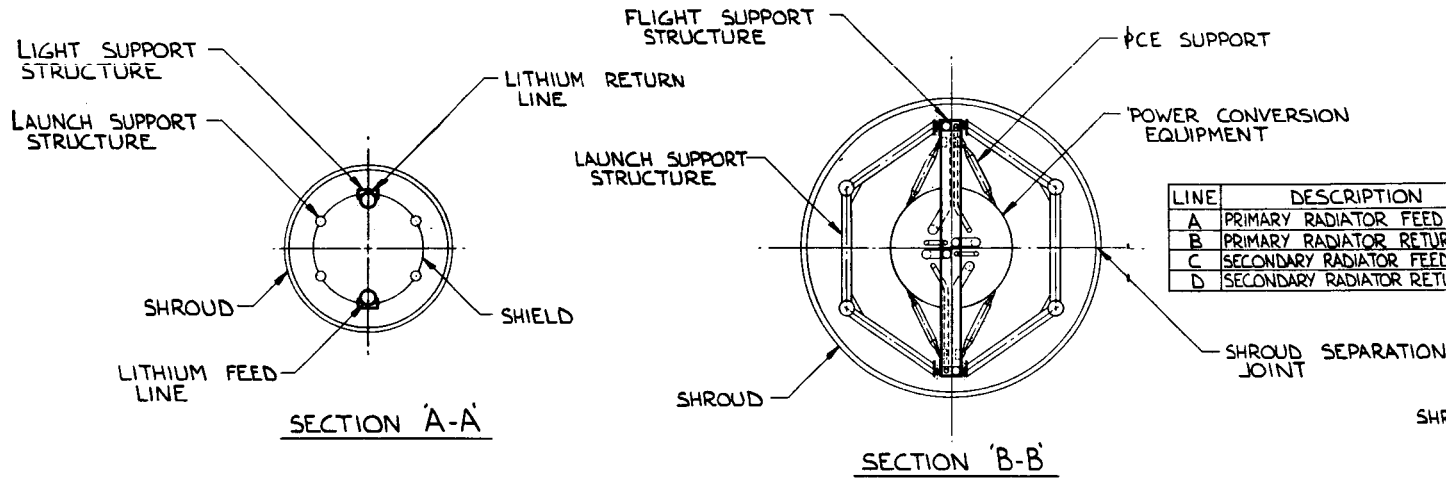
The reactor and shield of the powerplant are located at the nose of the spacecraft, and the power conversion unit is located immediately aft of the shield. The power conversion equipment is shown as a sealed container. This concept has several advantages for unmanned missions where component access is not required. The container permits a controlled inert atmosphere for all components and provides meteoroid protection. Assembly and integration with the remainder of the powerplant are also greatly simplified.

The parameters defining the flat panel radiators, as determined from the optimization process of the SPARTAN III computer code, are listed in Table 3-1 for the 300 kWe powerplant and in Table 3-2 for the 1200 kWe powerplant. The meteoroid protection requirements are predominant in determining the weight of the radiator. This is illustrated by the full size views of tube cross sections for the primary radiator on the 1200 kWe spacecraft, shown in Figure 3-3. The armor accounts for 65 percent of the total radiator weight at the highest survival probability.

TABLE 3-1. FLAT PANEL RADIATOR PARAMETERS  
FOR 300 kWe POWERPLANT

PARAMETERS		PRIMARY	SECONDARY
Heat Rejected	(kW)	2460	480
Area	(ft <sup>2</sup> )	460	325
Radiator Wt	(lb)	3589	1281
Inlet Temp	(°F)	1300	850
* Fluid ΔT in Rad	(°F)	110	150
No. of Panels		6	4
* No. of Tubes/Panel	(Average)	15	17
* Tube ID	(in.)	0.61	0.35
Tube Length	(ft)	11.05	8.18
Average Header Length	(ft)	6.6	9.5
* Header ID	(in.)	3.341	2.041
* Fin Thickness	(in.)	0.125	0.080
Fin Length	(in.)	1.624	2.647
Fin Efficiency	(%)	69.9	64.1
Tube Armor Thk	(in.)	0.683	0.503
* Basic Feed Line ID	(in.)	2.2	1.3
Radiator ΔP	(psi)	3.812	4.989
Feed Line ΔP	(psi)	2.848	8.765
Feed Line Wt	(wet, lb)	402.5	257.3
Coolant Flow Rate	(lb/sec)	99.07	24.87
Hydraulic Pump Power	(kW)	2.908	1.452

\* Optimized Variables



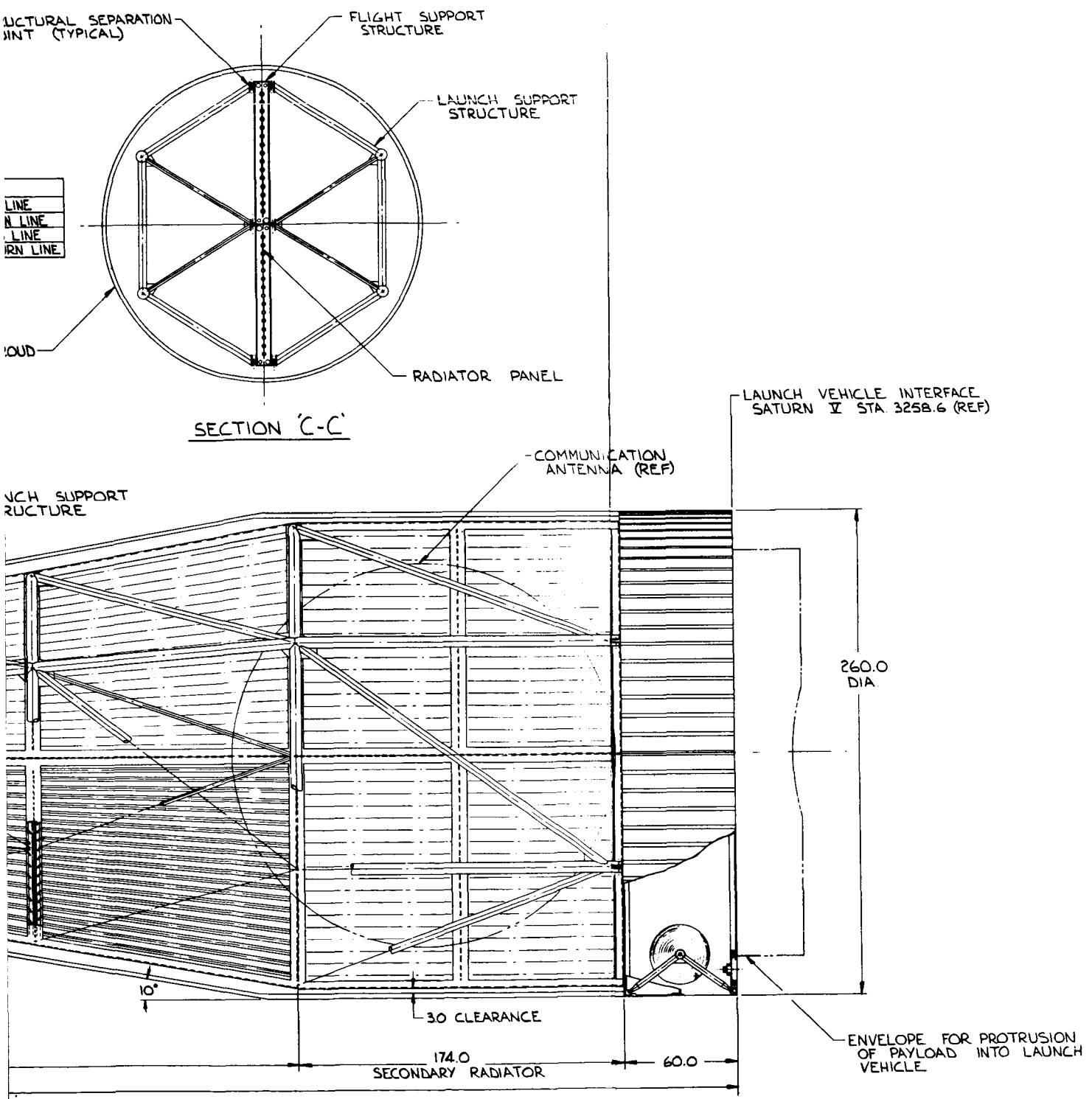
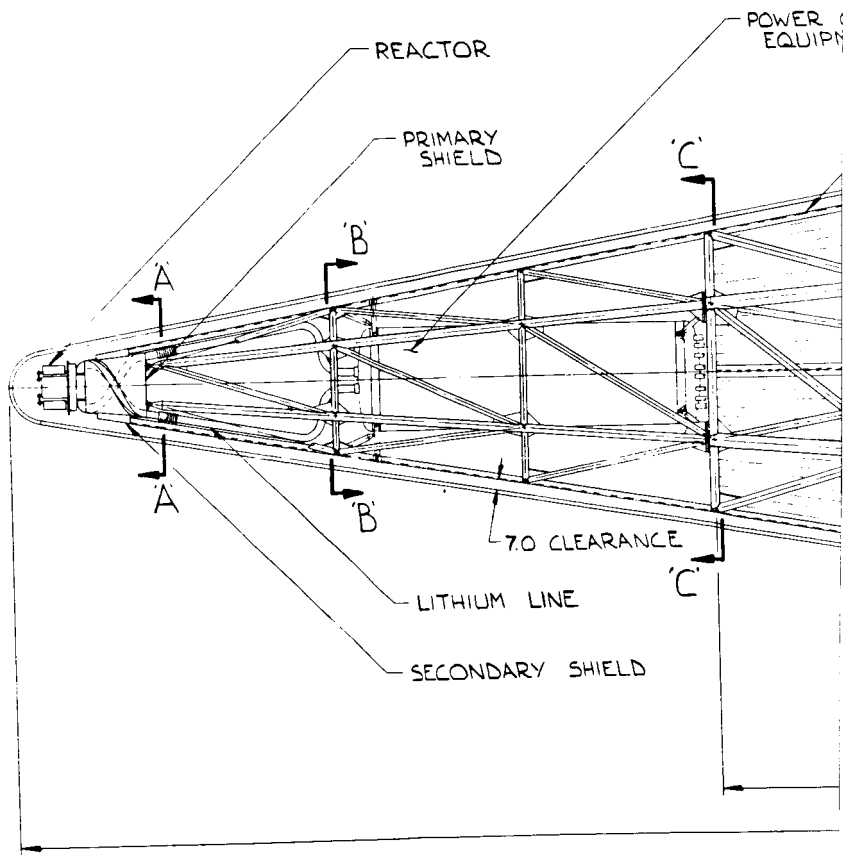
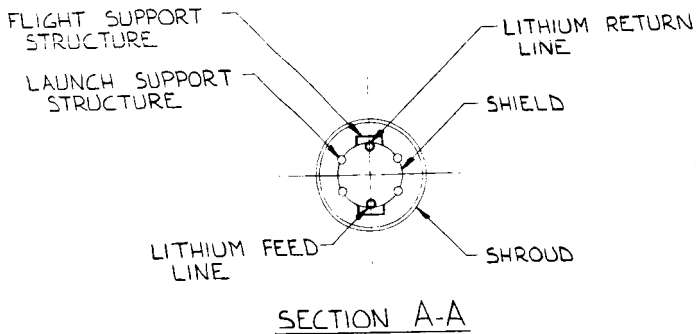
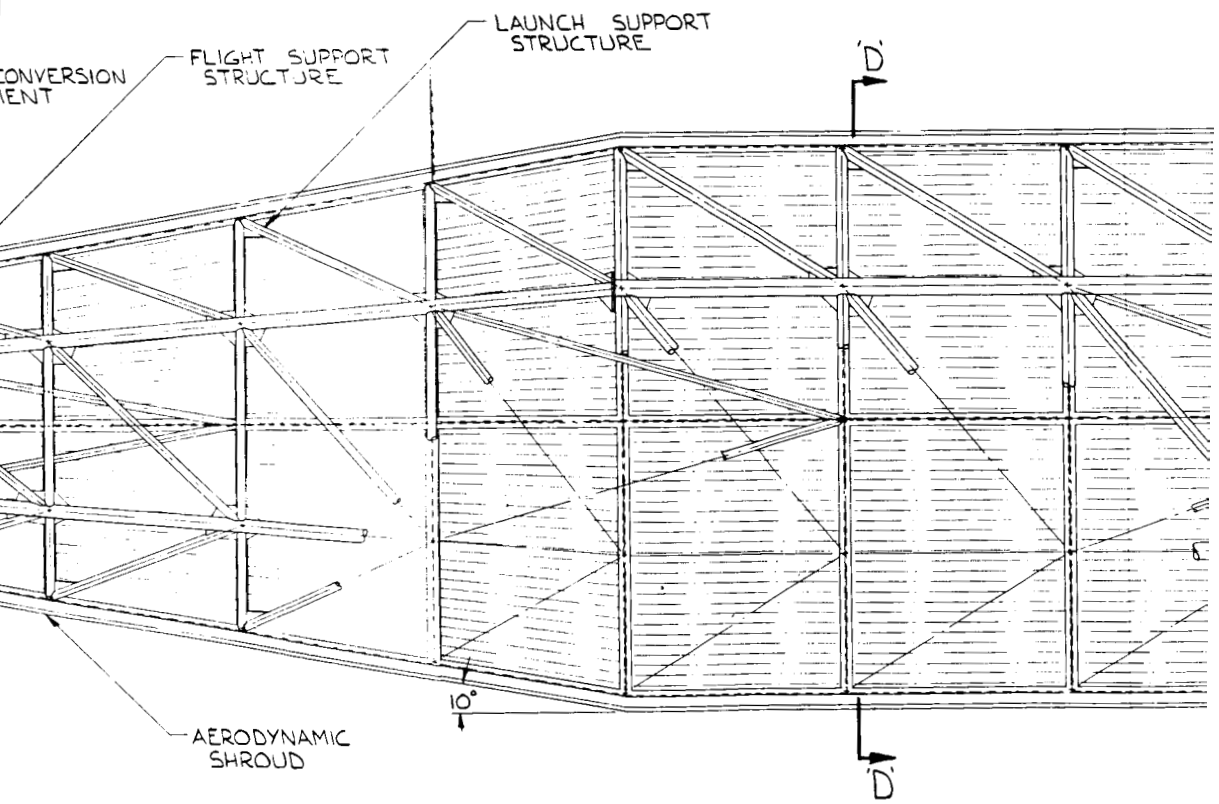
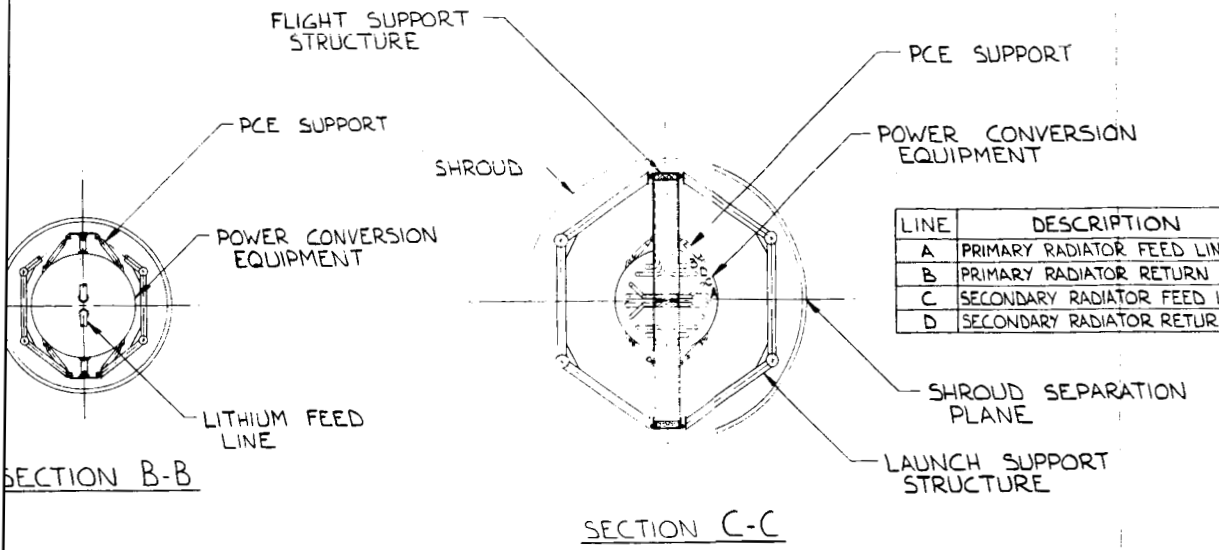


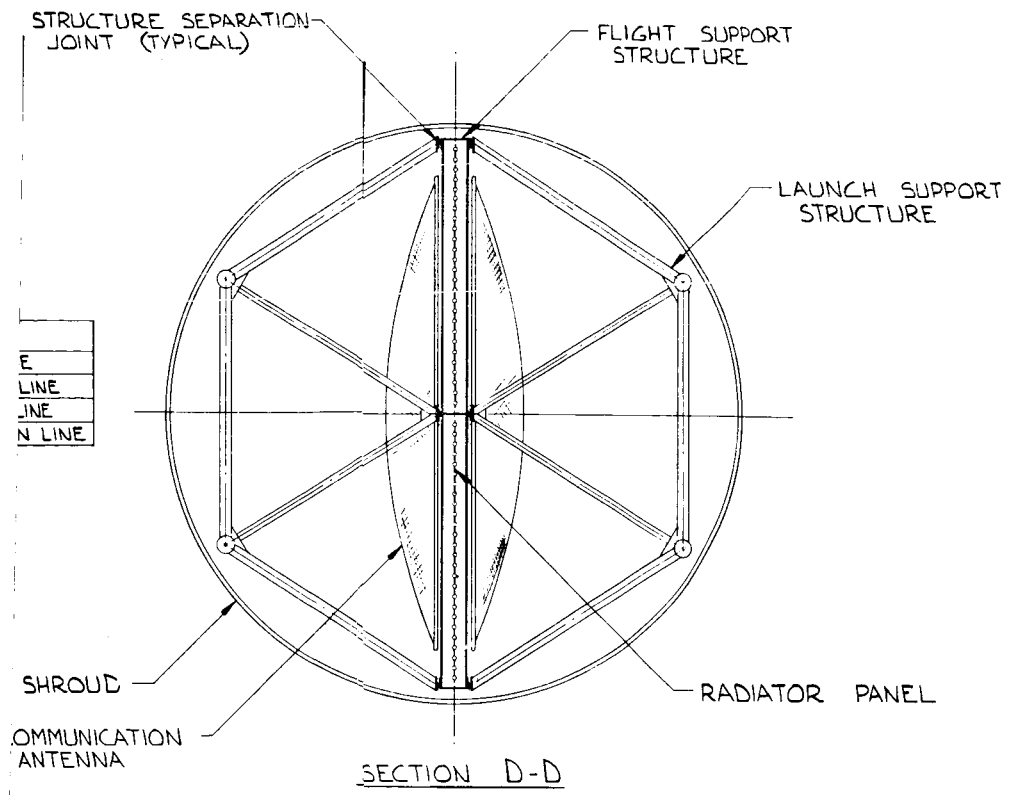
Figure 3-1. Spacecraft Concept for 300 kW Powerplant with Flat Panel Radiator





9800  
PRIMARY RADIATOR

1908.0



LAUNCH VEHICLE INTERFACE  
SATURN V STA 2555.0 (REF)

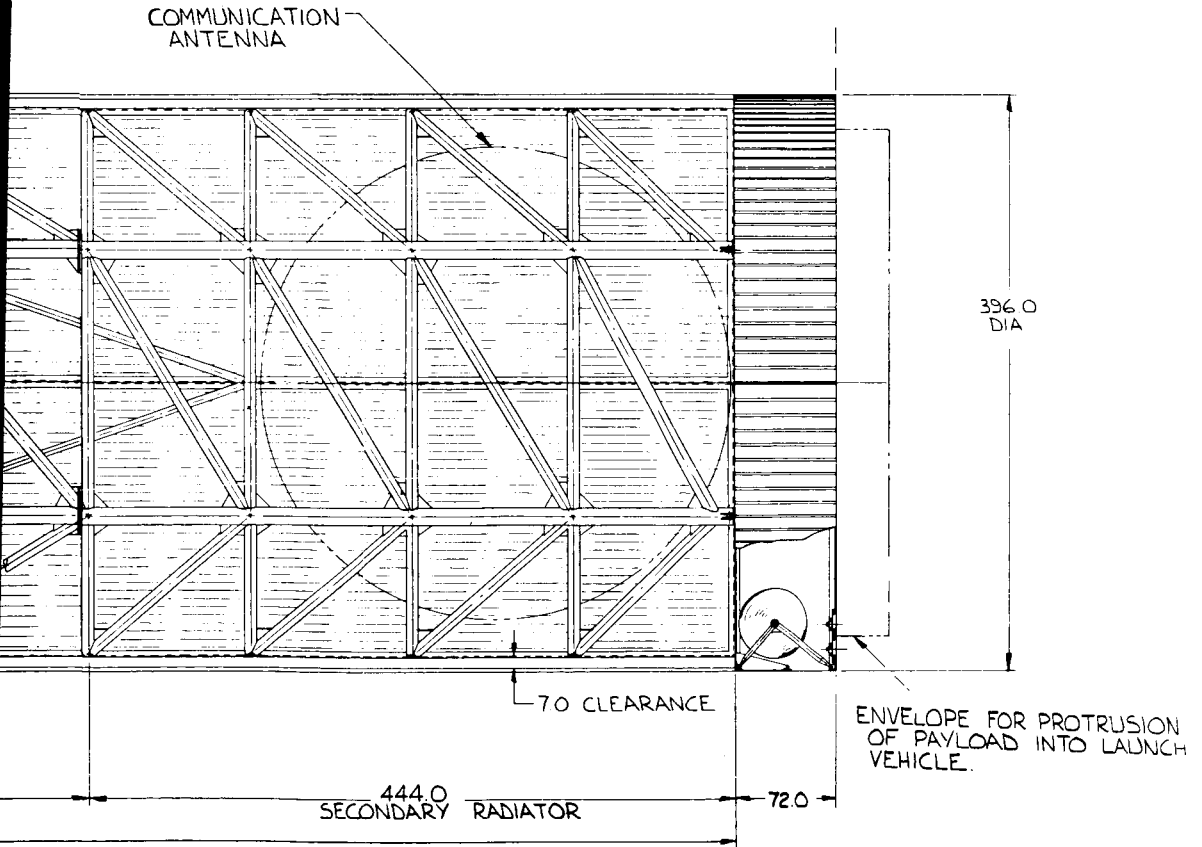
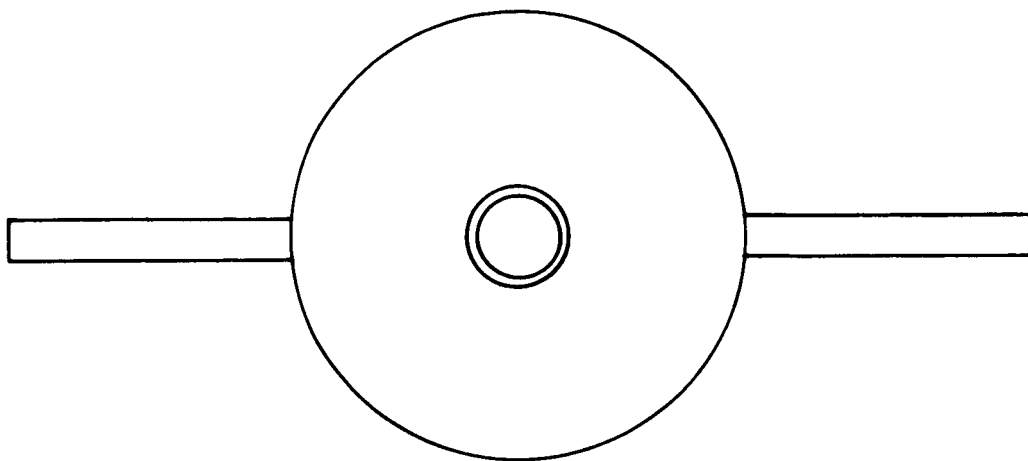


Figure 3-2. Spacecraft Concept for 1200 kW Powerplant with Flat Panel Radiator

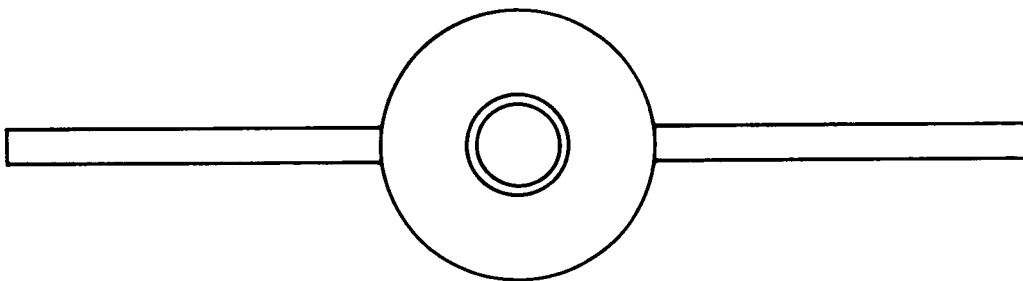
TABLE 3-2. FLAT PANEL RADIATOR PARAMETERS  
FOR 1200 kWe POWERPLANT

PARAMETER		PRIMARY	SECONDARY
Heat Rejected	(kW)	9,840	1,920
Area	(ft <sup>2</sup> )	2,070	1,070
Radiator Wt	(lb)	21,335	8,897
Inlet Temp	(°F)	1,300	850
* Fluid $\Delta T$ in Rad	(°F)	160	150
No. of Panels		14	8
* No. of Tubes/Panel	(Average)	22	32
* Tube ID	(in.)	0.56	0.325
Tube Length	(ft)	10.93	8.48
Average Header Length	(ft)	12.8	15.0
* Header ID	(in.)	3.715	2.6
* Fin Thickness	(in.)	0.24	0.145
Fin Length	(in.)	2.18	1.84
Fin Efficiency	(%)	72.4	84.8
Tube Armor Thk	(in.)	1.003	0.782
* Basic Feed Line ID	(in.)	2.5	1.9
Radiator $\Delta P$	(psi)	3.708	8.04
Feed Line $\Delta P$	(psi)	3.936	11.44
Feed Line Wt	(wet, lb)	2,364	2,141
Coolant Flow Rate	(lb/sec)	272.4	99.46
Hydraulic Pump Power	(kW)	9.177	8.225

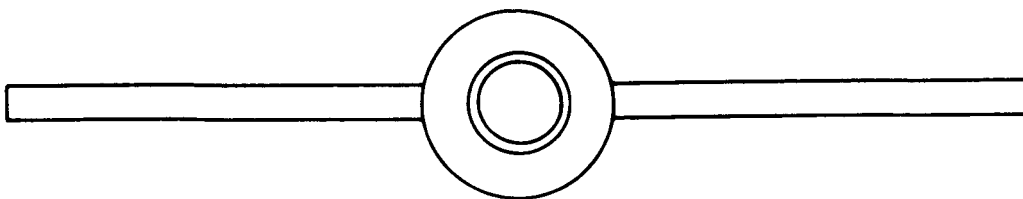
\* Optimized Variables



Po = 0.999



Po = 0.99



Po = 0.9

Figure 3-3. Tube Cross-Sections for Primary Radiator  
on 1200 kWe Spacecraft

It may be noted that the tube inside diameter does not change significantly with changes in the meteoroid survival probability. When the armor thickness is large, changes in the tube diameter have a relatively small effect on the tube exterior circumference. Since the vulnerable area is based on the outside surface area of the tube, the corresponding armor weight is relatively insensitive to changes in the inside tube diameter. At the lower survival probability, when the armor thickness is not large, pump power penalty has a stronger influence on tube diameter than the meteoroid protection requirements.

Compared with the conical configuration, the flat panel radiator has a relatively large tube diameter as a result of rejecting heat from both fin surfaces rather than one. This difference is amplified by the longer feed lines of the flat panel radiator which strengthens the influence of the pump power penalty. The relative influence of the meteoroid protection requirements is shown in Figure 3-4 where the weights of the flat panel and conical radiators are compared. It should be noted that the differences are small, amounting to three to six percent over the whole range of probabilities shown.

The flat panel radiator is supported by a structural frame which, together with disposable truss frames, forms the launch structure of the spacecraft. The structural frame and the truss frames have bay lengths determined by the radiator panel sizes, which in turn were selected to approximate the optimum tube length. The dimensions of the frame members surrounding each panel were chosen to satisfy the requirements of the radiator and not the structural loads. Open sections were used to facilitate the installation of feed lines and headers, with inside dimensions suited to the sizes of tubing to be accommodated.

The thickness of these members was determined by the meteoroid protection requirements, assuming a bumpered reduction factor. The structural capability of these members was found to be consistent with the overall launch structure requirements. The reactor and shield, and the power conversion equipment are supported by the radiator frame structure in such a manner, that when the disposable truss frames are removed, the frame becomes the entire spacecraft structure. This occurs during the mission only after all high thrust propulsion is completed. Hence the frame is also designated as the "flight structure."

Figure 3-5 shows the separation sequence for the 1200 kWe spacecraft, from launch (1) to escape (8). The aerodynamic fairing is ejected (2) early in the trajectory, as soon as

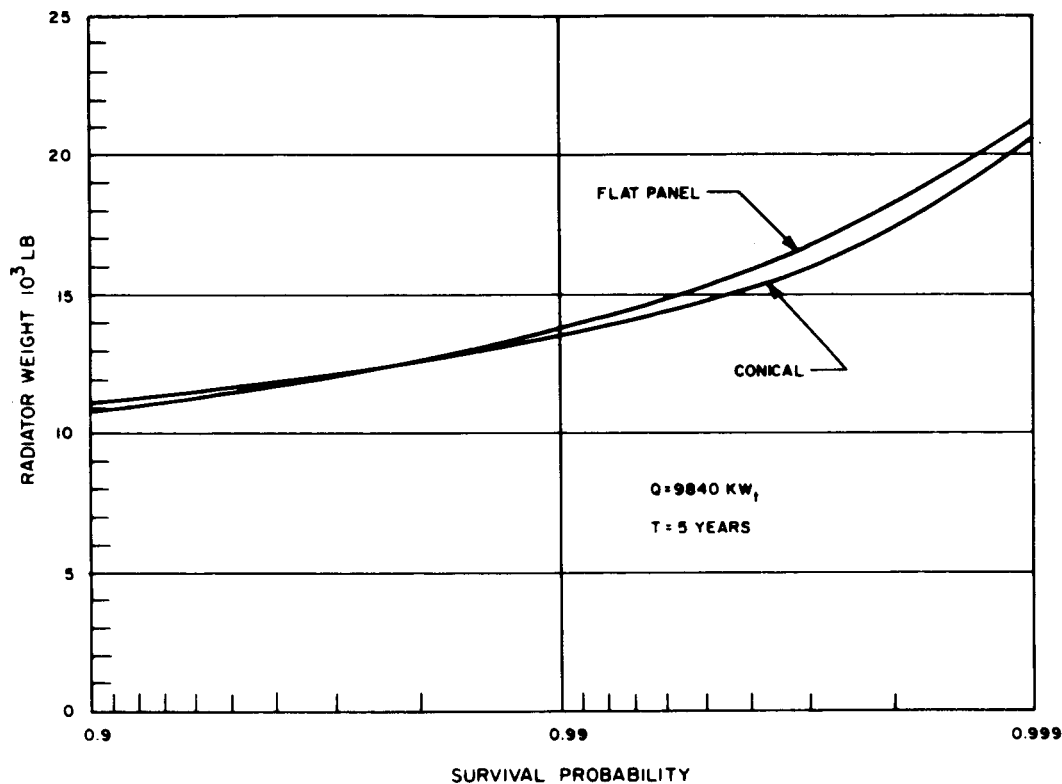


Figure 3-4. Weight Comparison for Flat Panel and Conical Radiator Configuration

aerodynamic loads are no longer significant, e.g., 200,000 ft. The S-IC stage carries the payload to 593,000 feet before separating (3), along with the adapter section (4) joining the S-IC and S-II stages. The S-II places the spacecraft in a parking orbit before separating (5). The disposable structure can then be separated (6) before the nuclear powerplant is started and all systems checked out (7). Electric propulsion thrusting (8) would then carry the spacecraft to beyond escape. A similar sequence would be used for the 300 kWe spacecraft, except that electric propulsion thrusting would not begin until the S-IVB had boosted the spacecraft beyond escape.

Support of the radiator panels within the structure frame is accomplished by means which preclude structural loads from being introduced into the radiator. If the radiator were rigidly supported, bending deflections in the plane of the radiator would load the radiator panels as the shear web in a beam. In addition, relative thermal expansion will occur as the radiator temperature increases from the launch condition to operating temperature. These relative displacements would be particularly severe if a material other than beryllium were used for the flight structure. The solution shown is to clamp the radiator panels at the edges by fittings attached through oversize holes. The clamping force is light enough so that excessive in-plane load will overcome friction and permit sliding.

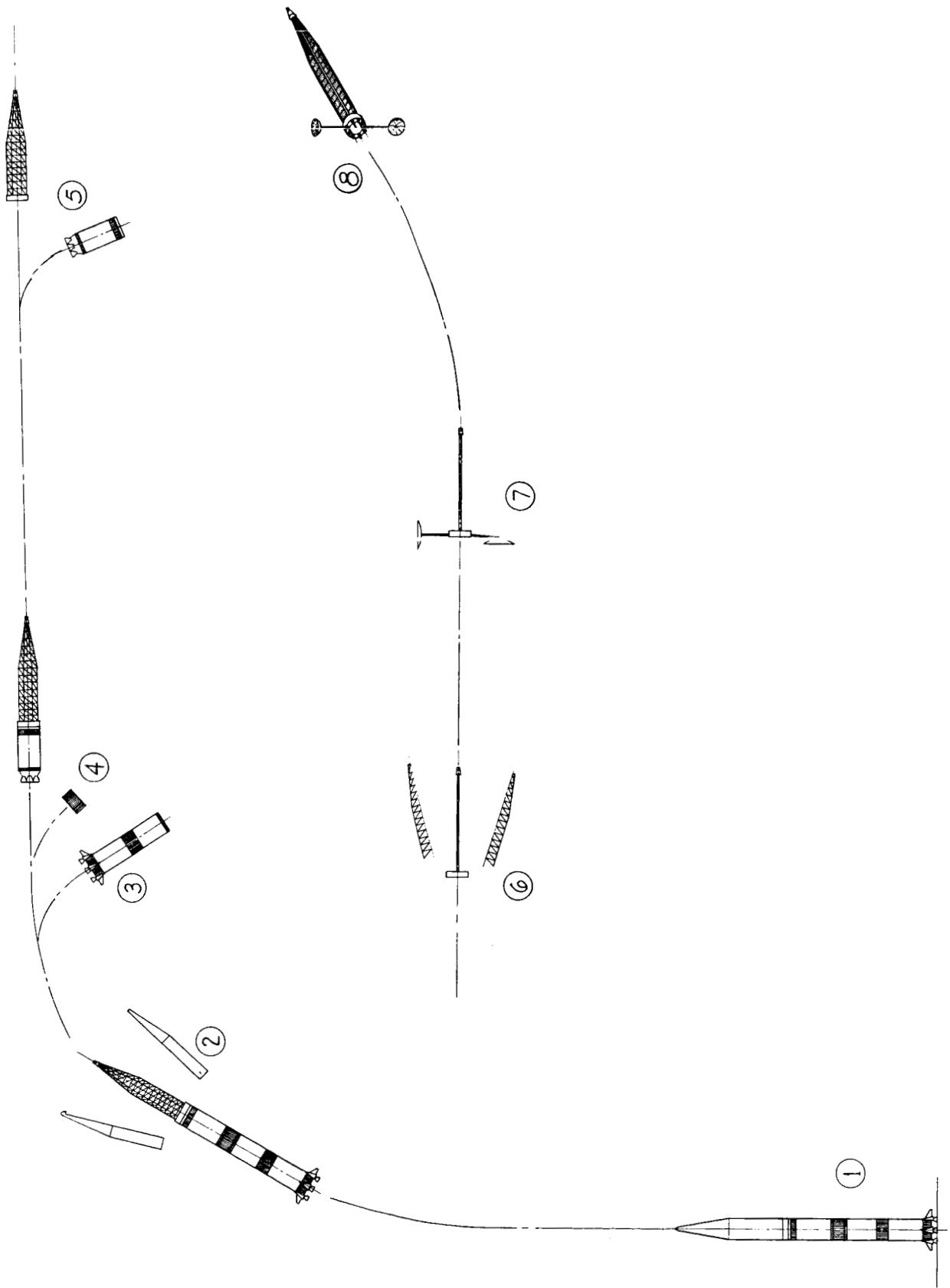


Figure 3-5. Separation Sequence for 200 kW Spacecraft

Support for the power conversion equipment is shown in Figure 3-6. Primary support fittings are located at the forward end, attached directly to the axial members of the flight structure. Lateral support is supplemented by struts at the aft end. The disposable launch structure attaches to the flight structure at fittings close to power conversion equipment supports in order to distribute the lateral loads with a minimum of bending in the flight structure.

The disposable part of the launch structure consists of two truss frames that attach to the flight structure through pyrotechnic release devices. As shown in Figure 3-7, these devices are explosively actuated pin pullers in a clevis fitting. Twenty-eight such attachments are required for the 300 kWe spacecraft and 62 for the 1200 kWe spacecraft. To enhance reliability, redundant squibs are used on each pin puller. The joint between the truss frame and the payload structure at the base of the powerplant must also be separated. A concept for this joint is shown in Figure 3-8. The vertical truss members are severed by a linear shaped charge, similar to that used for stage separation. The truss frames are then free to rotate about the "fly away" hinges shown in Figure 3-8. Positive separation is ensured by actuators located just below the shield.

The truss frame assembly is ideally designed as tubular struts with welded cluster joints as shown in Figure 3-9. This presumes a material that can be readily welded, and will retain a high percentage of its strength in the as-welded condition. Beryllium does not meet these requirements with present technology, although it is conceivable that it may in the future. Since beryllium will give the lightest weight launch structure and therefore will establish a lower limit to structural weight, it will be assumed for the purposes of this study, but with reservations on the manufacturing feasibility. A more conservative assumption, consistent with the level of technology assumed throughout the remainder of this study is that beryllium would not be chosen for the launch structure. However, it will be shown later that the material assumed for the launch structure does not alter the conclusions of the comparison between a load bearing and non-load bearing radiator.

Table 3-3 lists the significant mechanical properties of candidate materials for the launch structure at a temperature of 300°F. All the materials listed have acceptable mechanical properties at 1300°F. The outstanding advantage of beryllium for a stiffness limited structure is apparent, as indicated by the ratio  $E/\rho$ . Of the more conventional materials, Inconel X-750 is the best suited to fabrication of a large welded structure and would represent a choice made on the basis of present materials technology.

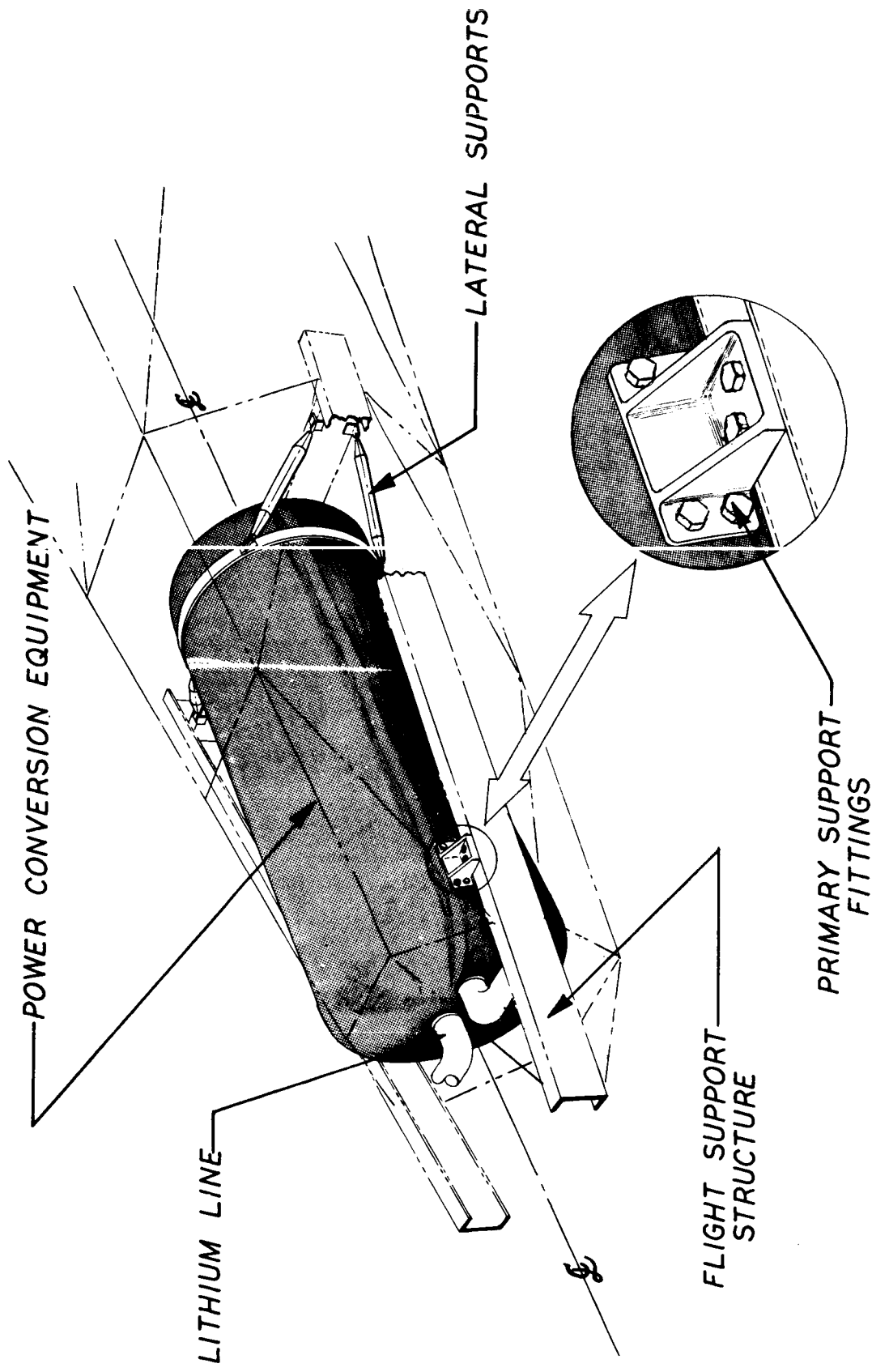


Figure 3-6. Support Structure for Power Conversion Equipment

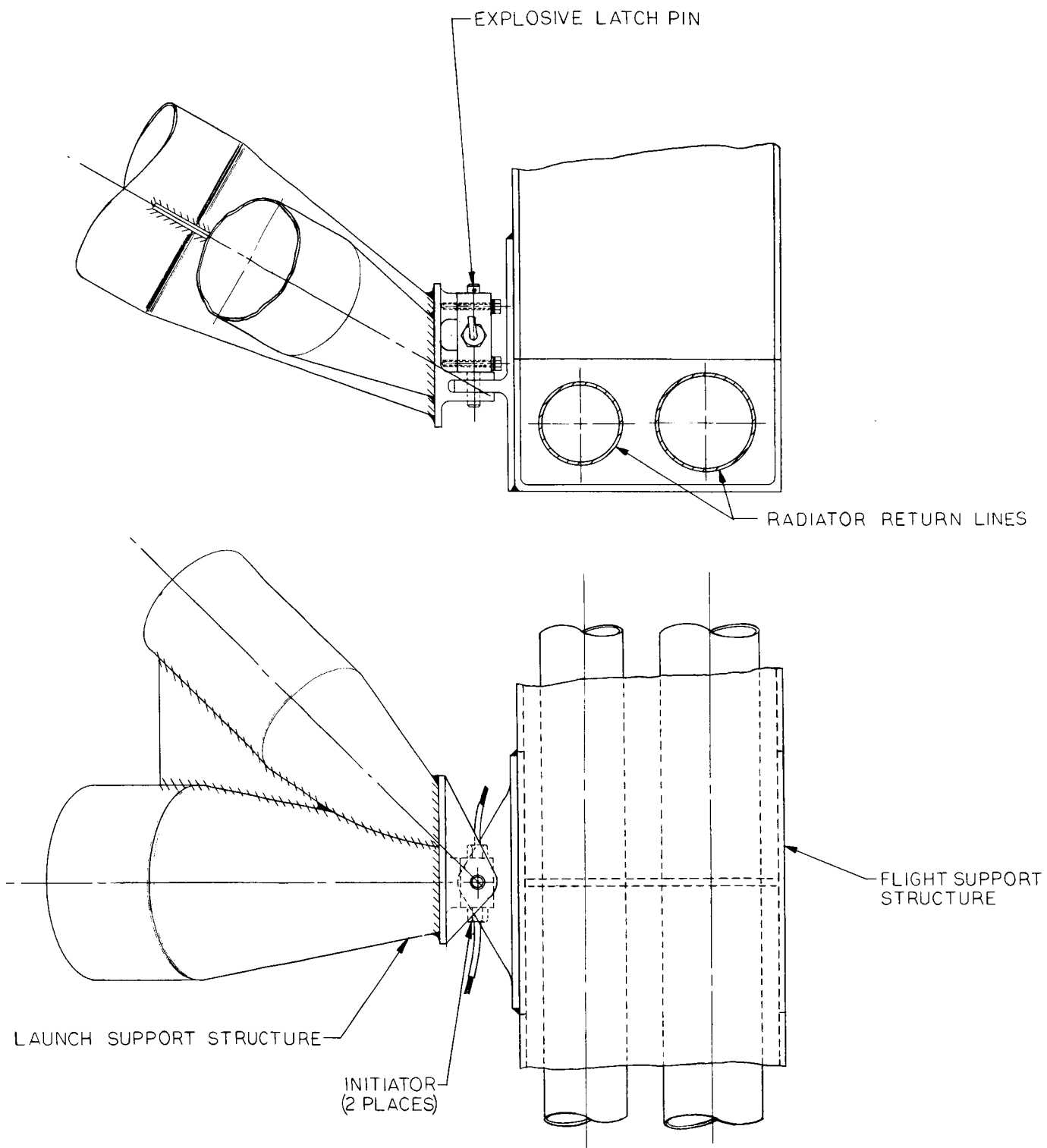


Figure 3-7. Detail of Launch Structure Separation Device

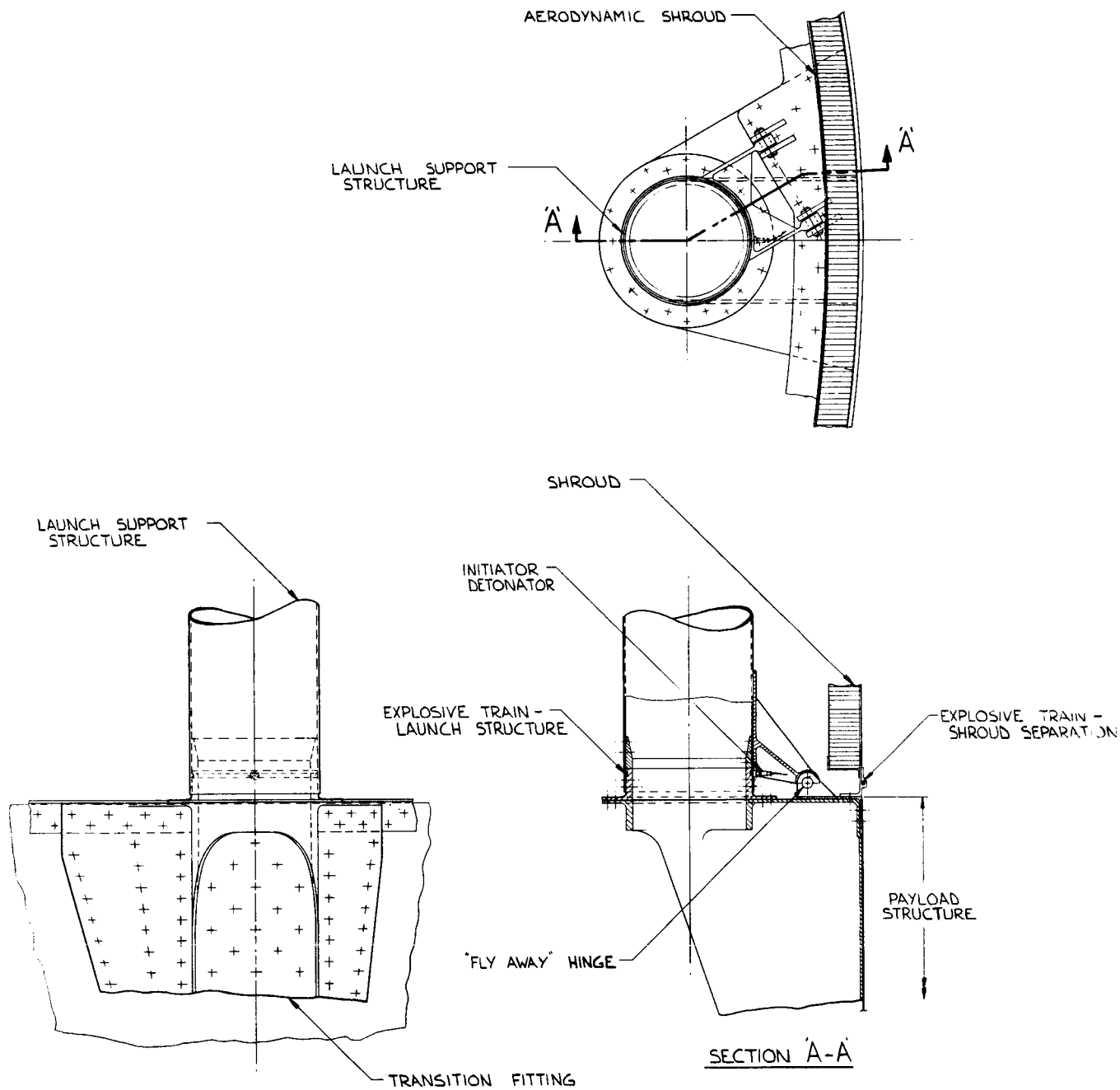


Figure 3-8. Detail of Launch Structure to Payload Structure Joint

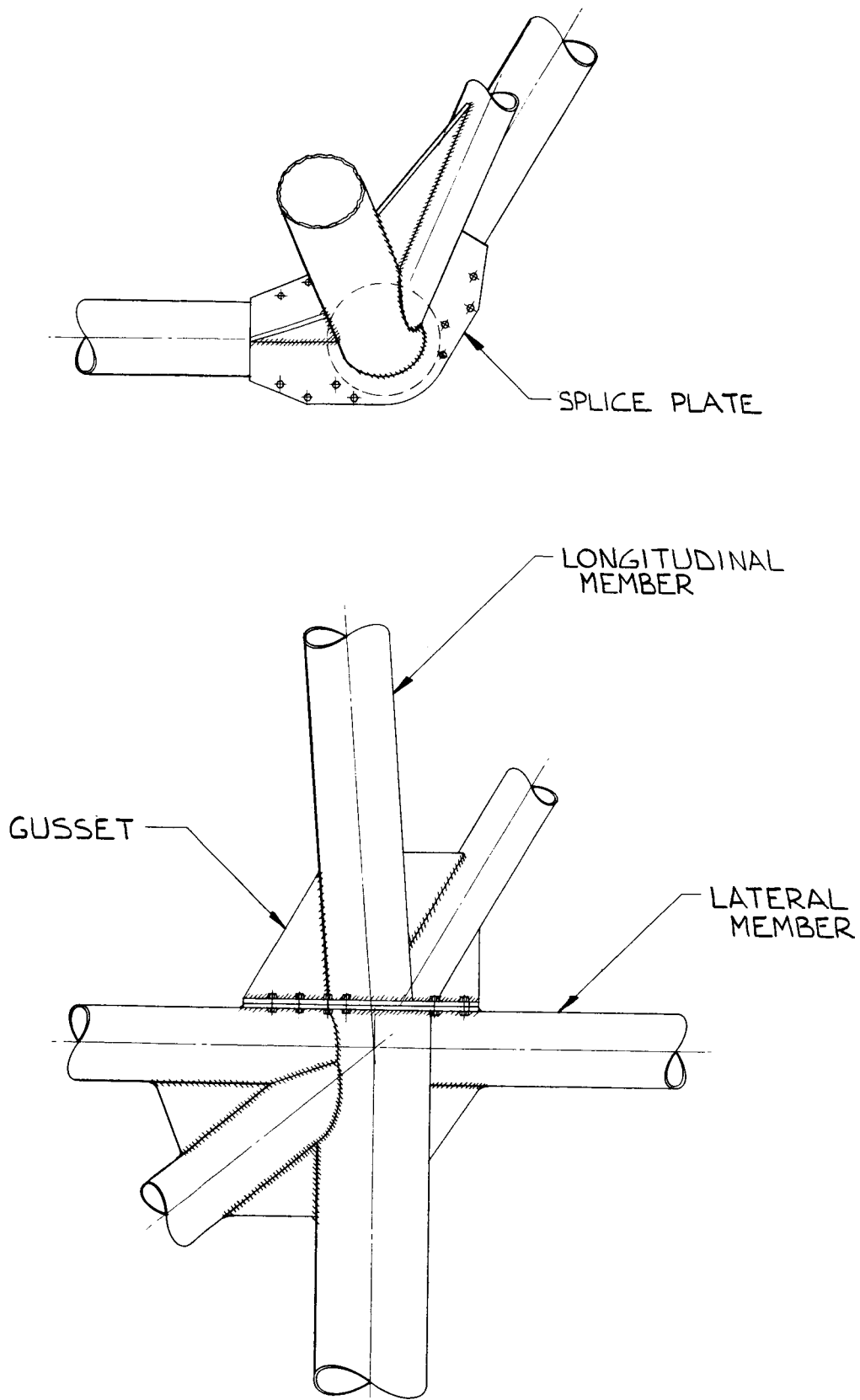


Figure 3-9. Detail of Tubular Cluster Joint in Truss Frame

TABLE 3-3. COMPARISON OF CANDIDATE MATERIALS  
FOR LAUNCH STRUCTURE AT 300° F

MATERIAL	ELASTIC MODULUS (10 <sup>6</sup> PSI)	DENSITY (LB/IN. <sup>3</sup> )	$\frac{E}{\rho}$ (10 <sup>6</sup> IN.)	TENSILE YIELD STRESS (10 <sup>3</sup> PSI)
Beryllium	42	0.065	646	55
Molybdenum	45	0.369	122	70
Inconel X-750	30	0.298	100	93
Titanium	14.8	0.160	92.5	101
L-605	31	0.330	93.9	53
301 SS	27	0.286	94.3	28

For ease in assembly, the truss frame is assumed to be spliced at several stations with mechanical attachments as shown in Figure 3-9.

### 3.2 STRUCTURAL ANALYSIS

A structural analysis of the launch structure used with the non-load bearing radiators was performed for the loading conditions and stiffness criteria discussed in paragraph 2.3. The analysis was iterated with design changes in order to arrive at a minimum weight. The analysis was performed using the MASS computer code (Reference 3-1) which determines deflections, stresses, and strain energy in each of the members. From these data, the natural frequency of the structure was calculated using Rayleigh's method as described in Reference 3-2. Sample calculations are shown in Appendix A for a typical truss member. The members are identified by the figures in the appendix showing mathematical models for the 300 kWe and 1200 kWe spacecraft.

Design iterations were performed only on the smaller of the two structures, and computer runs were made on the larger structure only to the extent necessary to permit extrapolation of the weight estimates. Preliminary analysis showed the structure to be stiffness dependent rather than stress dependent. Effort was therefore directed at meeting the lateral stiffness requirement, that is 4.04 cps in the first free-free bending mode for the larger spacecraft, and 4.13 cps for the smaller spacecraft.

A measure of the degree to which the structure had been optimized was obtained by comparison to the ideal mass distribution described in Reference 3-3. In Figure 3-10, the normalized structural weight distribution for the 300 kWe spacecraft is shown in comparison with the ideal distribution. As shown, some improvement can be made. However, the weight reduction that can be obtained by such improvements are not significant in this study. The weight of the launch structure used with the non-load bearing radiator is based on the weight of the truss with an additional weight increment for fittings and hardware. A study and test program reported in Reference 3-7 shows that for beryllium truss frames, as much as 80 percent of the weight is in the fittings.

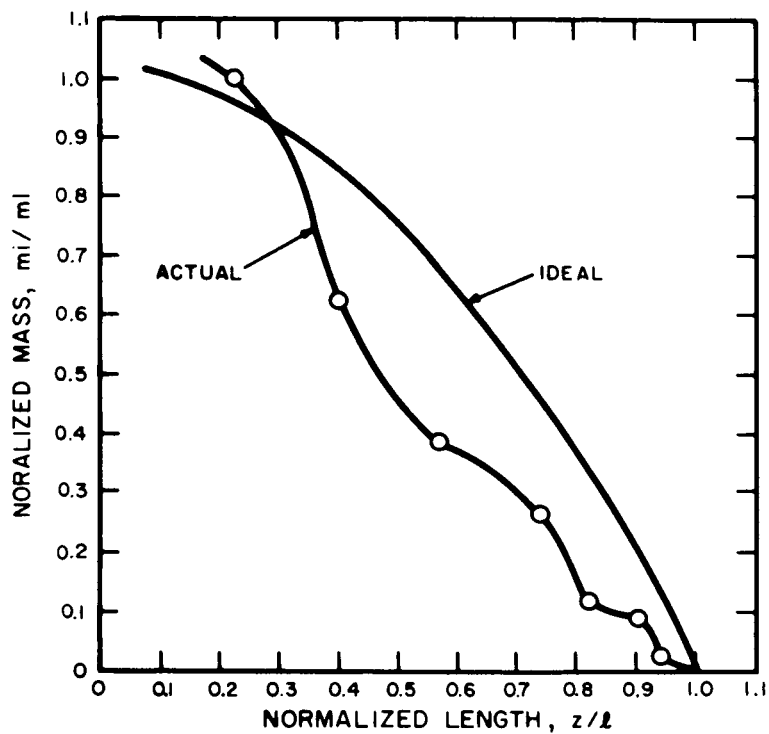


Figure 3-10. Comparison of Launch Structure Weight Distribution, Actual with Ideal

### 3.3 THERMAL STRESSES

An analysis was made of thermal stresses in the flat panel radiator for three conditions:

- a) Temperature gradients from tube to fin when the radiator is at operating temperature,
- b) Differential thermal expansion between the radiator panel and the headers,
- c) Residual stresses due to brazing.

A summary of the results of these analyses are given in Table 3-4, and the methods of analysis are described in Appendix B. The analysis was performed for a typical panel using the cross-section dimensions and temperature gradients for the primary radiator of the 1200 kWe powerplant. The dimensions and temperature gradients of the primary radiator for the 300 kWe powerplant and of the secondary radiator for both powerplants, are judged to be less critical.

The temperature gradient between the tubes and fins when the radiator is operating places the tube armor in compression and the fins in tension. Analysis shows that the stresses are less than allowable stresses for most forms of beryllium, even when the regions of high stress have been embrittled by brazing. Although the stresses are acceptable for the cross-section analyzed in this study, a less favorable distribution of stresses would result if the fin thickness were less or the tube spacing greater.

TABLE 3-4. SUMMARY OF THERMAL STRESS ANALYSES

CONDITION	LOCATION	MAXIMUM STRESS	ALLOWABLE STRESS
a. Thermal Stress due to Temperature Gradient from Tube to Fin	Fin root	9,000 psi Compression	52,500 psi
	Fin center line	21,000 psi tension	735,000 psi
b. Bending Stress due to Differential Thermal Expansion between Headers and Radiator	Pigtail piping	118,000 psi	700,000 psi
c. Residual Stress due to Brazing	Fin root	23,000 psi	40,000 psi
	Liner	17,600 psi	High

At operating temperatures, the thermal expansion of the beryllium radiator is less than that of the stainless steel headers. This difference is accommodated by bending of the pigtail piping connections. Although the fictitious elastic stresses computed are high, the stainless steel piping is ductile and shows a substantial margin of safety, even for repeated thermal cycles. Since the flat panel radiator is non-load bearing it must be flexibly supported by the launch structure. This flexible mounting also assures that thermal growth relative to the support structure does not induce significant stresses.

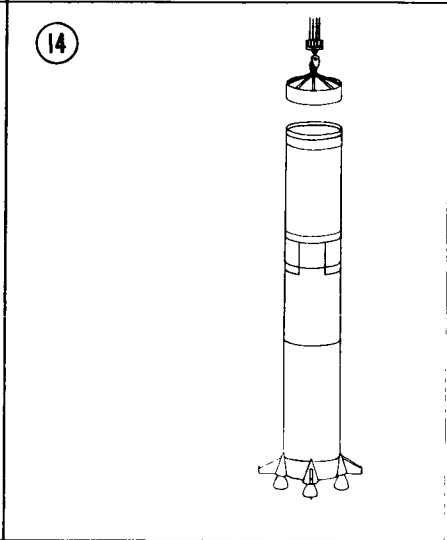
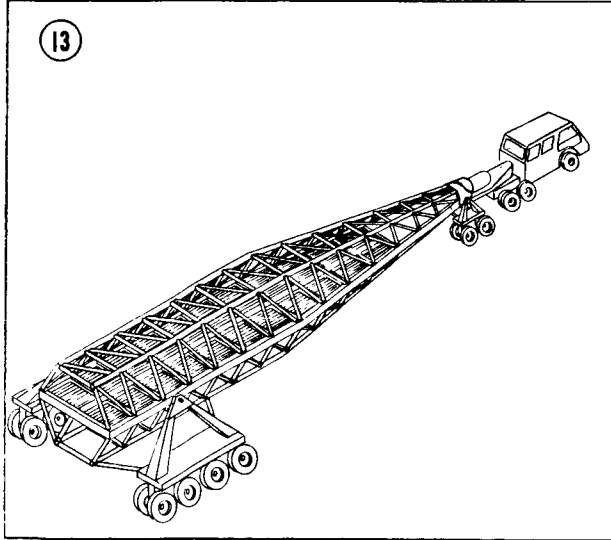
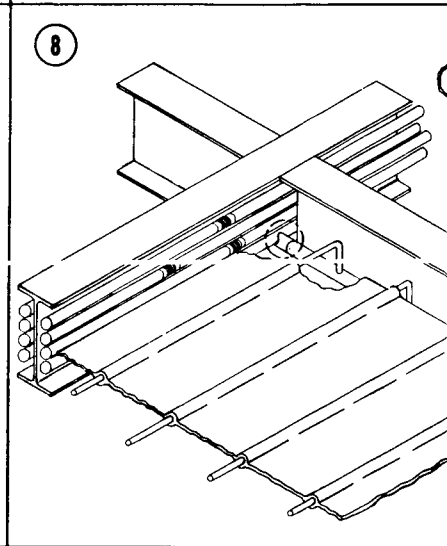
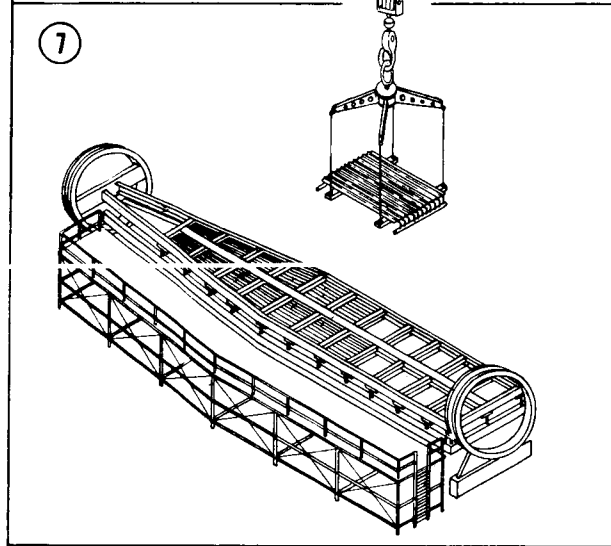
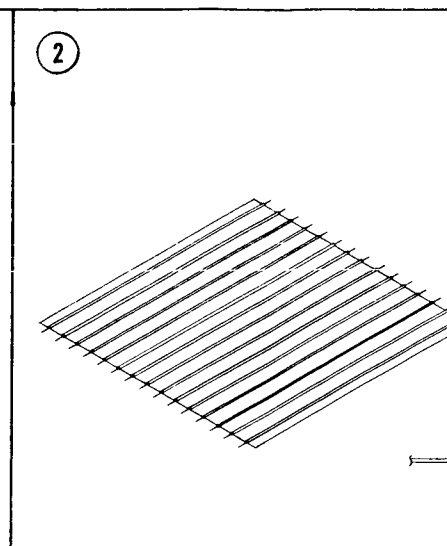
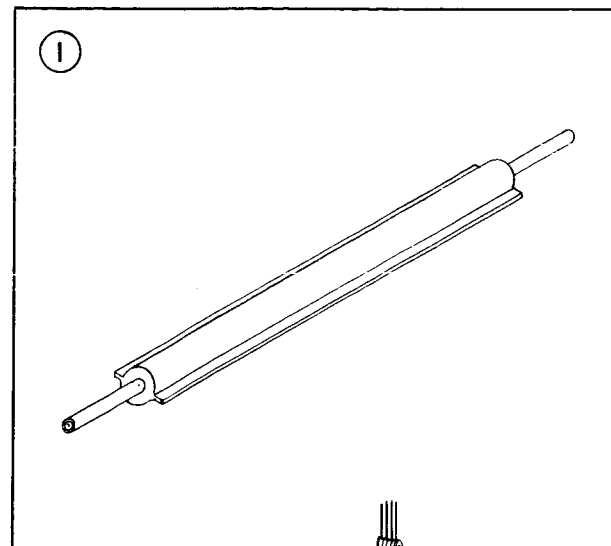
The analysis of residual stresses due to brazing was performed to illustrate the importance of matching the thermal expansion coefficients ( $\alpha$ ) of the beryllium forms used for armor and fin material. Mismatch is greatest between highly wrought forms, such as cross-rolled sheet and forms with disordered grain structure, such as hot pressed block. A mismatch of  $10^{-6}/^{\circ}\text{F}$ , for example, which could result from using the hot pressed block for armor and the cross rolled sheet for fins, would give stresses exceeding 90,000 psi.

Although experience with brazed fins on the SNAP-27 generator has shown that theoretical thermal stresses in excess of 100,000 psi can be sustained without failure, triaxial stresses in the presence of embrittlement due to brazing can cause failure at much lower stresses. Thermal expansion mismatch can also be significant even for the same forms of beryllium taken from different billets. Problems such as this may dictate that brazing be excluded from highly stressed areas, or eliminated entirely from the radiator fabrication procedure.

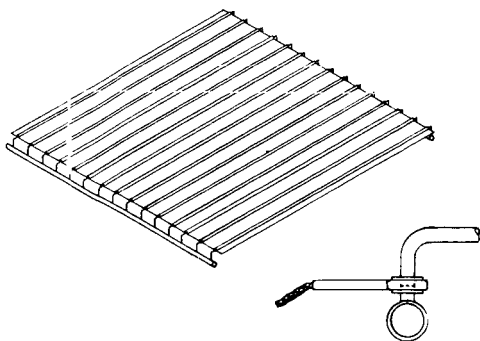
### **3.4 FABRICATION AND ASSEMBLY OF NON-LOAD BEARING RADIATOR**

As part of the preliminary design of the radiator assembly, a detailed consideration of the fabrication methods and assembly sequence was made. This was necessary to identify many of the "real world" factors that influence the design and contribute to the nonfunctional or parasitic weight of the assembly. Figure 3-11 shows a proposed assembly sequence for the non-load bearing radiator, from the fabrication of armored tube elements to the final mating with the launch vehicle.

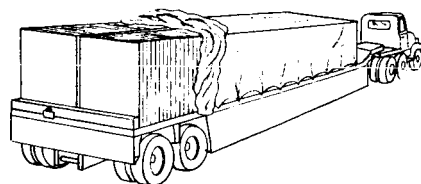
Step (1) in the fabrication sequence is the joining of beryllium armor to stainless steel liner. Several joining techniques, including coextrusion, brazing, and diffusion bonding have been developed for making such armored tubes. (References 3-5, 3-6, and 3-7.) Much remains to be done, however, in developing these techniques to achieve acceptable thermal conductance



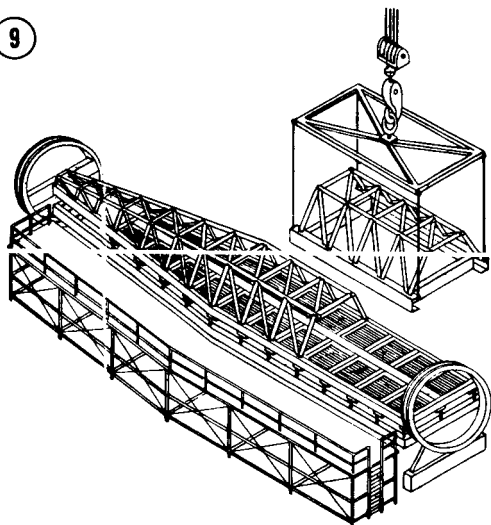
3



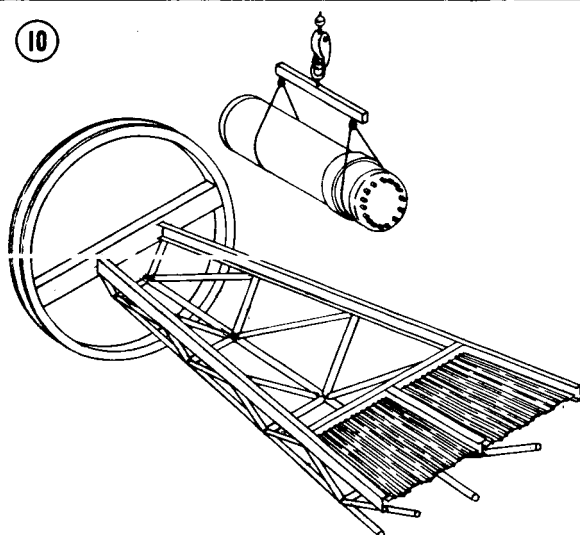
4



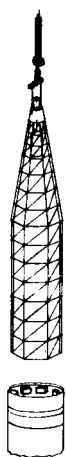
9



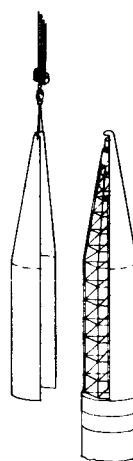
10



15



16



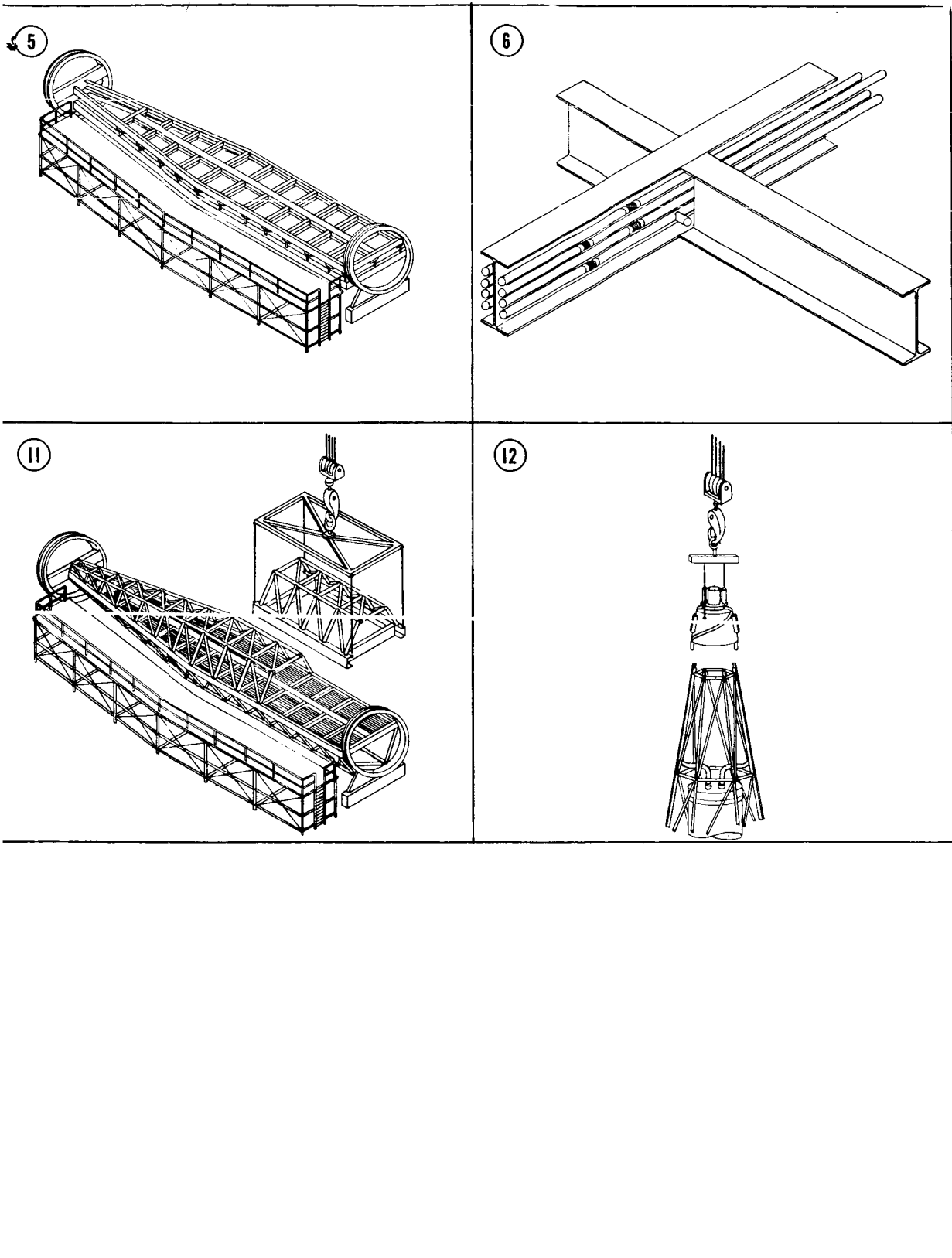


Figure 3-11. Assembly Sequence for Flat Panel Radiator

between the armor and liner, and in producing tubes of the required length in one piece. Experience with aluminum armor tubes in lengths up to ten feet, suggests that, with development, similar results might be feasible with beryllium.

The next step in the assembly sequence shown in Figure 3-11 is joining the armored tubes to the fins. If the armored tube has extruded or machined tabs as shown, the fins can be joined by a lap braze, or a braze welded butt joint. Several suitable techniques for making this joint are under development and are reported in a recent survey report (Reference 3-7). Experience with brazed beryllium fins on the SNAP-27 generator has shown the importance of allowing for embrittlement in the braze area, especially in the presence of triaxial stresses. The analysis of thermal stresses that result from brazing, presented earlier, showed the importance of minimizing the difference in thermal expansion coefficient between the fin and armor material, even though both are beryllium. Further evaluation of these brazing problems may, in the future, suggest that it is best to avoid all brazing by casting or extruding armored tubes with fins, then fasten mechanically fin-to-fin to form a panel. The largest panel shown on either flat panel radiator measures 145 by 180 inches. This is within the capacity of many facilities for high temperature brazing, for example, those used to fabricate the brazed stainless steel sandwich panels used on the XB-70 aircraft.

After assembly of the individual radiator panels, the next step is to join the tube liners to the feed and return headers, as shown in step (3) of Figure 3-11. Because of the large number of tube joints to be made, it is essential that the joining technique used be one that is rapid, repeatable and highly reliable. A portable tool (Figure 3-12) having a programmed, orbiting head, is ideally suited for this purpose and may become an industry standard (Reference 3-8). After leak testing of these joints and the application of a high emissivity coating, the panels are shipped to the launch center for assembly into a radiator (4).

The flight structure that supports the radiator panels is shown in step (5) in a turn-over fixture. The feed liner and panels are assembled into the frame in steps (6) and (7), and

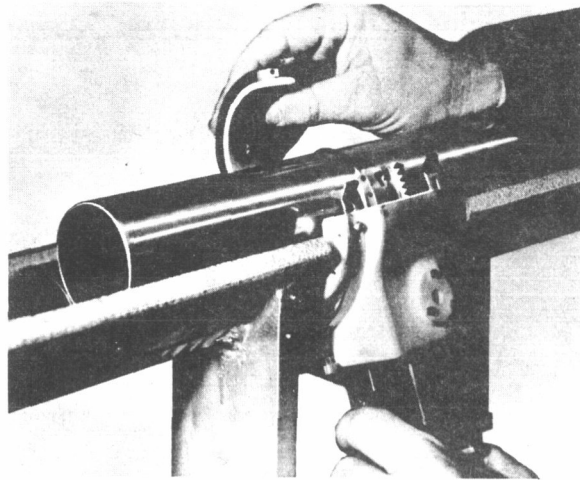


Figure 3-12. Portable Welding Tool, 2-inch Diameter Tube

the header to feed line joints made with a portable tube welder. Figure 3-13 shows how a typical complex junction is arranged to permit access for the tube welder. Table 3-5 lists typical clearance requirements for tubes of various diameters.

After the radiator panel support fittings have been installed and adjusted, one-half of the tubular space frame can now be attached to the flight structure as shown in step (9). Since the frame sections are not closed, stable structures until they are attached to the flight structure, they are handled and assembled with tooling bars in place, to be removed when the assembly is complete. The attachments to the flight structure are explosively actuated pin pullers. At this stage in the assembly, dummy initiators would be installed in all explosive devices to permit safe handling and installation and checkout of electrical harnesses. The dummy initiators would be removed at the same time that similar pyrotechnic devices on the launch vehicles are armed.

With one-half of the tubular frame in place, the flight structure can now be rotated in its fixture and the power conversion equipment installed as shown in step (10). The remainder of the tubular frame is installed, step (11), and the entire assembly rotated into a vertical position for installation of the reactor and shield assembly, step (12). From this step on, the requirements of nuclear safety would predominate.

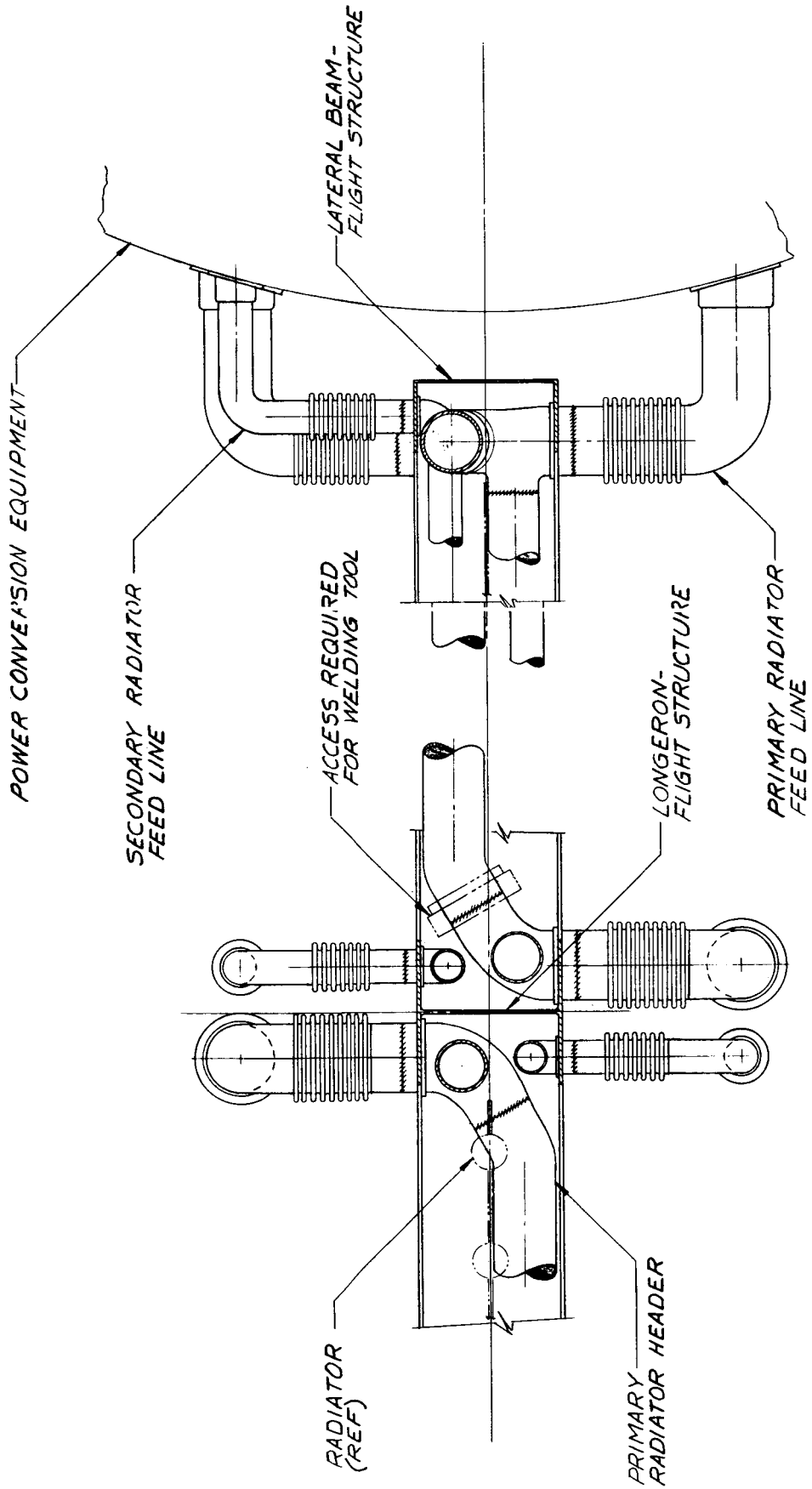
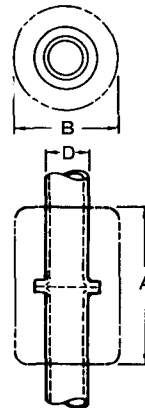


Figure 3-13. Detail of Feed Line to Header Joints

TABLE 3-5. SPACE REQUIREMENTS FOR WELDING EQUIPMENT

SPECIAL TUBE JOINING TOOLS

TUBE OD (INCHES)	A (INCHES)	B (INCHES)
1/4	1.7	1.5
3/8	2.0	1.6
1/2	2.2	1.7
5/8	2.5	1.9
3/4	2.6	2.0
1	2.8	3.0
1-1/4	3.0	3.2
1-1/2	3.1	3.5
2	3.4	4.0
2-1/2	3.6	4.5
3	3.9	5.0
4	4.0	6.5
7	5.0	9.5
8	5.0	10.5



The complete power system, having been charged and tested, is transported, (step 13), and the payload section, step (14), and then the powerplant, step (15), are lifted on to the Saturn V launch vehicle. The final event in the sequence is the installation of the aerodynamic fairing. The assembled launch vehicle can now be transported to the launch complex.

**3.5 REFERENCES**

- 3-1 "MASS System- The Computer Program for General Redundant Structures With Vibratory and General Static Loading," R66FPD172, General Electric, 1966.
- 3-2 "Shock and Vibration Handbook," Harris and Crede, McGraw-Hill, 1961.
- 3-3 "Design of Minimum Mass Structures with Specified Natural Frequencies," M.J. Turner, AIAA Journal, Volume 5 No. 3, March, 1967.
- 3-4 Siergiej, J.M. , "Long Beryllium Extrusions With Complex Cross Sections," Space/ Aeronautics, March, 1965.

- 3-5 Patenaude, C.J. and W.H. Santschi, "Casting of Beryllium-Columbium Impact Target Composites," NASA CR-54144, 1964.
- 3-6 Diersing, R.J., et al, "Gas-Pressure Bonding of Stainless Steel - Reinforced Beryllium Hypervelocity Impact Targets," NASA CR-54222, 1964.
- 3-7 National Academy of Sciences, "Sixth Progress Report by the Committee on Beryllium Metallurgy of the Materials Advisory Board," National Research Council Publication MAB-199-M(6), Washington, April, 1966.
- 3-8 Meredith, R., "Special Tooling for Joining Tubing in Place," Engineering Development Laboratory, North American Aviation Inc., In Symposium of Technology Status and Trends, NASA SP-5030, 1966.

## 4. LOAD BEARING RADIATORS

### 4.1 SPACECRAFT DESCRIPTION

Load bearing radiators are shown in spacecraft concepts with a 300 kWe powerplant in Figure 4-1, and a 1200 kWe powerplant in Figure 4-2. Similar concepts are shown for both spacecraft. The radiators act as primary structures supporting the other components of the powerplant. An aerodynamic shroud covers only the reactor and shield so that the radiator is subjected to both aerodynamic and inertial loads during launch. This presumes that a thermal shroud over the radiator is not required during launch to prevent radiator coolants from freezing before the nuclear powerplant is started.

The conical radiator configuration does not require as large an envelope as the flat panel radiator of the same heat rejection capability. Therefore, at the power levels used in this study, the conical radiators are not area limited. The choice of a 10 degree half-cone angle is based on minimizing the nuclear radiation shielding weight and launch loads (Reference 4-1). As shown in Figure 4-1, the optimum radiator area for a 300 kWe powerplant is less than that available with a 10 degree half-cone angle so that the base of the primary radiator does not match the diameter of the launch vehicle. A payload section is therefore used to act as an adapter, as well as to support the electric propulsion system, communication and guidance systems, and scientific instrumentation. As for the spacecraft with non-load bearing radiators, the payload section is largely undefined. However, unlike the flat panel radiator, the conical radiator provides excess volume on the inside so that extensions into the Instrument Unit are unnecessary.

The power conversion unit is supported by a cone structure inside the radiator. A cone structure is used rather than struts so that it might also serve as an insulated bulkhead to prevent radiation from the interior of the primary radiator to the cooler secondary radiator and power conversion equipment.

The radiators are divided into bays to provide tube lengths which are close to the thermal optimum and are within feasible manufacturing capabilities. The headers in each bay are alternated inlet and outlet so that temperature gradients across bay joints are eliminated. The rings which splice adjacent bays together support the headers and provide them with

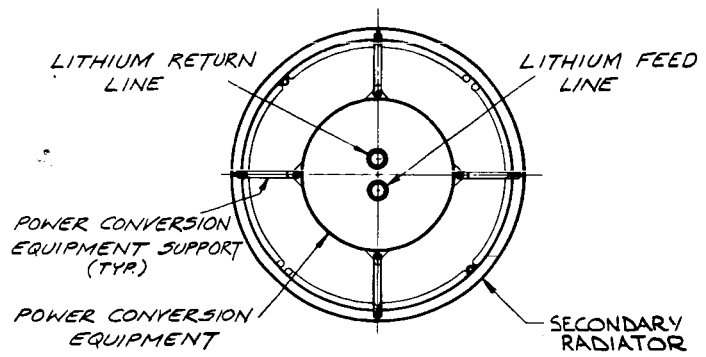
additional meteoroid protection. All headers and feed lines derive meteoroid protection from the radiator as well as blockage by the power conversion equipment and its support cone.

The parameters defining the radiators for the 300 kWe powerplant are listed in Table 4-1 and for the 1200 k We powerplant, in Table 4-2. These parameters are the direct output from the SPARTAN III computer code. Note that in comparison with the flat panel radiators, the conical radiators have optimized with many of the parameters in a favorable direction.

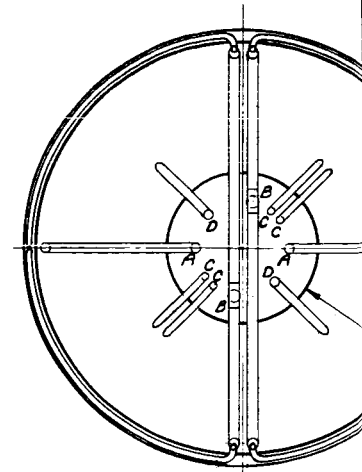
TABLE 4-1. CONICAL RADIATOR PARAMETERS FOR 300 kWe POWERPLANT

		PRIMARY	SECONDARY
Heat Rejected	(kW)	2460	480
Area	(ft <sup>2</sup> )	1077	564
Radiator Wt.	(lb)	3598	1245
Inlet Temp.	(°F)	1300	850
Fluid Δ T in Rad. *	(°F)	250	150
No. of Panels		8	8
No. of Tubes/Panel*	(Average)	29	12
Tube ID*	(in.)	0.258	0.31
Tube Length	(ft)	10.71	11.11
Average Header Length	(ft)	12.2	6.2
Header ID*	(in.)	1.965	1.519
Fin Thickness	(in.)	0.172	0.105
Fin Length*	(in.)	2.203	2.79
Fin Efficiency	(%)	78.3	78.4
Tube Armor Thickness	(in.)	0.768	0.539
Tube Armor Thk, Bumpered	(in.)	0.164	0.127
Basic Feed Line ID*	(in.)	1.3	1.3
Radiator Δ P	(psi)	7.265	5.802
Feed Line Δ P	(psi)	4.33	0.4589
Feed Line Wt (wet)	(lb)	251.1	112.6
Coolant Flow Rate	(lb/sec)	43.59	24.87
Hydraulic Pump Power	(kW)	2.23	0.6609

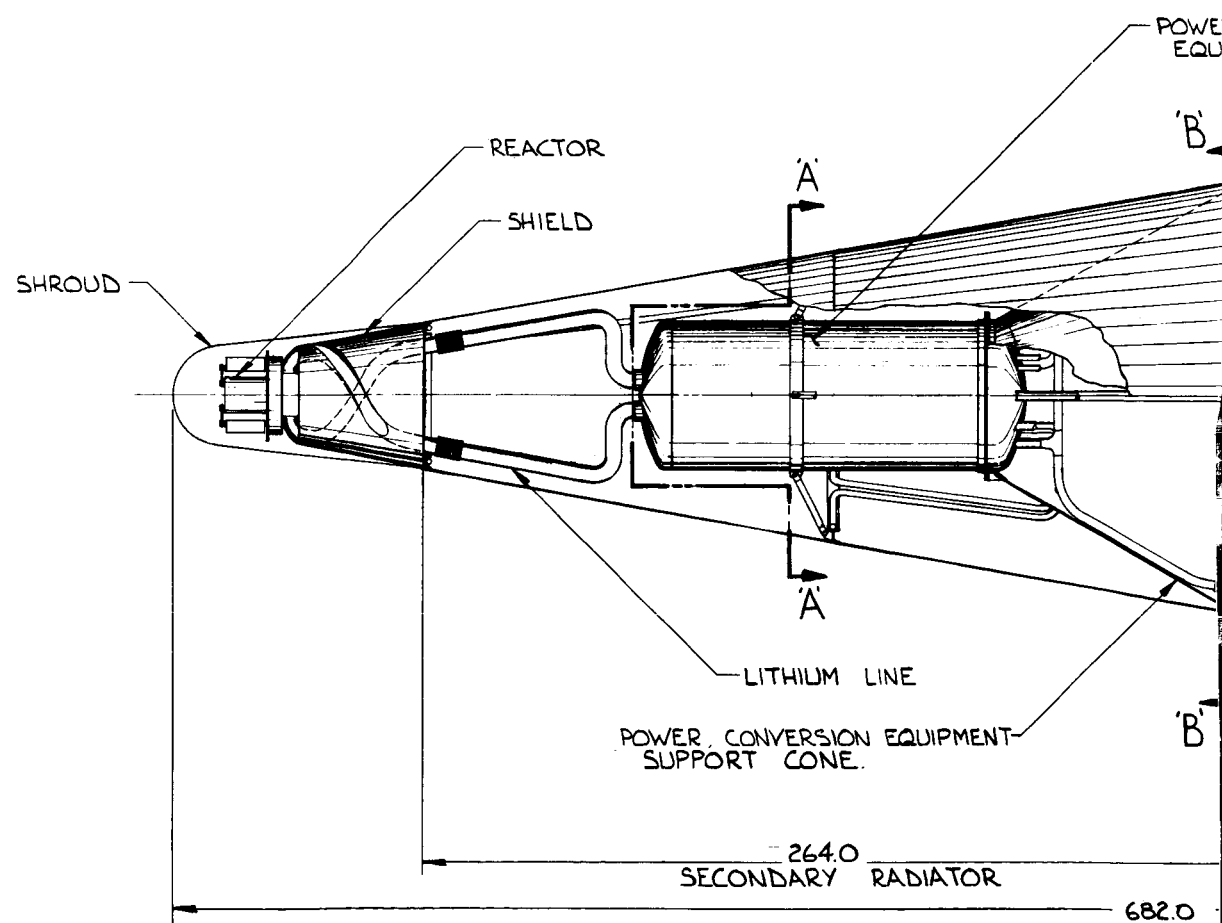
\*Optimized Variables

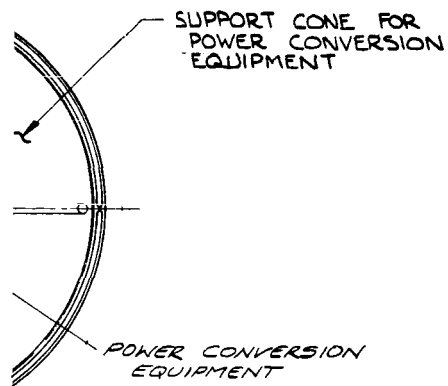


SECTION 'A-A'



SECTION 'B-B'





LINE	DESCRIPTION
A	PRIMARY RADIATOR FEED LINE
B	PRIMARY RADIATOR RETURN LINE
C	SECONDARY RADIATOR FEED LINE
D	SECONDARY RADIATOR RETURN LINE

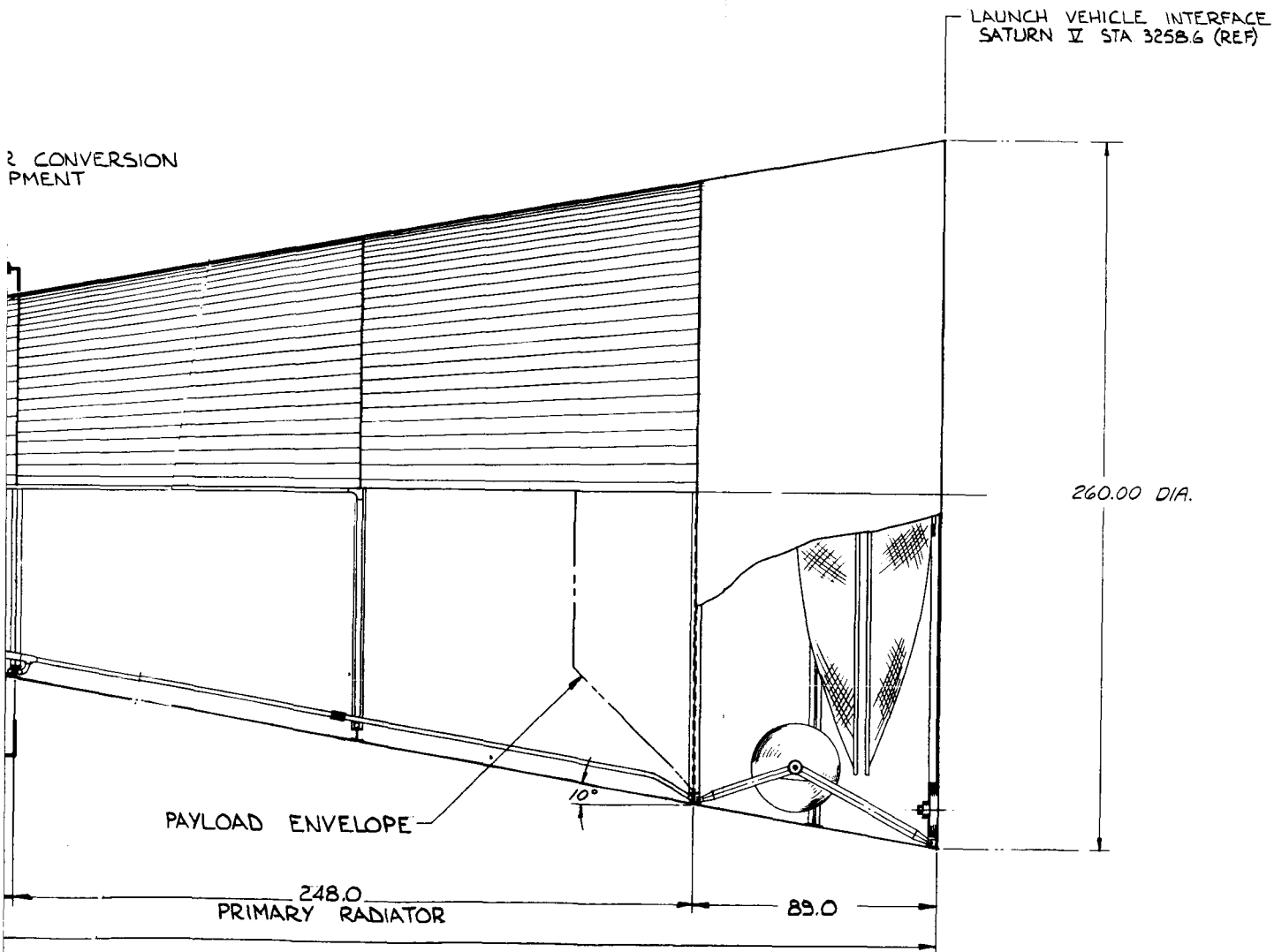
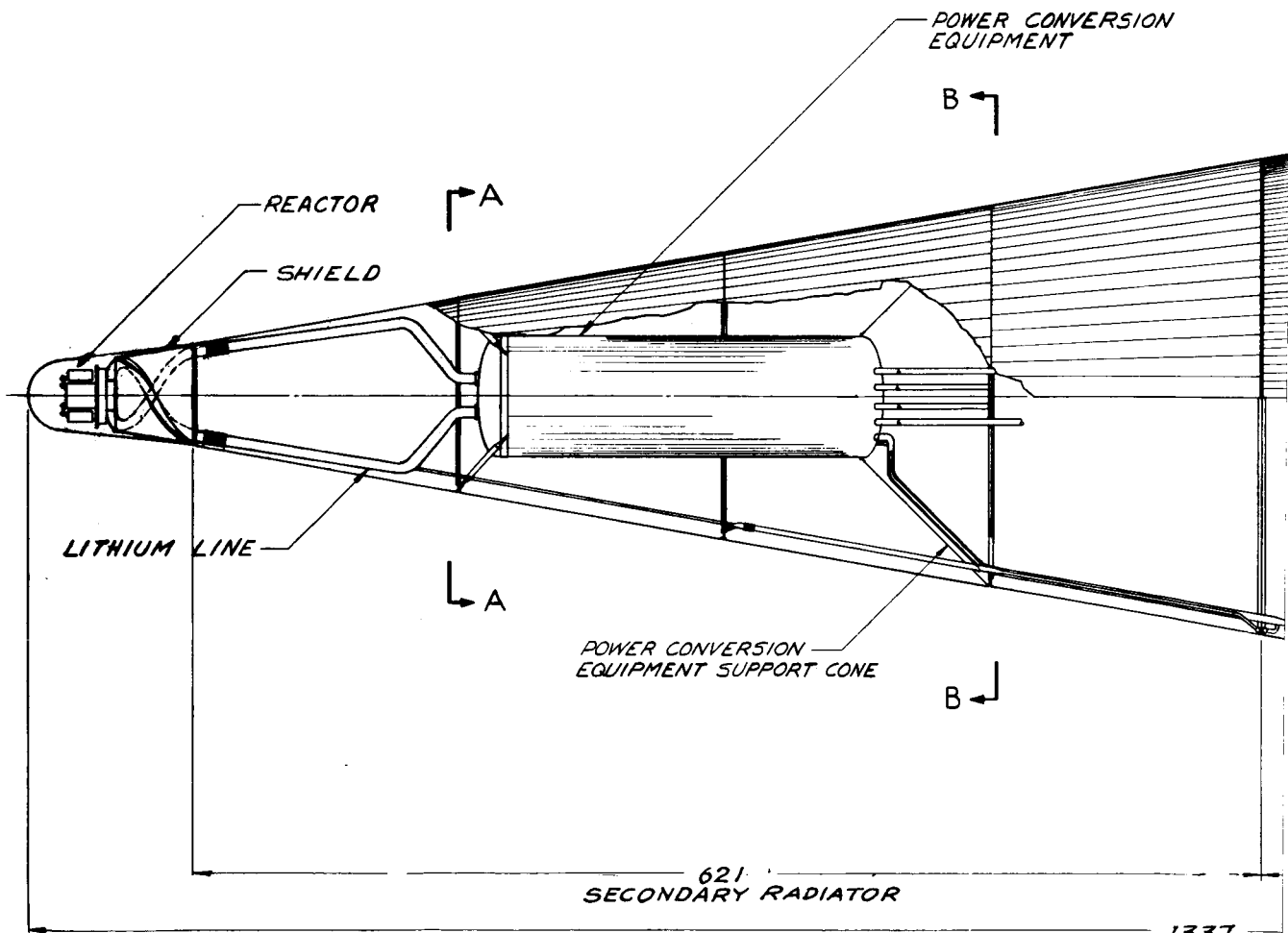
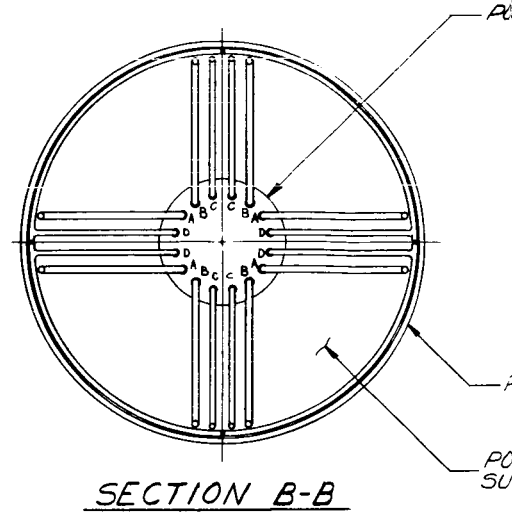
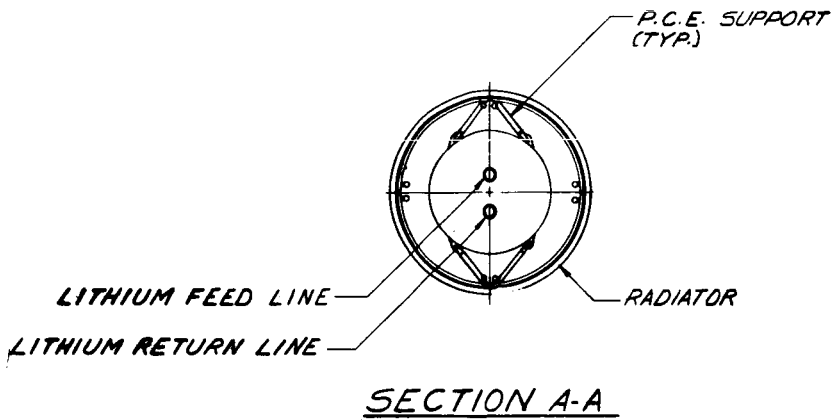


Figure 4-1. Spacecraft Concept -300 kWe Powerplant with Conical Radiator



1337

POWER CONVERSION EQUIPMENT

LINE	DESCRIPTION
A	PRIMARY RADIATOR FEED LINE
B	PRIMARY RADIATOR RETURN LINE
C	SECONDARY RADIATOR FEED LINE
D	SECONDARY RADIATOR RETURN LINE

RADIATOR

POWER CONVERSION EQUIPMENT  
SUPPORT CONE

LAUNCH VEHICLE INTERFACE  
SATURN V STA. 2555-0 (REF)

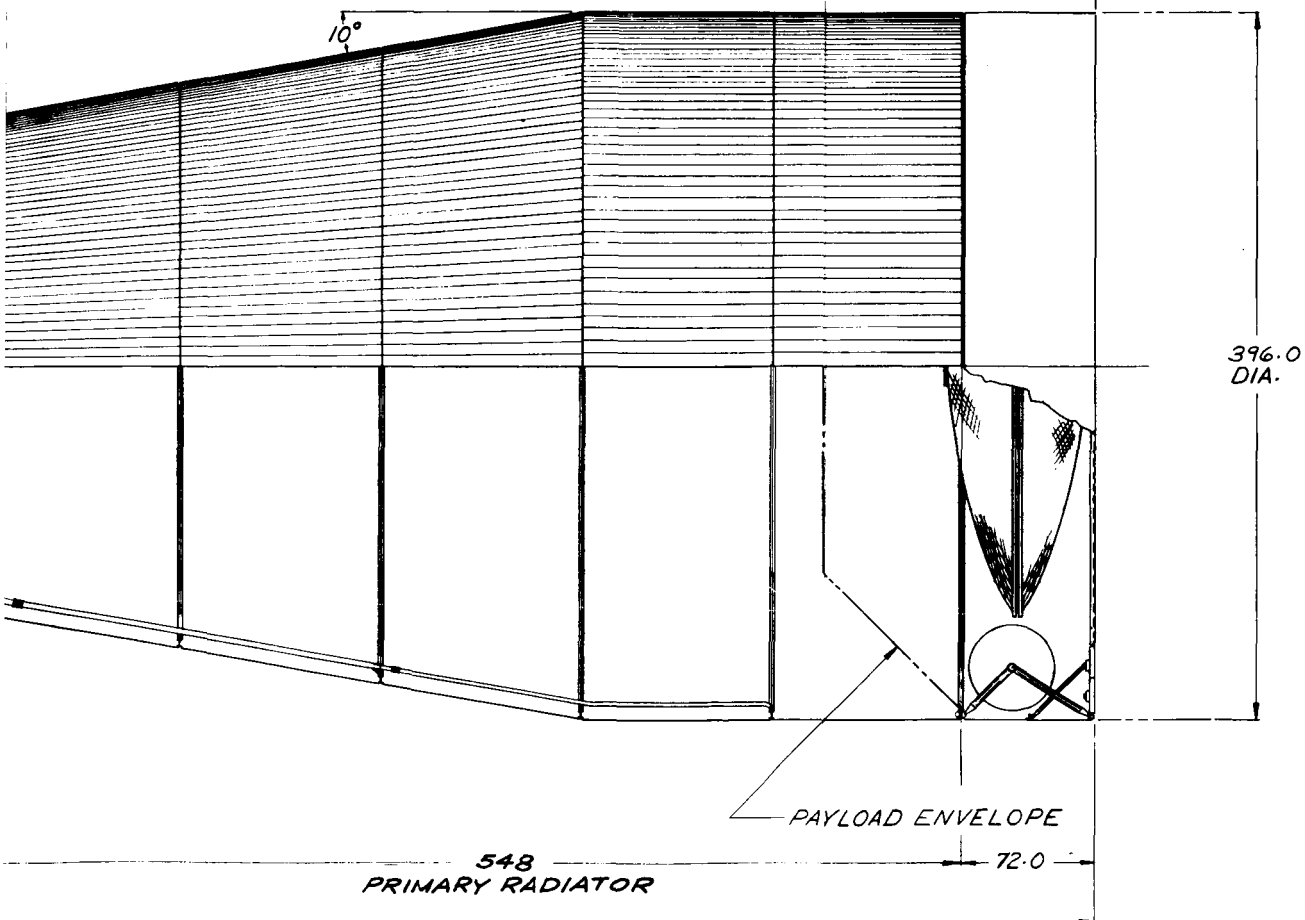


Figure 4-2. Spacecraft Concept -1200 kWe Powerplant with Conical Radiator

TABLE 4-2. CONICAL RADIATOR PARAMETERS FOR 1200 kWe POWERPLANT

		PRIMARY	SECONDARY
Heat Rejected	(kW)	9840	1920
Area	(ft <sup>2</sup> )	3995	2291
Radiator Wt.	(lb)	20075	7502
Inlet Temp.	(°F)	1300	850
Fluid Δ T in Rad. *	(°F)	180	150
No. of Panels		20	16
No. of Tubes/Panel*	(Average)	49	17
Tube ID*	(in.)	0.27	0.35
Tube Length	(ft)	8.12	12.67
Average Header Length	(ft)	23.3	11
Header ID*	(in.)	2.673	2.041
Fin Thickness*	(in.)	0.26	0.16
Fin Length	(in.)	2.45	3.49
Fin Efficiency	(%)	80.4	78.1
Tube Armor Thickness	(in.)	1.11	0.790
Tube Armor Thk, Bumpered	(in.)	0.242	0.192
Basic Feed Line ID*	(in.)	1.6	1.6
Radiator Δ P	(psi)	7.884	6.932
Feed Line Δ P	(psi)	9.366	3.28
Feed Line Wt. (wet)	(lb)	1354	965
Coolant Flow Rate	(lb/sec)	242.2	99.5
Hydraulic Pump Power	(kW)	18.41	4.312

\*Optimized Variables

This is a reflection of the meteoroid bumper advantage of the conical radiator which permits the optimization to approach more closely the thermal-hydraulic optimum.

Because of differences in radial thermal expansion, separation joints must be provided between the secondary and primary radiators and between the primary radiator and the payload section. These separation joints are conceived as rings held by mechanical fasteners during launch that are released explosively before the nuclear powerplant is started up. A second set of fasteners would permit radial displacements, but have sufficient tension capability to withstand flight loads after launch. Release of contact pressure across this joint would also permit an effective reduction in thermal conductance across the joint. This joint concept was first described in Reference 4-2.

## 4.2 STRUCTURAL ANALYSIS OF THE CONICAL RADIATOR

The load bearing conical radiator acts as a longitudinally stiffened shell in axial compression. Critical design loads occur during launch at the maximum "q $\alpha$ " condition, as determined in Reference 4-1. The loads on the radiator at the maximum "q $\alpha$ " condition were shown in terms of equivalent axial load for both the three-stage and two-stage versions of the SATURN V launch vehicle in Figures 2-7 and 2-8.

The limit loads obtained from these figures are multiplied by a factor 1.25, appropriate for unmanned missions, to obtain the ultimate loads used in the structural analysis. Structural analysis was performed using the Conical Radiator Analysis of Stability Stress (CRASS) computer code. This code analyzes each bay at three locations namely the top, center, and bottom, for each of three failure modes; local instability, panel instability, and general instability. Definitions of these failure modes are given in Table 4-3. The computer code treats a conical bay as an equivalent cylinder by using the slant length and by resolving axial loads into the cone surface. This is equivalent to the assumption that:

$$P_{cr} = P_{cyl} \cos^2 \alpha$$

where

$$P_{cr} = \text{buckling load of the cone}$$

$$P_{cyl} = \text{buckling load of an equivalent cylinder}$$

$$\alpha = \text{half-cone angle}$$

The buckling stress for local instability is given by:

$$\sigma_l = \frac{k_l \pi^2 E}{12(1 - \nu^2)} \left( \frac{t}{b} \right)^2$$

where

$$\sigma_l = \text{critical buckling stress for local instability}$$

$$k_l = \text{buckling coefficient}$$

$$E = \text{elastic modulus}$$

$\nu$  = Poisson's ratio

$t$  = thickness

$b$  = width

For a radiator, the thickness is that of the fin and the width is the distance between tubes. The buckling coefficient is conservatively taken as 4.0, representing a "long" panel with edges simply supported and no curvature.

For panel instability, the stiffening element, which is the armored tube with effective fin, is analyzed as an Euler column:

$$\sigma_p = c \pi^2 E \left( \frac{\rho}{\ell} \right)^2$$

where

$\sigma_p$  = critical buckling stress in panel instability

$c$  = "fixity factor" (structural support coefficient)

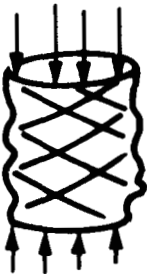
$\rho$  = radius of gyration

$\ell$  = stiffener length

When prior local instability is prevented, the fin can be assumed to be fully effective, that is, its entire cross sectional area can be lumped with the stiffener. Simple support of the ends is assumed, corresponding to a coefficient  $c$  of 1. If it is found that the panel instability stress is below the ultimate design stress, the CRASS code will determine the size and spacing of additional stiffening rings required to bring the radiator up to strength. Sizing of these intermediate rings makes use of the Shanley criteria (Reference 4-3). For general instability, the method of Becker and Gerard from Reference 4-4 is used. This theory uses a relation in the form:

$$\sigma_x = \frac{k_x \pi^2 E I_s}{t_s L^2}$$

TABLE 4-3. DEFINITIONS OF STRUCTURAL FAILURE MODES

<p>Local Instability</p>	<p>Buckling of the skin between the boundaries formed by the longitudinal and circumferential stiffeners</p>	 <p>A schematic diagram of a rectangular panel under uniform vertical compression. The panel is bounded by stiffeners on all four sides. A dashed line indicates the buckled shape of the skin, which has formed a single half-wave between the stiffeners.</p>
<p>Panel Instability</p>	<p>Buckling of the longitudinal stiffeners by bowing into one or more longitudinal half-waves between circumferential stiffeners</p>	 <p>A schematic diagram of a rectangular panel under uniform vertical compression. The longitudinal stiffeners are shown bowing outwards between the circumferential stiffeners, forming a half-wave.</p>
<p>Crippling</p>	<p>The final ultimate compressive failure of a longitudinal stiffener which has sufficient support to prevent panel instability</p>	 <p>A schematic diagram of a rectangular panel under uniform vertical compression. One of the longitudinal stiffeners has failed, causing a localized buckling and crushing of the stiffener.</p>
<p>General Instability</p>	<p>The simultaneous buckling of skin, longitudinal and circumferential stiffeners. The mode may be asymmetric (diamond shaped buckles) or axisymmetric (convolutions)</p>	 <p>A schematic diagram of a cylindrical shell under uniform vertical compression. The skin, longitudinal stiffeners, and circumferential stiffeners all buckle simultaneously, forming a diamond-shaped pattern of buckles.</p>

where

$\sigma_x$  = critical buckling stress for general instability

$k_x$  = buckling coefficient

$I_s$  = distributed moment of inertia of the stiffeners

$t_s$  = distributed thickness of the stiffeners

$L$  = length of the shell

The buckling coefficient  $k_x$  is a complex function of stiffener and frame properties, fin thickness, shell radius and length. For shells in the moderate length range, the buckling stress is independent of shell length.

The results of structural analysis of the load bearing radiators are summarized in Table 4-4 for the 300 kWe powerplant and in Table 4-5 for the 1200 kWe powerplant. Because of the relatively severe meteoroid protection requirements, it was found that the radiator has considerably greater load carrying capacity than is required to sustain the launch loads.

TABLE 4-4. SUMMARY OF STRESS ANALYSIS FOR 300 kWe CONICAL RADIATOR

BAY	LOCATION	ULTIMATE DESIGN STRESS (psi)	LOCAL INSTABILITY STRESS (psi)	PANEL INSTABILITY STRESS (psi)	GENERAL INSTABILITY STRESS (psi)	MINIMUM MARGIN OF SAFETY
1	top	2290	203,450	----	248,217	0.82
	center	2491	82,004	4544	176,222	
	bottom	2692	44,004	----	134,010	
2	top	2148	134,305	----	130,992	0.94
	center	2568	81,401	4574	107,586	
	bottom	2358	54,558	----	90,571	
3	top	1353	445,439	----	112,962	4.54
	center	1673	314,083	8376	99,105	
	bottom	1513	234,580	----	87,944	
4	top	1523	396,550	----	86,444	3.91
	center	1696	305,563	8327	87,208	
	bottom	1870	242,643	----	71,238	

TABLE 4-5. SUMMARY OF STRESS ANALYSIS FOR THE 1200 kWe CONICAL RADIATOR

BAY	LOCATION	ULTIMATE DESIGN STRESS (psi)	LOCAL INSTABILITY STRESS (psi)	PANEL INSTABILITY STRESS (psi)	GENERAL INSTABILITY STRESS (psi)	MINIMUM MARGIN OF SAFETY
1	top	3773	$4.96 \times 10^6$	5295	182,943	0.29
	center	4118	$1.27 \times 10^6$		141,171	
	bottom	4463	$0.57 \times 10^6$		114,923	
2	top	3008	$2.55 \times 10^6$	5458	97,037	0.46
	center	3735	$1.41 \times 10^6$		85,861	
	bottom	4463	$0.89 \times 10^6$		76,997	
3	top	3569	$2.18 \times 10^6$	5344	69,414	0.32
	center	4061	$1.38 \times 10^6$		63,076	
	bottom	4554	$0.96 \times 10^6$		57,799	
4	top	3836	$1.98 \times 10^6$	5316	53,118	0.26
	center	4233	$1.39 \times 10^6$		49,262	
	bottom	4630	$1.03 \times 10^6$		45,923	
5	top	2407	$13.8 \times 10^6$	14,484	50,862	4.31
	center	2728	$10.7 \times 10^6$		48,767	
	bottom	3048	$8.5 \times 10^6$		46,841	
6	top	2832	$13.3 \times 10^6$	14,316	44,730	3.95
	center	2893	$10.7 \times 10^6$		43,102	
	bottom	2954	$8.7 \times 10^6$		41,590	
7	top	2779	$12.4 \times 10^6$	14,500	40,124	3.60
	center	3149	$10.1 \times 10^6$		38,745	
	bottom	3519	$10.8 \times 10^6$		37,459	
8	top	3291	$10.8 \times 10^6$	14,582	36,479	2.77
	center	3871	$10.8 \times 10^6$		36,479	
	bottom	4450	$10.8 \times 10^6$		36,479	
9	top	4450	$10.8 \times 10^6$	14,383	36,479	1.98
	center	4829	$10.8 \times 10^6$		36,479	
	bottom	5207	$10.8 \times 10^6$		36,479	

Since additional stiffening is not required, there is no opportunity to optimize the thermal-meteoroid structural interrelations as discussed in Reference 4-1. Ultimate stresses do not exceed 5500 psi, well below the compression yield stress of beryllium. The allowable stresses for local and general instability are high and therefore not critical. The critical failure mode is panel instability. The fact that the buckling stresses for local and general instability are very much greater than those for panel instability is indicative of an off-optimum structural configuration. Optimum structural design would occur when the critical stresses for all failure modes are identical. No intermediate stiffening rings are required between the rings joining bays together. Panel instability is the critical mode in every case and the margins of safety for this mode are listed.

### **4.3 THERMAL STRESSES**

The analyses of thermal stresses discussed in paragraph 3.3 apply with few differences to the conical radiator. The stresses that occur while the radiator is at operating temperature have no effect on the load bearing capability of the radiator since temperatures will be relatively moderate during launch with no significant temperature gradients. The restraints offered by adjacent bays of the conical radiator will not induce thermal stresses because the headers have been alternated to eliminate temperature changes across the bay joints. Exceptions are the joint between primary and secondary radiators, and the joint between the radiator and payload sections. At these locations, the difference in radial growth across the joint is so great that radial restraint must be eliminated when the radiators are at operating temperature. A concept for these joints was discussed previously.

The analysis of pigtail piping stresses for the flat panel radiator can be applied to the conical radiator. However, if deflections are to be limited to the same magnitude as for the flat panel radiator, the headers must be divided by a bellows expansion joint wherever their length exceeds twelve feet.

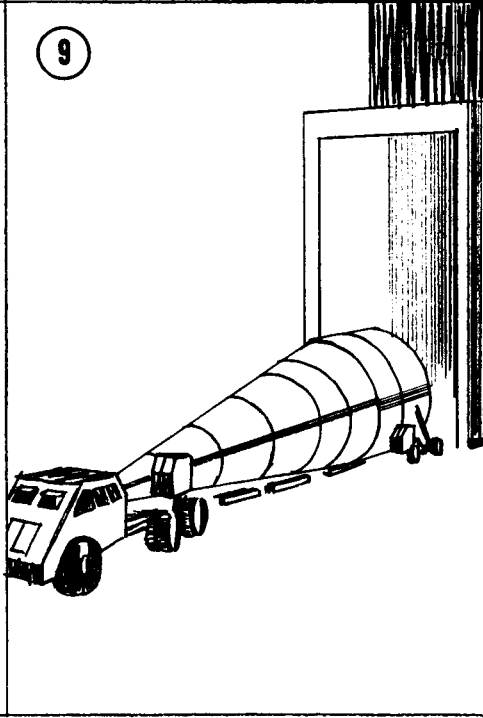
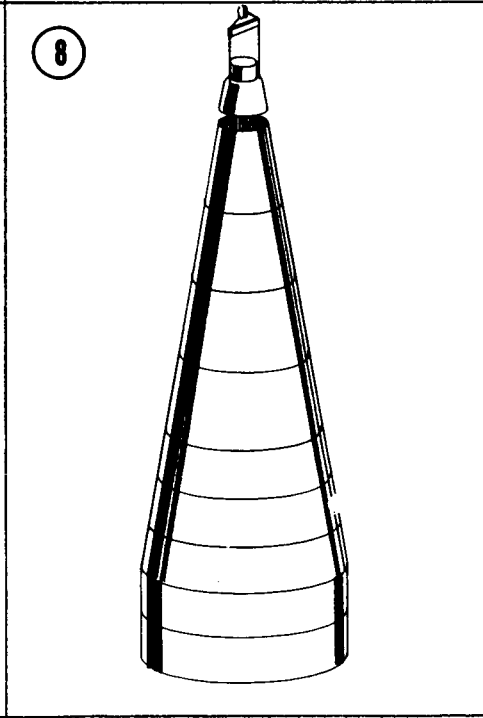
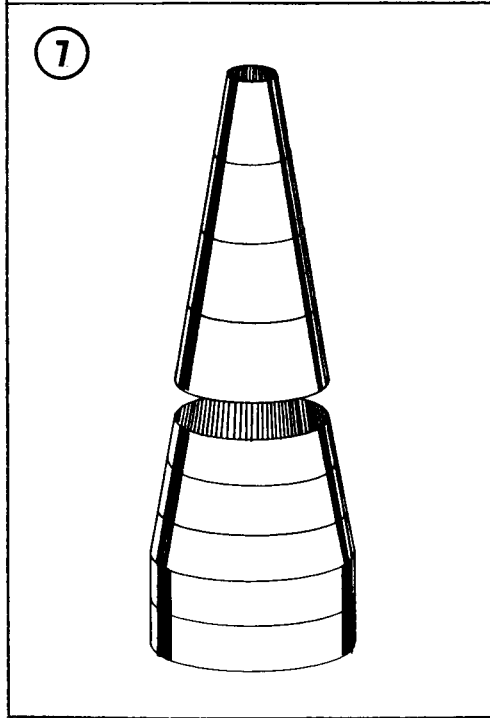
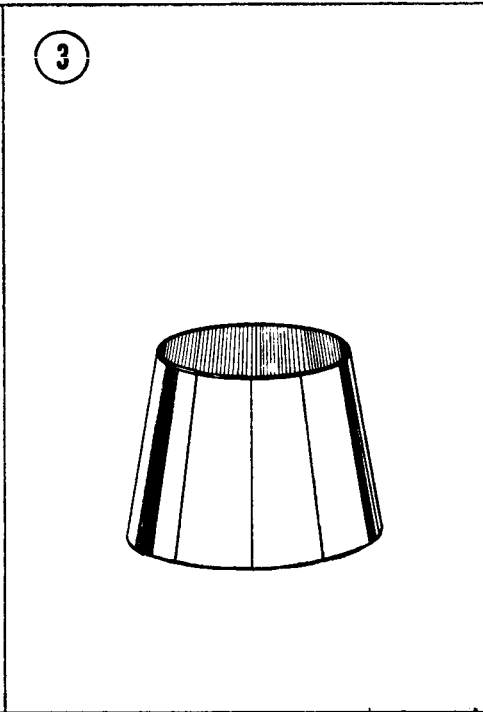
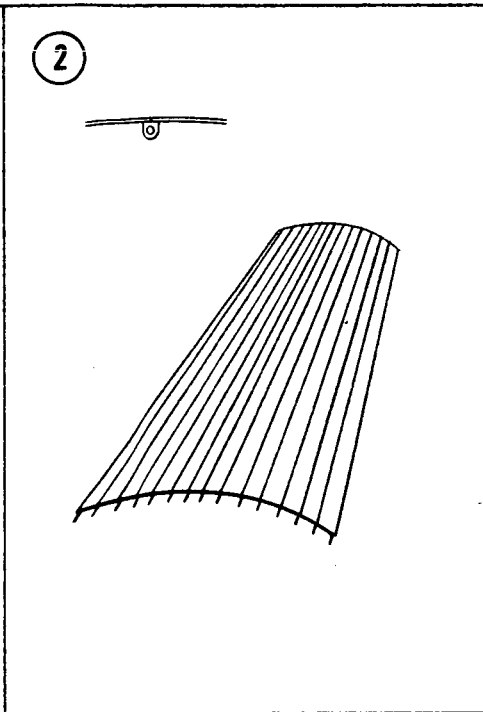
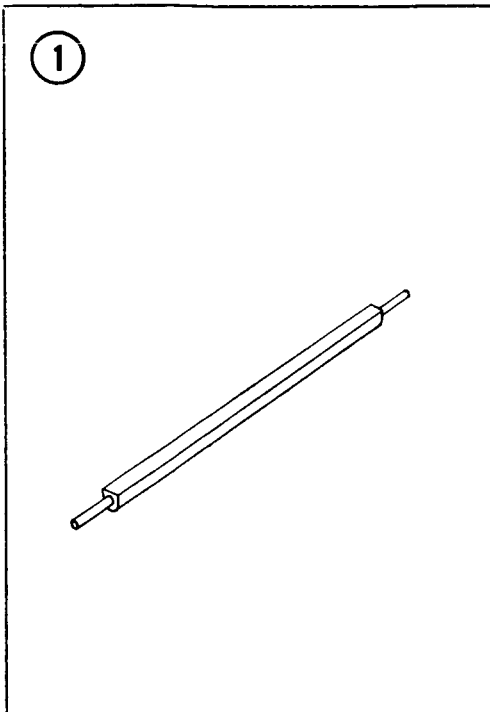
The analysis of residual stresses in the radiator due to brazing has particular significance to the load bearing radiator since these stresses must be superimposed with the stresses due to launch loads. Although the analysis of launch loads has shown that stresses are generally insignificant during launch, the combined loads may result in failure if the thermal expansion coefficients are not closely matched. Whereas the thermal stresses are self-limiting, the stresses due to launch loads are not. Failure of stiffened shells in axial

compression is generally catastrophic when yielding occurs. In addition, initial imperfections may greatly reduce the critical instability stresses of a shell in compression. The distortions that occur as a result of brazing will have a similar effect. It may be concluded that for a load bearing radiator it is highly desirable to eliminate assembly by brazing unless thermal expansion coefficients of the parts being joined can be closely matched.

#### **4.4 FABRICATION AND ASSEMBLY-LOAD BEARING RADIATOR**

A sequence of events for fabrication and assembly of a load bearing radiator, similar to that previously discussed for the non-load bearing radiator, is shown in Figure 4-3. The first two steps of the sequence are similar to those for the flat panel radiator with the exception that the armored tube is machined to an offset armor configuration, and the tubes are assembled into a curved panel that is part of a cone or cylinder. For the load bearing radiator, it is even more essential to avoid a mismatch in thermal expansion coefficient between armor and fin material if the panel is assembled by brazing, because residual thermal stresses from the brazing process will be superimposed on the stresses occurring during launch. Even though the stresses due to launch loads are relatively low, the beryllium should be initially in a stress free state if it is to be used as primary structure.

After transporting to the launch site, the panels are assembled into structural bays by attaching to stiffening rings (Step 3). These joints, and the joints between adjacent panels in a bay, would be made with mechanical fasteners. Beyond step (3), the radiator bay assemblies have sufficient structural capability that they can be handled and transported with very little fixturing. The headers and power conversion equipment, and feed lines, are installed in steps (4), (5), and (6), with all tube joints being made by a portable tube welder as described previously for the flat panel radiator. After mating the primary and secondary radiators, step (7), the reactor and shield assembly are installed in step (8) to complete the powerplant. The powerplant is then transported, step (9), and the payload, step (10), and the powerplant, step (11), are then mated with the Saturn V launch vehicle. The small aerodynamic shroud which covers only the reactor and shield can be installed in one piece as shown in step (12).



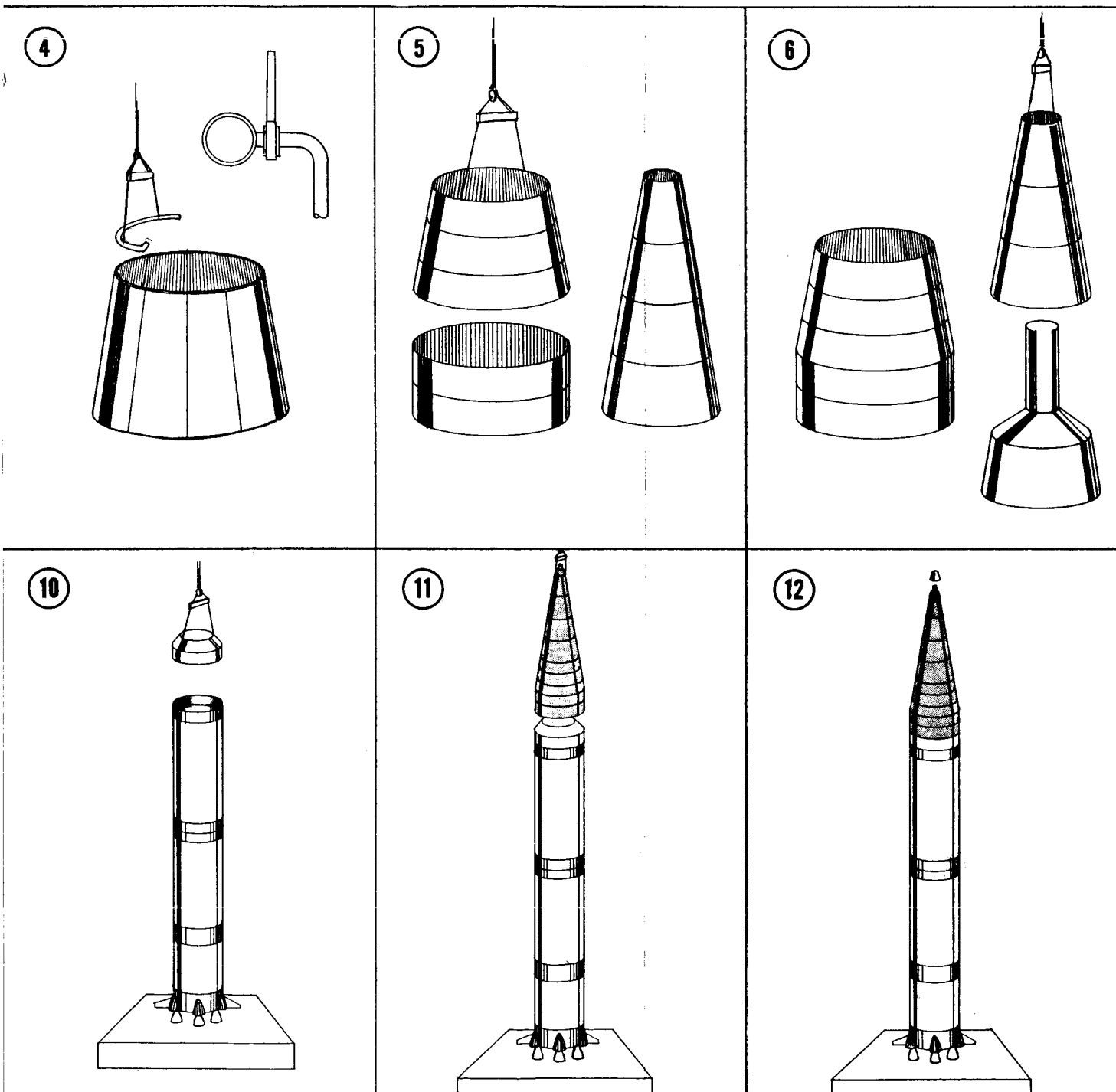


Figure 4-3. Assembly Sequence  
for Conical Radiator

It can be seen that the relative simplicity of the load bearing radiator leads to a less complex assembly sequence than is required for the non-load bearing radiator. Significant differences are:

- a) The less elaborate tooling requirements
- b) Elimination of pyrotechnic devices required for separation
- c) A simpler aerodynamic fairing installation

#### **4.5 REFERENCES**

- 4-1 Cockfield, R.D., "Definition of Spacecraft and Radiator Interrelations, for Nuclear Rankine Systems," NASA CR-72245, January 26, 1967.
- 4-2 Larson, J. W., "Research on Spacecraft and Powerplant Integration Problems - Spacecraft Analysis," NASA CR-54159, July 24, 1964.
- 4-3 Shanley, F.R., "Weight-Strength Analysis of Aircraft Structures," Dover Publications, 1952.
- 4-4 Becker, H. and G. Gerard, "Elastic Stability of Orthotropic Shell," Journal of the Aerospace Sciences, May, 1962.

## 5. CONCLUDING REMARKS

A weight breakdown for spacecraft with load bearing and non-load bearing radiators, at two power levels, is given in Table 5-1. The radiator, shield, and structural weights were derived from analyses previously discussed. Reactor weights were estimated from data presented in Reference 5-1 and power conversion equipment weights from the data in Reference 5-2. The latter two items are the same for both radiator configurations and have no significant influence on the comparison. Aerodynamic shroud weights for the non-load bearing radiators were determined from the data presented in Reference 5-3, while the smaller shrouds required for the reactor and shield on the spacecraft with load bearing radiators, were estimated from data in Reference 5-4.

To provide a meaningful basis for comparison, payload weights were determined for a typical unmanned Jupiter fly-by mission. The mission analysis, discussed further in Appendix C, showed that the spacecraft launched on the three-stage Saturn V had optimum staging for a 500 day trip when the S-IVB provided an hyperbolic excess velocity of 16,800 feet per second. Payload capability of the Saturn V to this velocity is approximately 68,000 pounds (Reference 5-5). Therefore, the comparison between the load bearing and non-load bearing radiator concepts was made on the basis of equivalent payloads of 68,000 pounds, taking into account the propellant weight penalty of the aerodynamic shroud. To compute the shroud weight penalties, ejection was assumed to take place at 200,000 feet altitude when the velocity had reached 9,000 feet per second, and the specific impulse of the upper stages was assumed to be 440 seconds. As a result of using this basis for comparison, the spacecraft weights at launch are not identical.

For the spacecraft launched on the two-stage Saturn V, a similar basis was used. Mission analysis for this case showed an optimum parking orbit of 200 nmi for an 800 day trip. Saturn V capability to this orbit is approximately 190,000 pounds, and this mass was used in the comparison in Table 5-1.

The electrical propulsion system and cesium propellant weights were determined from the mission analysis described in Appendix C.

The trip times were chosen as a result of the comparison shown in Figure 5-1. The three-stage Saturn has an advantage over the two-stage Saturn V only for trip times less than 690

TABLE 5-1. WEIGHT COMPARISON FOR JUPITER FLY-BY MISSION

	300 kWe SYSTEMS		1200 kWe SYSTEMS	
	LOAD BEARING	NON-LOAD BEARING	LOAD BEARING	NON-LOAD BEARING
<u>POWERPLANT</u>				
Reactor	14,450	14,150	44,400	46,950
Shield	2,400	2,400	3,500	3,500
Power Conversion Equipment	3,900	2,900	5,100	3,500
Radiators	3,200	3,200	8,000	8,000
Primary	4,850	4,900	27,600	30,250
Secondary	(3,600)	(3,600)	(20,100)	(21,350)
Structure	(1,250)	(1,300)	(7,500)	(8,900)
	100	450	200	1,700
<u>PAYLOAD</u>	53,500	51,850	145,550	122,850
Propellant (Cesium)	17,900	17,400	66,000	59,100
Tankage, Feeds, Etc.	2,000	1,950	7,500	6,650
Thrustor Array	2,200	2,200	7,900	7,900
Scientific Payload & Structure	31,400	30,300	64,150	49,200
<u>SPACECRAFT WEIGHT AT START OF ELECTRIC PROPULSION</u>	67,950	66,000	189,950	169,800
Disposable Structure		1,400		13,700
Struts		(250)		(2,700)
Joint Fittings & Hardware		(1,100)		(10,850)
Separation System		(50)		(150)
<u>SPACECRAFT WEIGHT AT END OF CHEMICAL PROPULSION</u>	67,950	67,400	189,950	183,500
Propellant Weight Penalty for Shroud	50	600	50	6,500
Launch Vehicle Capability	68,000	68,000	190,000	190,000
Aerodynamic Shroud	250	5,000	300	21,300
<u>SPACECRAFT WEIGHT AT LAUNCH</u>	68,200	72,400	190,200	204,800

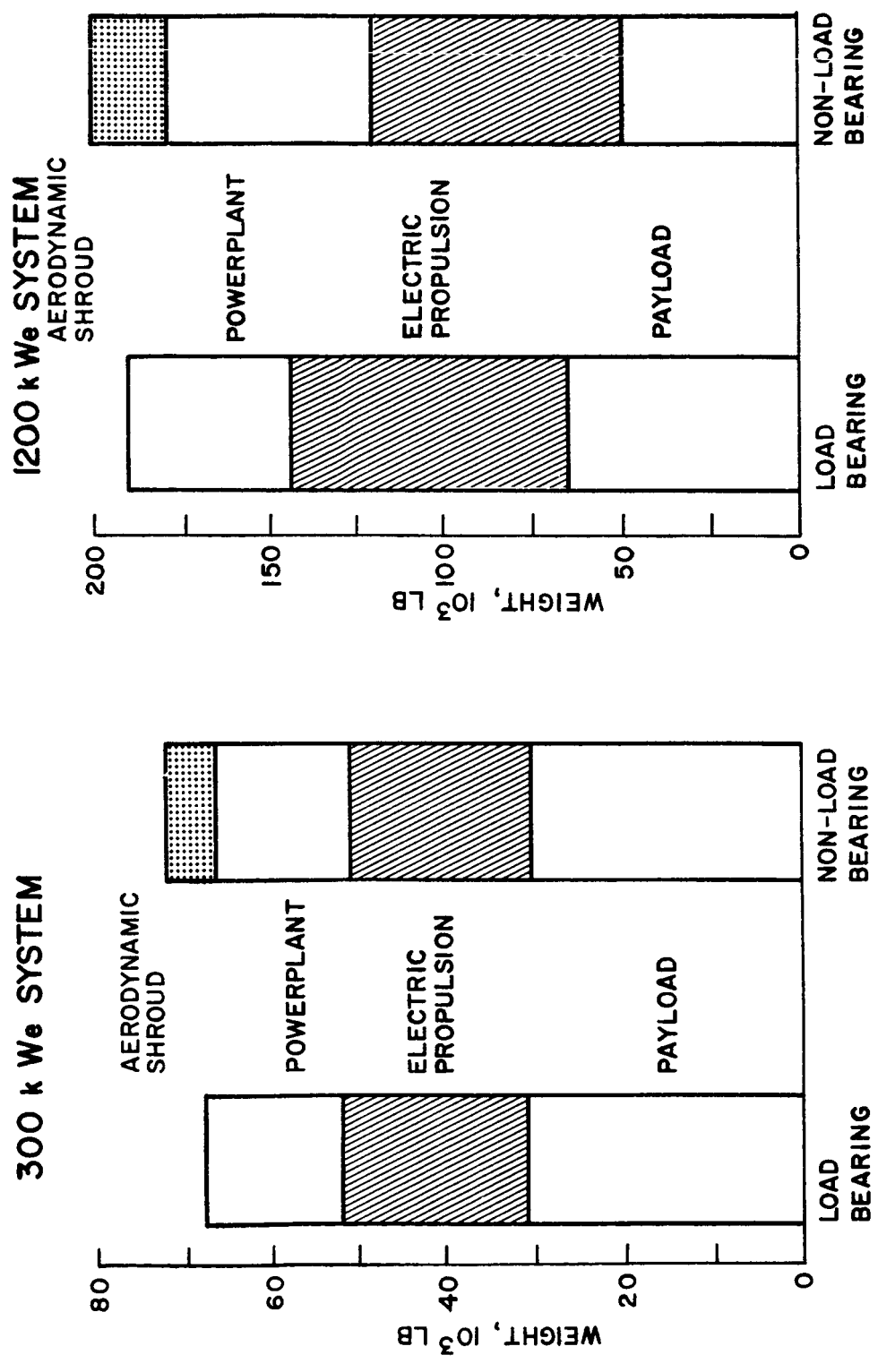


Figure 5-1. Weight Comparison For Jupiter Fly-By Mission

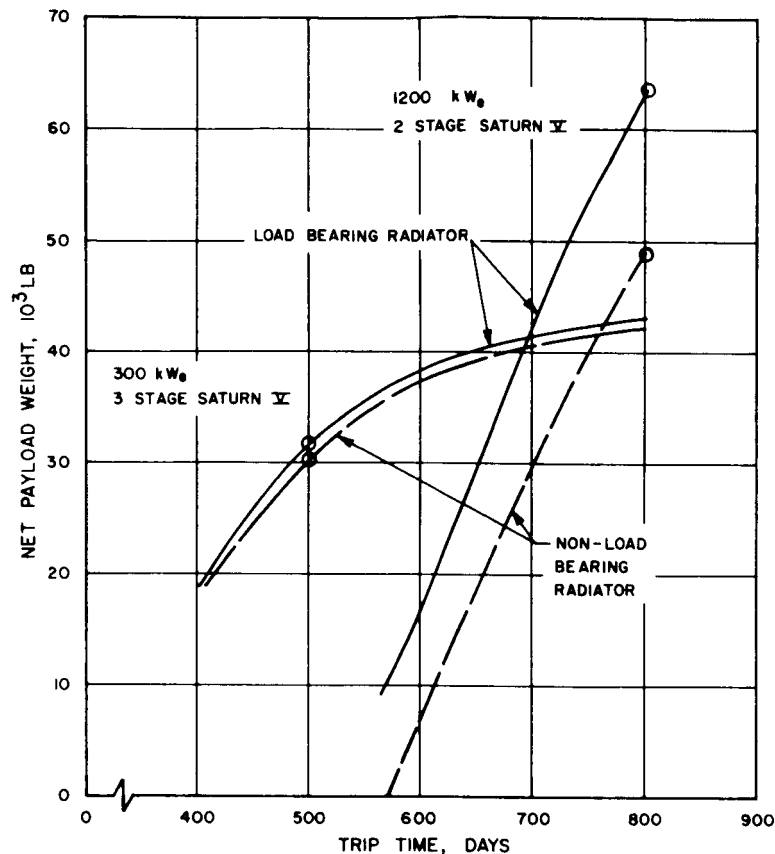


Figure 5-2. Payload Comparison for Jupiter Fly-by Mission

days. Therefore, a 500-day trip was chosen for the comparison of 300 kWe spacecraft, representing a mission which only the three-stage Saturn V can accomplish. For shorter trip times, the nuclear electric propulsion stage has less of an advantage over a fourth chemical stage. For trip times greater than 690 days, the two-stage Saturn V has a payload advantage that increases with trip time. An 800-day trip was chosen as a mission for which the payload advantage is greatest. Trip times greater than 800 days were not considered in this study since, as the geocentric phase of the trajectory increases, aerodynamic drag, which was neglected in the performance analysis, becomes significant.

It should be noted that the payload capabilities shown in Figure 5-1 are applicable only to the assumptions used in this study for the purpose of comparing radiator concepts. Increased payload capabilities of 10 to 15 percent can be shown by optimizing the power level.

As shown in Table 5-1, for the assumed trip times, the load bearing radiator concept results in a payload advantage of four percent at a power level of 300 kWe and an advantage of 30 percent at a power level of 1200 kWe. Although the exact payload differences are dependent

to some extent on the assumptions used in this study, the comparison suffices to show that the non-load bearing radiator does not offer the advantage that may have been anticipated for an interplanetary mission. It is also evident that the conclusion would not be altered by refinement in the design of the disposable launch structure; since the powerplants have nearly equal weights, the disposable launch structure for the flat panel is almost all penalty. Furthermore, should real design constraints demand a heavier launch structure composed of steel or titanium, the flat panel design payload capability would be further penalized.

Examination of the weights in Table 5-1 shows that the advantage of the load bearing radiator can be attributed to some extent to the weight penalty of the aerodynamic shroud. For the three-stage Saturn V, the velocity to which the shroud is carried before ejection is a fraction of the total velocity increment provided by the chemical stages so that the propellant penalty is small. The launch structure, on the other hand, is carried beyond escape velocity so that little is gained by disposal of the structure. The result is that the difference in payload capability between the load bearing and non-load bearing concepts launched on the three-stage Saturn V is small.

On the two-stage Saturn V, however, the shroud, in addition to being considerably heavier, is carried to a velocity which is a greater fraction of the total velocity increment provided by the chemical stages. The launch structure in this case is carried only to a 200 nmi orbit. Although electric propulsion provides a larger velocity increment, the advantage in disposing of the launch structure is not as predominant because of the high specific impulse of electric propulsion. Hence the shroud penalty predominates and the load bearing radiator concept shows a greater payload capability than the non-load bearing.

Mission requirements may also have an influence on the realizable payload advantage. For the Jupiter fly-by mission considered in this study it was noted that a two-fold increase in payload was obtained at the expense of a four-fold increase in nuclear power and a 60 percent increase in trip time. Cost effectiveness may show the shorter trip time at lower power level to be more desirable. Therefore, the 30 percent payload advantage of the load bearing radiator at the higher power level would be of no significance.

## REFERENCES

- 5-1 Freedman, S. I., "Reactor for Nuclear Brayton Cycle Power Systems," NASA CR-54397, (CRD), August 5, 1965.
- 5-2 Larson, J. W., "Research on Spacecraft and Powerplant Integration Problems - Spacecraft Analysis," NASA CR-54159, July 24, 1964.
- 5-3 , "The Atlas Launch Vehicle Family for Spacecraft Contractor Planning," General Dynamics Report, GDC-BGJ66-018, October, 1966.
- 5-4 Hendrix, E. S., and D. L. Bacchus, "Launch Vehicle Nose Shroud Optimization," Lockheed Technical Report, Contract NAS 8-11148.
- 5-5 Shulte, L. O., "Saturn V Payload Planner's Guide," Douglas Report, No. SM-47274, November, 1965.

## APPENDIX A

### SAMPLE CALCULATION FOR STRUCTURAL ANALYSIS OF LAUNCH STRUCTURE

The launch structure for the non-load-bearing radiators was analyzed with the MASS computer code, using the mathematical models shown in Figures A-1 and A-2. The maximum ultimate stress in each member was compared with the following allowable stresses:

$$\text{Crippling stress} = \frac{1.52 Et^2}{A}$$

where E = elastic modulus =  $42 \times 10^6$  psi

t = wall thickness = 0.040 inches

A = cross-sectional area = 1.507 in.<sup>2</sup>

Crippling stress = 67,700 psi

$$\text{Buckling stress} = \frac{\pi^2 EI}{Al^2}$$

where  $l$  = member length = 141 inches

I = moment of inertia = 27.13 in.<sup>4</sup>

∴ Buckling stress = 376,000 psi

Margin of safety =  $\frac{67,700}{7,840} - 1 = \text{large}$

The natural frequency of the launch structure is computed by use of Rayleigh's method:

$$\omega_n^2 = \frac{g \int_0^l EI (\delta'')^2 dx}{\sum_{i=1}^M P_i \delta_i^2}$$

where  $P_i$ 's are the concentrated loads, and  $\delta_i$ 's are the deflections.

Since  $\int_0^l EI (\delta'')^2 dx = 2 \times$  (total strain energy)

$$\omega_n^2 = \frac{2g \text{ (total strain energy)}}{\sum P_i S_i^2}$$

The total strain energy is obtained by summing the strain energies of all members from the computer output.

Example: total strain energy = 82,530 in.-lb

$$\sum P_i S_i^2 = 2.108 \times 10^6 \text{ lb in.}^2$$

$$\omega_n^2 = 772 \times \frac{82,530}{2.108 \times 10^6} = 30.2$$

$$\omega_n = 5.50 \text{ radians/sec}$$

$$f_n = 0.874 \text{ cps}$$

Since the structure was analyzed as a cantilever, the natural frequency in the free-free mode is as follows:

$$f_n = 0.874 \times \frac{22.4}{3.52} = 5.57 \text{ cps}$$

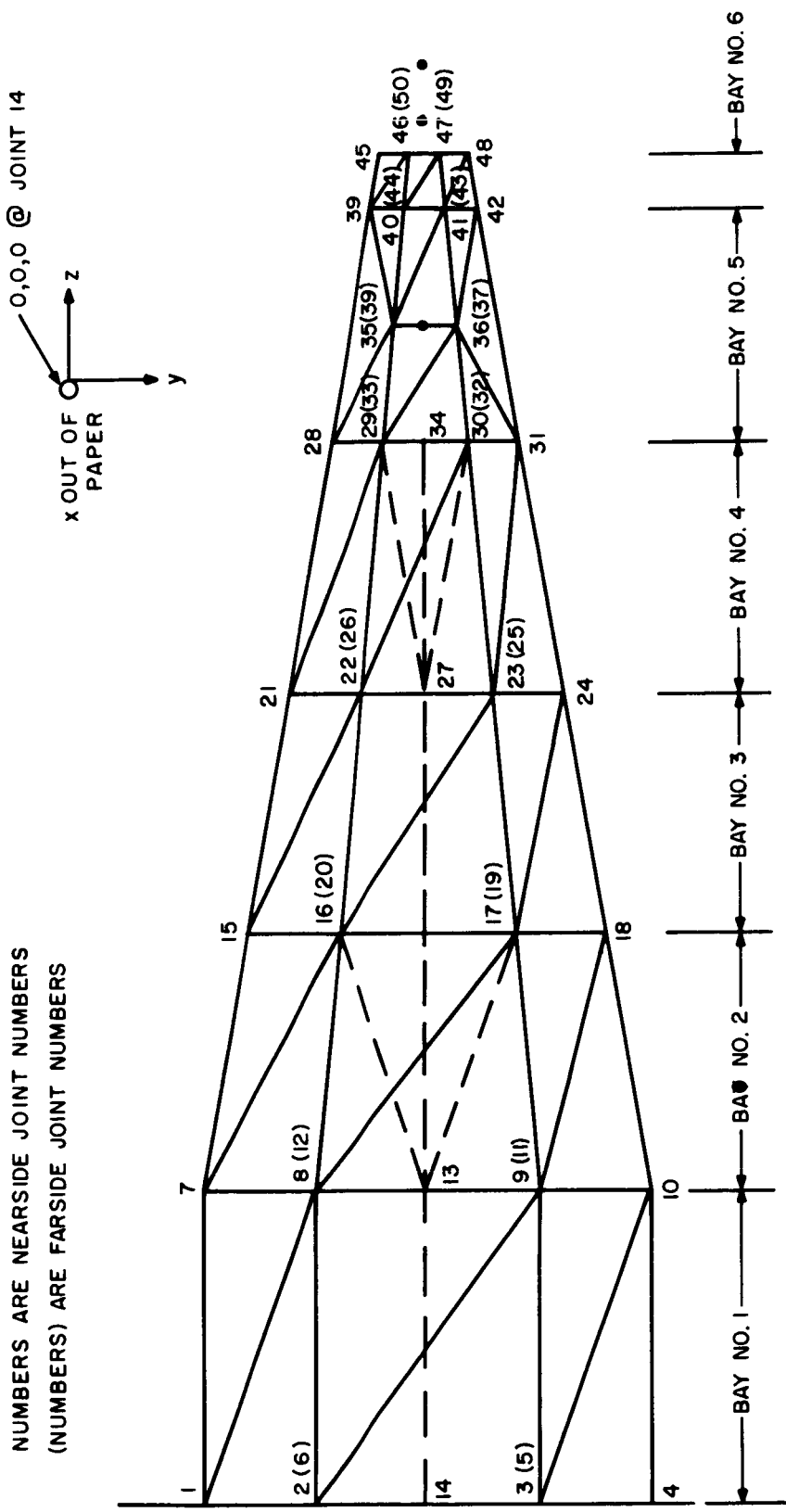


Figure A-1. Mathematical Model of the Small Radiator Support Structure

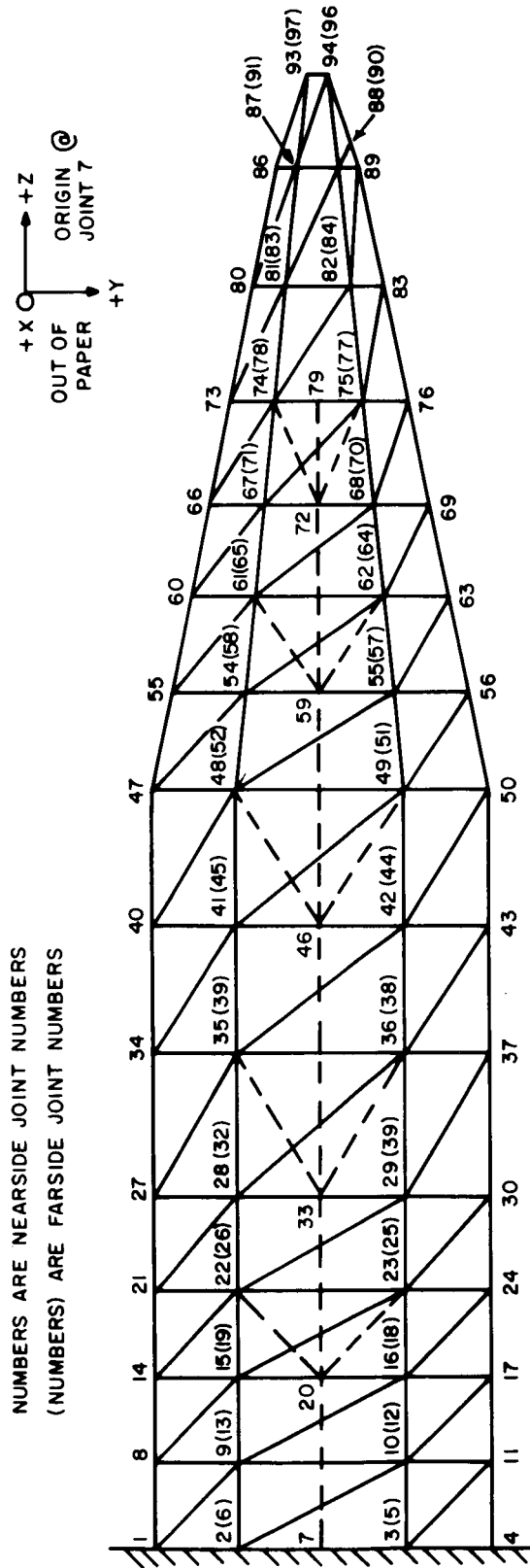


Figure A-2. Mathematical Model of the Large Radiator Support Structure

## APPENDIX B

### STRESSES DUE TO TUBE TO FIN THERMAL GRADIENTS

The temperature gradient between the radiator tubes and the cooler fins, when the radiator is operating, places the tubes in compression and the fins in tension. The relative magnitudes of the two peak stresses will depend upon the relative stiffness of the armor and fins. When the fin efficiency is low (that is, thin fins and large tube spacing), the tension stresses in the fins will be greater.

A two-dimensional analysis of thermal stresses was made for a typical section from a primary radiator used with a 1200-kWe powerplant. The analysis was made for the offset tube configuration used with the conical radiator, since this configuration had higher thermal gradients than the central fin shape. However, the results would not be significantly different for a central fin configuration; therefore, the results can be applied to both types. The temperature gradients were obtained from the SPARTAN III code thermal analysis, using temperatures at the hot end of the tube.

As shown in Figure B-1, peak stresses occur at the fin center line, where the maximum compressive stress is 22,000 psi. This stress is less than the compressive yield stress of beryllium at this temperature for many of the forms that might be used for radiator construction; e. g., extrusion, plate, and cross-rolled sheet.

In addition, thermal stresses are self-limiting (in that yielding will produce relaxation of the loads); as a result, recognized practice for reactor pressure vessels permits allowable stresses above the yield stress when compared to thermal stresses calculated by elastic theory. (Reference B-1) A fracture stress to be compared with the thermal stress calculated by elastic theory can be approximated by the elongation times the elastic modulus.

For cross-rolled sheet at 1100<sup>o</sup>F, the elongation is 7 percent and the elastic modulus is  $21 \times 10^6$  psi. The fracture stress is therefore as follows:

$$\begin{aligned}\text{Fracture stress} &= 0.07 \times 21 \times 10^6 \\ &= 1.47 \times 10^6 \text{ psi}\end{aligned}$$

Applying a factor-of-safety of 2, the allowable stress, therefore, is 735,000 psi.

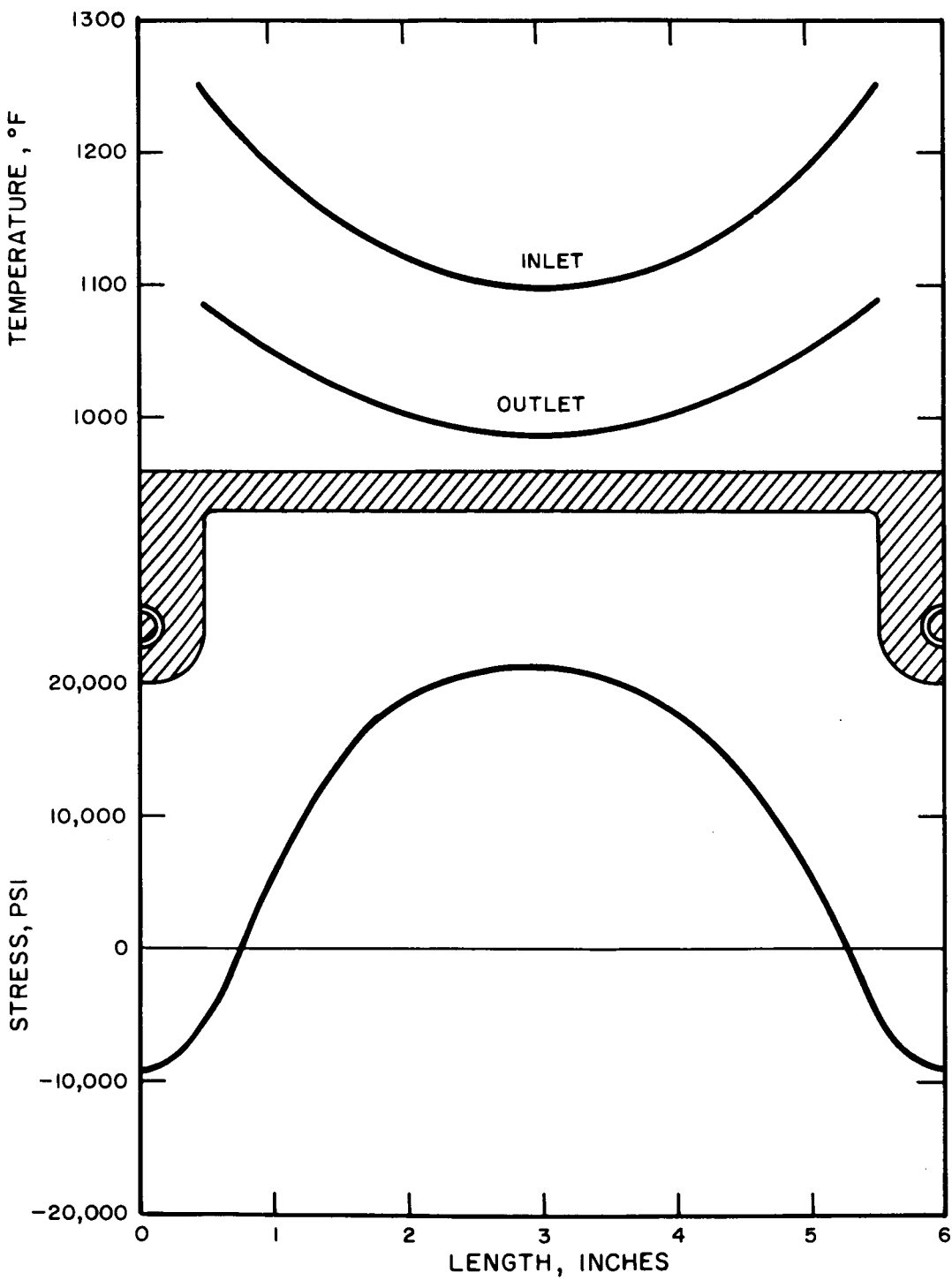


Figure B-1. Thermal Stresses Due to Temperature Gradient

At the tube center line, the maximum compressive stress shown in Figure B-1 is only 9000 psi. However, if the tube-to-fin joint is made by brazing, the effects of braze embrittlement must be considered; these may limit the allowable stresses to less than yield.

Although experience with the brazed beryllium fins on the SNAP-27 generator has shown that theoretical thermal stresses in excess of 100,000 psi can be sustained without failure in the presence of triaxial stresses and braze embrittlement, failure due to thermal stresses can occur at much lower stresses.

Without defining the actual braze alloy to be used in joining the radiator tubes to the fins, it is difficult to predict the embrittlement effects. However, if it is assumed that the braze alloy chosen reduces the elongation by the same factor as that experienced on SNAP-27 with a silver base braze alloy, then the elongation of the fin material could be as low as 1/2 percent. The fracture stress would then be:

$$\begin{aligned}\text{Fracture stress} &= 0.005 \times 21 \times 10^6 \\ &= 105,000 \text{ psi}\end{aligned}$$

The allowable stress, with a factor of safety of 2, would be 52,500 psi. Therefore, by comparison with the computed stress, it can be seen that the thermal stresses at operating temperature are acceptable, even when the beryllium is greatly reduced in elongation by a braze joint in the region of peak stresses.

However, it should also be noted that the forms of beryllium used in the radiator assembly should be chosen for high ductility rather than for high strength alone.

## **DIFFERENTIAL THERMAL EXPANSION BETWEEN RADIATOR AND HEADER**

The difference in thermal expansion between the beryllium radiator and the stainless steel headers occurs because of the combined effect of a difference in thermal expansion coefficients and a difference in average temperatures. The maximum difference occurs at the hot end of the panel having the longest continuous header. The difference is accommodated by bending of the pigtail piping connections. The center of the panel and header can be assumed to remain fixed; the deflection that must be accommodated by each pigtail then increases with distance from the panel center line. The following symbols are used in the analysis;

- A = cross section area of piping (sq. in.)  
 c = radius of piping (in.)  
 E = modulus in tension (psi)  
 G = modulus in torsion (psi)  
 I = moment of inertia about axis (in.<sup>4</sup>)  
 I<sub>p</sub> = polar moment of inertia (in.<sup>4</sup>)  
 l = piping length (in.)  
 L = header or radiator length from center to farthest piping connection (in.)  
 M = bending moment (in./lb)  
 P = force (lb)  
 T = torque (in./lb.)  
 ΔT = temperature increase above assembly temperature  
       = operating temperature -70°F (°F)  
 U = strain energy (in./lb)  
 α = thermal expansion coefficient (1/°F)  
 δ = deflection (in.)  
 σ = normal stress (psi)  
 τ = shear stress (psi)

Expansion of the header is:

$$\begin{aligned}
 \delta_H &= \alpha_H L \Delta T_H \\
 &= 10^{-5} \times 76 \times 1230 \\
 &= 0.935 \text{ inches}
 \end{aligned}$$

Expansion of the radiator panel is:

$$\begin{aligned}
 \delta_R &= \alpha_R L \Delta T_R \\
 &= 9.7 \times 10^{-6} \times 76 \times 1055 \\
 &= 0.780 \text{ inches}
 \end{aligned}$$

The difference that must be accommodated by the farthest piping connection is:

$$\begin{aligned}\delta_H - \delta_R &= 0.935 - 0.780 \\ &= 0.155 \text{ inches}\end{aligned}$$

The stresses caused by this deflection can be found from Castigliano's theorem:

$$\begin{aligned}\delta &= \frac{\partial U}{\partial P} \\ U &= \int_0^L \left( \frac{M}{2EI} + \frac{T}{2GI_p} \right) dx\end{aligned}$$

Since the piping has one 90-degree bend, it will be analyzed in two sections, neglecting the bend radius.

$$\delta = \delta_1 + \delta_2$$

$$\delta_1 = \frac{\partial U_1}{\partial P}$$

$$= \int_0^{\ell_1} \frac{M_1}{EI} \frac{\partial M_1}{\partial P} dx + \int_0^{\ell_2} \frac{T_1}{C} \frac{\partial T_1}{\partial P} dx$$

$$\delta_2 = \frac{\partial U_2}{\partial P}$$

$$= \int_0^{\ell_2} \frac{M_2}{EI} \frac{\partial M_2}{\partial P} dx + \int_0^{\ell_2} \frac{T_2}{GI_p} \frac{\partial T_2}{\partial P} dx$$

Solving for the shear load and bending moment, we obtain:

$$P = \frac{\delta}{\frac{\ell_1^3}{3EI} + \frac{\ell_1 \ell_2^2}{2GI_p} + \frac{7\ell_2^3}{12EI}}$$

$$M = \frac{\delta}{\left[ \frac{l_1^3}{3EI} + \frac{l_1 l_2^2}{2GI_p} + \frac{l_2^3}{3EI} \right] \frac{2}{l_2} + \frac{l_2^2}{2EI}}$$

Substituting the following:

$$E = 22 \times 10^6 \text{ psi}$$

$$G = 8.5 \times 10^6 \text{ psi}$$

$$I = 0.00221 \text{ in.}^4$$

$$I_p = 0.00442 \text{ in.}^4$$

$$l_1 = 4 \text{ inches}$$

$$l_2 = 2 \text{ inches}$$

We obtain:  $P = 208 \text{ lb}$

$$M = 224 \text{ in. -lb}$$

The bending, direct shear, and torsional shear stresses, respectively, are given by the following equations:

$$\sigma_b = Pl_1 c/I$$

$$\tau = P/A$$

$$\tau_t = (Pl_2 - M) c/I_p$$

The principal combined stress is:

$$\begin{aligned} \sigma_p &= \frac{\sigma_b}{2} + \sqrt{\frac{(\sigma_b)^2}{4} + (\tau^2 + \tau_t^2)} \\ &= 118,000 \text{ psi} \end{aligned}$$

Note that this stress, computed by use of elastic theory, exceeds the yield stress of stainless steel (approximately 15,000 psi for 316 at 1300° F). However, thermal stresses are self-limiting, and recognized practice permits allowable stresses many times yield stress when compared with such fictitious elastic stresses.

Since the radiator may be subjected to several thermal cycles during ground tests, the following equation from Reference B-2 is used to compute an allowable stress:

$$\sigma_{\text{all}} = \frac{E}{4\sqrt{N}} \log_e \frac{100}{100 - RA} + \sigma_e$$

where N = number of cycles

RA = reduction in area

$\sigma_e$  = endurance limit stress

Assuming N = 10, RA = 60%,  $\sigma_e = 29,000$  psi, we obtain:

$$\sigma_{\text{all}} = 1.4 \times 10^6 \text{ psi}$$

With a factor of safety of 2, the allowable limit stress is 700,000 psi. Comparing with the computed stress of 118,000, the margin of safety, M. S., is:

$$\text{M. S.} = \frac{700,000}{118,000} - 1 = + \text{high}$$

## RESIDUAL STRESSES DUE TO BRAZING

Residual stresses are produced in the radiator panels as they cool from brazing temperature as the result of mismatch in the thermal expansion coefficients of the parts being joined. The mismatch between the stainless steel liner and beryllium armor is not a serious problem if the liner thickness is small, because the strain will be taken almost entirely by the more ductile stainless steel.

From the previous analysis of thermal stresses, we know that the stainless steel will not fail at thermal stresses computed by elastic theory of many times the yield stress. However, the mismatch between the fin and armor is a more serious problem, even though both are beryllium, because small strains may be associated with very high stresses. Residual

stresses will be a maximum at room temperature and will be reduced as the radiator temperature rises.

The offset tube configuration was chosen for analysis in order to show the worst case for residual stresses in the liner. However, the stresses computed for mismatch between the armor and fins can be applied to the central fin configuration with some conservatism.

As shown in Figure B-2, the maximum principal stress is 22,000 psi in tension, occurring at the fin root. As discussed previously in the analysis of tube to fin temperature gradients, this stress is acceptable, even in the presence of braze embrittlement. However, if the armor material were hot-pressed block or some similar form, and the fins were cross-rolled sheet, the thermal expansion mismatch could be as much as  $10^{-6}/^{\circ}\text{F}$ , with the result that stresses would exceed 90,000 psi. Mismatch can also occur between identical forms of beryllium taken from different billets. To avoid possible fracture when the radiator cools from brazing temperature, it is important, therefore, to select the forms and grades of beryllium to minimize differences in thermal expansion coefficient.

Figure B-3 shows the results of analysis of residual stresses in the stainless steel liner, assuming that the same brazing process is used to make this joint. The maximum tensile stress occurs at the center of the tube, and does not exceed 18,000 psi. This is below the yield stress of most of the grades of stainless steel that might be used for liner material. If the armor material is joined to the liner by some process other than brazing (e. g., coextrusion), the residual stresses, including the effects of a subsequent brazing process, cannot be found by this simple analysis.

## REFERENCES

- B-1 Langer, B. F., "Design Values for Thermal Stress in Ductile Materials," 58-Met-1, ASME, April, 1958
- B-2 Langer, B. F., "Design of Pressure Vessels for Low-Cycle Fatigue," WAPO-T-1324, Bettis Atomic Power Laboratory, January 31, 1961

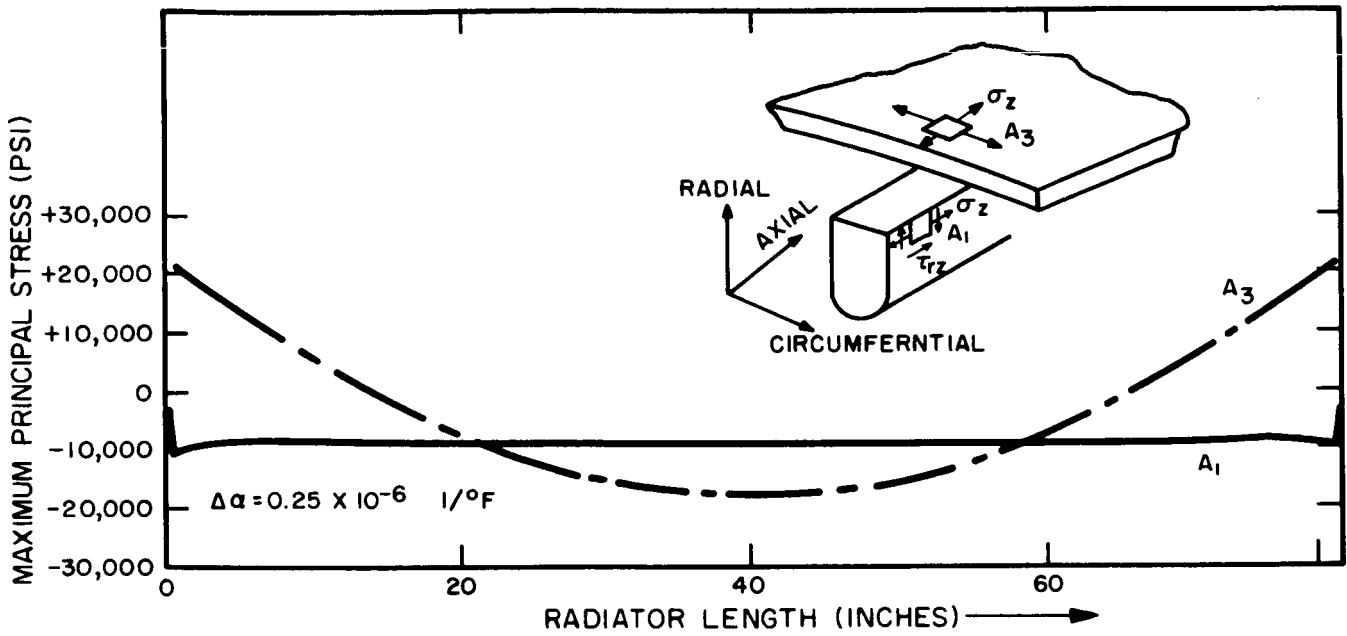


Figure B-2. Residual Stresses due to Brazing

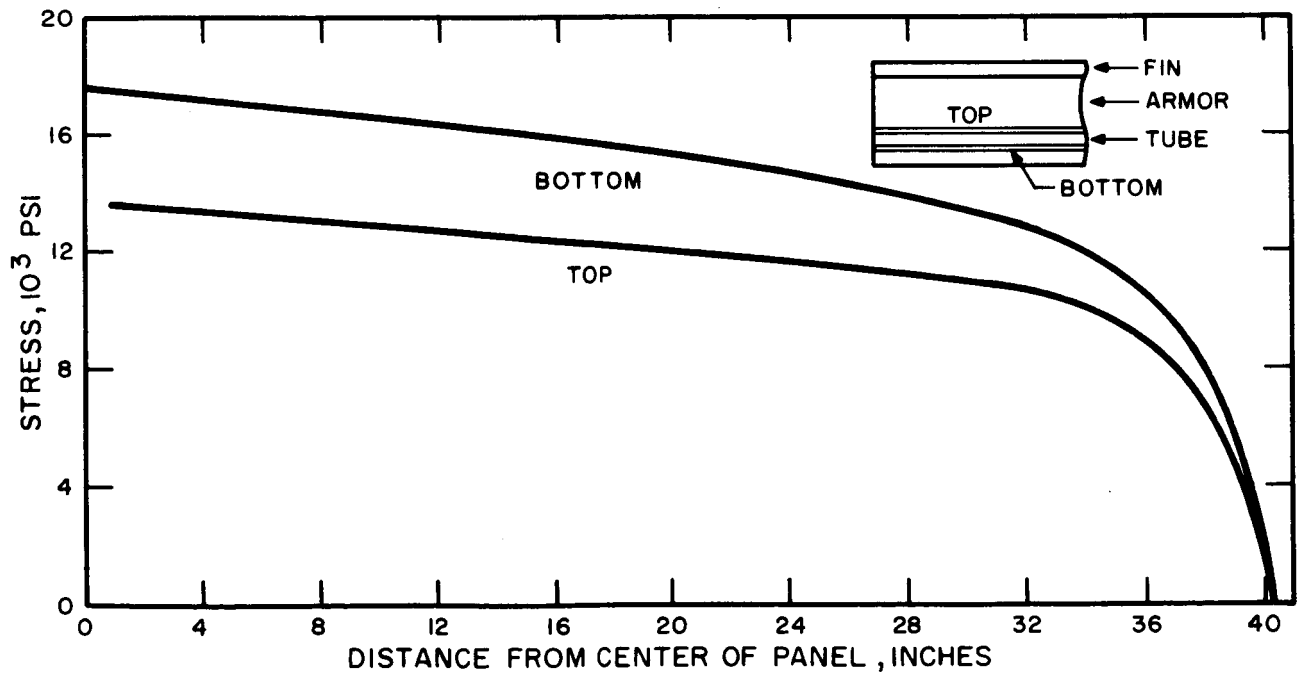


Figure B-3. Residual Stresses in Stainless Steel Tubing Due to Brazing



## APPENDIX C

### MISSION PERFORMANCE ANALYSIS

A mission performance analysis was performed for the spacecraft defined in this study in order to provide a basis for the comparison between load-bearing and non-load-bearing radiator concepts. The mission chosen was an unmanned Jupiter fly-by, representing an interplanetary mission of sufficient difficulty to warrant the choice of nuclear electric propulsion. Although the powerplant is assumed to have a 5-year life, the Jupiter fly-by trip time was assumed to be in the range of 400 to 800 days. Secondary mission objectives, such as additional planetary visits, might be included within the performance capability.

Analysis was performed with use of a computer code written specifically for this mission. An empirical model of the Saturn V launch vehicle payload capabilities, derived from data in Reference C-1, was used in the program. Electrical propulsion system characteristics were assumed, based on anticipated state of the art. The optimization procedure described in Reference C-2 was employed to maximize the payload weight. Departure date, electric propulsion specific impulse, and hyperbolic excess velocity were the parameters varied.

The electric propulsion system was assumed to employ cesium electron-bombardment thrusters. Specific power requirements were assumed to be related to specific impulse by the expression: (Reference C-3)

$$\text{Power/thrust} = 63.92 + 1.192 \times 10^{-2} \text{ Isp} + 59.75 \times 10^{-8} \text{ Isp}^2$$

Thruster weight was obtained from the following equation, assuming 25 percent redundancy:

$$W_T = 83.5 \frac{(\text{Isp})^{-2}}{1000} P \eta_{pc}$$

where

P = powerplant power output

$\eta_{pc}$  = power conditioning efficiency = 93%

The corresponding power conditioning specific weight was assumed to be 4.2 lb/kWe and the weight of propellant tanks, propellant reserves, feed system and structural support were assumed to be 11.3 percent of the propellant weight. (Reference C-4)

For the two-stage Saturn V mission, the low-thrust propulsion requirements for Earth escape were obtained from the characteristic velocity equation of Reference C-5:

$$V = V_o - 0.7 (a_o G)^{0.25}$$

where

$V_o$  = orbital velocity of the initial parking orbit

$a_o$  = initial low-thrust acceleration

$G$  = Earth gravitational constant

The characteristic length correlation of Reference C-6 was used as the basis for obtaining the low-thrust propulsion requirements for the heliocentric phases of both the two- and three-stage missions. The minimum characteristic length requirement for a Jupiter periapsis fly-by was obtained from the equation:

$$L = L_o - (L_o - L_m) \frac{T_T}{T_m} \left( 2 - \frac{T_T}{T_m} \right)$$

where

$L_o$ ,  $L_m$ , and  $T_m$  are obtained from the data in Reference C-6

$T_h$  = heliocentric trip time

The minimum characteristic length thus calculated was then increased by a factor to account for increased propulsion requirements imposed by a fly-by when Jupiter is not at its periapsis.

$$L_h = L + | A e \sin v |$$

where

$A$  = sine major axis of the Jovian orbit

$e$  = eccentricity

$v$  = true anomaly at arrival

The low-thrust characteristic length requirements for the three-stage missions were corrected for the hyperbolic excess velocity of the high-thrust departure stage by the relationship:

$$L_c = L_h \left[ 1 - \frac{V_h T_h}{L_h} \right]$$

where

$V_h$  = Earth departure hyperbolic excess velocity

The corrected characteristic length was then used to calculate the heliocentric mass ratio requirement from the equation of Reference C-6

$$W_2/W_1 = 1 - \frac{a_1}{V_j} \left[ (T_T + L_c/ZV_j) - \sqrt{T_T^2 - L_c \left( \frac{2}{a_1} - \frac{T_T}{V_j} \right)} \right]$$

where

$a_1$  = initial acceleration of heliocentric phase

$V_j$  = effective jet velocity

The final mission payload is then calculated from the following equation:

$$W_1 = W_2 - W_{pp} - W_t - W_t (W_1 - W_2) - W_{pc}$$

where

$W_{pp}$  = powerplant weight

$W_t$  = propellant tankage factor

$W_{pc}$  = power conditioning system weight

## REFERENCES

- C-1 Schulte, L.O. "Saturn V Payload Planner's Guide" Douglas Report No. SM-47274, November 1965
- C-2 Brown, H. and P. Ortiz, "CONTOUR Optimization Program," General Electric Co. Technical Information Series No. 67SD306, 25 August, 1967

and P. Ortiz, "Mission Engineering Study of Electrically Propelled Planetary Vehicles - Volume II, Mission Analysis Report," General Electric Company Document No. 6300-214, July 19, 1967.

C-4 Quillinan, J. H. , "Mission Engineering Study of Electrically Propelled Manned Planetary Vehicles - Volume IV, Systems Design Topical Report," General Electric Company Document No. 6300-216, July 19, 1967.

C-5 Brown, H. "Mission Analysis Topical Report" GE Document No. 64SD505, 26 February 1964.

C-6 Brown, H. "Mission Analysis" NASA CR-54324, Volume 1, March 1965.